

Nonlinear drift interactions between fluctuating colloidal particles: oscillatory and stochastic motions

By E. J. HINCH¹ AND LUDWIG C. NITSCHÉ²

¹Department of Applied Mathematics and Theoretical Physics, The University of Cambridge, Silver Street, Cambridge CB3 9EW, UK

²Department of Chemical Engineering, The University of Illinois at Chicago, 810 South Clinton Street, Chicago, IL 60607, USA

(Received 5 August 1992 and in revised form 10 March 1993)

In this work we consider how nonlinear hydrodynamic effects can lead to a mean force of interaction between two spheres of equal radius a undergoing translational fluctuations parallel or perpendicular to their line of centres. Motivated by amplitudes and Reynolds numbers characteristic of Brownian motion in colloidal systems, nonlinearities due to motion of the boundaries and to inertia throughout the fluid are treated as regular perturbations of the time-dependent Stokes equations. This formulation ultimately leads to a prescription for computing, at leading order, the time-average nonlinear force for the case of pure oscillatory modes – which represents the Fourier decomposition of more general motions. The associated hydrodynamic problems are solved numerically using a least-squares boundary singularity method. Frequency-dependent results over the whole spectrum are presented for a sphere–sphere gap equal to one radius; illustrative calculations are also carried out at other separations. Subsequently we extend the analysis of nonlinear drift to a Langevin equation formulation of the more complex problem of stochastic motion due to thermal fluctuations in the suspending fluid, i.e. Brownian motion. By integrating (numerically) over the spectrum of frequencies, we quantify how the mutual interactions of all translational disturbance modes give rise, on ensemble average, to a stochastic nonlinear force of interaction between the particles. It is particularly interesting that this net interaction – arising from a zero-mean random force – is of $O(1)$ on the Brownian scale kT/a , even though it represents a small $O(Re)$ correction at each frequency of pure oscillations. Finally, we discuss how the presence of stochastic nonlinear drift would lead to non-uniform equilibrium distributions of dilute colloidal suspensions, unless one adds to the random force in the Langevin equation a cancelling non-zero mean component.

1. Introduction

Traditionally it is believed that fluid inertia can be entirely neglected in modelling Brownian motion of colloidal particles, an approach which is motivated by two main considerations. Firstly, the actual spreading by diffusion is sufficiently slow that a Reynolds number based upon the characteristic spreading speed must obviously be very small. Secondly, despite the fact that short-time fluid-mechanical transients (e.g. Basset history dependence associated with the diffusion of vorticity) can affect certain

ensemble-average properties such as the velocity autocorrelation function, mean-square displacements are accurately reproduced using *quasi-static* mobility coefficients (Hinch 1975; Batchelor 1977; Russel 1981). Therefore, fluid inertia – which has a significant effect (e.g. added mass) only during the hydrodynamic relaxation time – would seem to be unimportant as well. Reflecting these considerations, particulate diffusion is generally modelled by incorporating quasi-static hydrodynamic mobility coefficients (obtained from the quasi-static Stokes equations) into a convective–diffusive parabolic equation describing the conservation of probability density in the space of particle positions and orientations.

In the linear theory of Brownian motion as described above, transient effects do not contribute to any *net* hydrodynamic interactions between particles even on the short timescale, although there is a well-known drift term associated with the configuration dependence of the *quasi-static* mobility coefficients (§7.1; cf. Russel, Saville & Schowalter 1989, Chap. 3). The present hydrodynamic problem is motivated by the observation that the transients *can* lead to systematic mean forces or motions if one accounts for (weak) inertia in the hydrodynamic equations – this despite the assumed zero-mean character of the driving thermal fluctuations. In principle, such interactions would affect the equilibrium spatial distribution of Brownian particles as well as the rate at which they spread apart from one another. Indeed, nonlinear stochastic drift could conceivably impact on the collective behaviour of large swarms of particles, as embodied, for example, in effective rheological coefficients. It is therefore of interest to quantify nonlinear drift interactions as functions of geometric and hydrodynamic parameters.

We assert that inertia of the suspending fluid represents an important and inseparable part of Brownian motion. The reason is simply this: if one decomposes the spectrum of random disturbances into its constituent modes, it is evident that each frequency leads to a nonlinear force of interaction between particles. Therefore, there is no *a priori* reason to dismiss the possibility that stochastic forcing with a zero mean value can produce either net attraction or net repulsion between diffusing particles. Although the magnitude and direction of this effect can only be decided by integrating over the spectrum of frequencies (which is the detailed calculation developed in this paper), the underlying physical concept appears straightforward. Moreover, our mechanistic picture of inertial drift does *not* contradict the ostensibly slow rate of Brownian spreading, it merely superimposes an additional systematic force upon the traditional formulation.

As a concrete model which captures some of the features of fluctuating motion of particles, and which represents a frequency decomposition (i.e. Fourier transform) of general motions, we first study nonlinear drift forces which arise from pure oscillatory modes of two identical spheres – either parallel or perpendicular to the line of centres, and with arbitrary relative phase.

Section 2 describes the case of potential flow, which represents the simplest possible example of net forces of interaction accompanying zero-mean oscillations of particles. This problem corresponds to the physical situation at extremely high frequencies, and therefore provides a useful check of consistency (for the general theory as well as for numerical computations) on the subsequent, more complex formulation for viscous fluids at arbitrary frequencies. We consider (i) the hydrodynamic approach, based upon Euler's equations; and (ii) Lagrange's equations, which encapsulate the fluid degrees of freedom in virtual masses that depend upon (generalized) particle coordinates. Our derivation of the latter from the former (§2.1) is conceptually more direct than traditional arguments (Lamb 1932; Birkhoff 1950; Milne-Thompson

1968). Subsequently, the general formulas are specialized to deal with two spheres of equal size (§2.2), and actual numerical calculations of the interaction force as a function of separation are carried out using virtual masses and Lagrange's equations (§2.3).

In §3 we develop a general formulation for calculating the mean sphere–sphere interaction force at arbitrary frequencies. Nonlinearities arising at the moving boundaries (finite-amplitude effects) and within the bulk fluid are treated as perturbations of the time-dependent Stokes equations posed on the fixed, zeroth-order fluid domain (§3.2). A reciprocal theorem then yields an expression for the time-average interaction force in terms of surface and volume integrals involving the leading-order nonlinear terms (§3.3). In §3.4 the dependence upon relative phase of oscillation is factored out by defining special drift-force coefficients. After examining asymptotic behaviour in the limits of high and low frequencies (§§3.5–3.8), we rewrite the coefficient formulas to take advantage of the axisymmetric geometry (§3.9).

Actual computations (§4) for the hydrodynamic problems – potential flow, quasi-static Stokes flow, transient Stokes flow – encountered in finding the drift-force coefficients are carried out with a least-squares boundary singularity method (Mathon & Johnston 1977; Bogomolny 1985; Dąbrosz 1985; Nitsche & Brenner 1990), by which the flow fields are expressed as linear combinations of singular basis functions whose poles lie inside the spheres. This numerical technique is general, and can readily be extended to treat more complicated geometries (e.g. involving particles in pores; see Nitsche & Brenner 1990). The discussion emphasizes the unsteady Stokes equations, the quasi-static case being entirely analogous. Algorithmic details are provided in §§4.2, 4.3 for the axisymmetric flows associated with oscillations along the line of centres. The numerical method is extended to transverse modes in §4.4, in a manner that exploits axisymmetry of the geometry even though the actual flows are no longer axisymmetric. The frequency-dependent friction coefficients are expressed in terms of the expansion coefficients in §4.5. Analogous calculations for transverse oscillations in potential flow are outlined in §4.6, leaving axial modes to be treated more simply by the method of images (Appendix A; cf. Lamb 1932). For very high frequencies, above a certain threshold value, the numerical scheme begins to lose accuracy. Although this would generally signal the need for a boundary-layer representation, the sphere–sphere interactions in the outer field are so weak that the first reflected field in the Brinkman-like solution gives very good results even at $O(1)$ separations. Formulas pertaining to this approximation appear in §4.7. Finally, §§4.8 and 4.9 indicate how the drift-force coefficients are calculated from the hydrodynamic flow fields, and establish the accuracy and consistency of our numerical results.

Our general formulation implicitly incorporates the nonlinear phenomenon of steady streaming, i.e. the second-order mean flow set up by oscillatory boundary layers when the outer field varies in the streamwise direction (Riley 1966; Batchelor 1967, §5.13; Hall 1974). In this connection it is worthwhile to mention the work of Tabakova & Zapryanov (1982*a, b*), who develop a singular perturbation analysis for steady-streaming interactions between two spheres in the limit of high frequencies and small amplitudes. Our results are examined in relation to theirs in §5.

Although part of the computed interaction force is ascribable to the steady-streaming flow field of one sphere impinging on the other sphere, and vice versa, the reciprocal theorem yields the forces directly, and systematically accounts for all of the leading-order nonlinear effects.

To provide insight into the role of nonlinear drift in Brownian motion, we conclude with a calculation of the mean nonlinear force of interaction for the case in which the

spheres undergo stochastic motion due to thermal fluctuations in the suspending fluid (§6). For all but pure oscillatory modes the nonlinear terms arising at the boundaries and throughout the fluid represent a ‘mixing’ of different frequencies. Our formulation of nonlinear drift – which utilizes results from the linear theory of Brownian motion (Case 1971; Chow & Hermans 1974; Hinch 1975; Batchelor 1977; Russel 1981) – indicates how different oscillatory disturbance modes interact with each other to yield a net drift interaction on ensemble average (§§6.1–6.3). Although the nonlinear terms are usually presumed to be vanishingly small (Hauge & Martin-Löf 1973), we argue that they should not be discarded – precisely because they represent a *systematic* component in an otherwise zero-mean stochastic process. The resultant nonlinear drift force is decomposed into two contributions: (i) a frictional term arising from a pole at zero frequency; and (ii) an inertial term obtained by integrating over the spectrum of frequencies. Both effects are of $O(1)$ on the Brownian scale kT/a . This order of magnitude of the drift force can be estimated as the result of pressure forces p acting over an area $O(a^2)$, with pressure fluctuations $O(\rho u^2)$ in which one uses the thermal velocity $u = O(kT/\rho a^3)^{1/2}$. The physical assumptions by which our analysis can be applied to colloidal particles are considered in §6.4. Finally, the stochastic drift force is calculated quantitatively by the above formalism in §6.5.

These results, which rigorously account for fluid degrees of freedom directly excited by translational motions of the particles at all frequencies, are compared with a simpler nonlinear Langevin equation that involves only particle degrees of freedom – the effects of fluid inertia being modelled approximately with virtual mass coefficients (§7.1). Finally, in §7.2 we consider how nonlinear drift would lead, at least in principle, to *non-uniform* equilibrium distributions of Brownian particles, unless one modified the forcing of the Langevin equation to include a non-zero mean component.

We should point out that in statistical mechanics there is no well-established general theory of nonlinear fluctuations to which we can appeal. In the colloidal systems of interest in this paper, however, the fluctuations are necessarily small in magnitude, as estimated in §6.4. For small fluctuations we expect that the classical and successful linear theory can be applied to leading order. The most interesting small correction for weak nonlinearities is a steady drift. We return to these issues in §7.3.

Copies of the tables 1, 3–11 and appendices A–E for this paper are available on request from the authors or the editorial office of the *Journal*.

2. Model formulation for two vibrating spheres in potential flow

Consider two spheres of radius a oscillating harmonically, with common frequency ω and amplitude ℓ , about mean positions that are separated by the gap spacing \mathcal{L} . The vibrations of both spheres are supposed to occur parallel to a specified unit vector \mathbf{b} , which – as far as concerns the general derivations to follow – may have any orientation relative to the line of centres (z -axis). Ultimately the nonlinear drift force will be decomposed into two contributions: (i) modes parallel to the line of centres ($\mathbf{b}^{\parallel} = \mathbf{e}_z$), and (ii) modes perpendicular to the line of centres, which – owing to transverse isotropy – are encapsulated in the single case $\mathbf{b}^{\perp} = \mathbf{e}_x$. Where it becomes necessary to make a distinction between these two cases, we will use the respective affixes ‘ \parallel ’ and ‘ \perp ’.

Since time-average properties must show themselves to be independent of the initial phase, we can – without loss of generality – specify a sine oscillation for the first sphere together with a relative phase shift for the other sphere. Making length and time dimensionless with respect to a and ω^{-1} , respectively, the positions of the particle

centres are given by

$$\mathbf{r}_1(t) = -h\mathbf{e}_z + \eta q_1(t)\mathbf{b}, \quad \mathbf{r}_2(t) = h\mathbf{e}_z + \eta q_2(t)\mathbf{b}, \quad (2.1)$$

with

$$q_1(t) = \sin t, \quad q_2(t) = \sin(t + \varphi) \quad (2.2)$$

and $\eta = \ell/a$, $L = \mathcal{L}/a$, $h = 1 + L/2$. Utilizing the inertial pressure scale $\rho a^2 \omega^2$, the Navier–Stokes equations appear in the following dimensionless form, posed on the time-varying fluid domain $\mathcal{V}(t)$:†

$$\frac{\partial \mathbf{V}}{\partial t} + \mathbf{V} \cdot \nabla \mathbf{V} = -\nabla P + \frac{1}{\Omega} \nabla^2 \mathbf{V}, \quad (2.3)$$

$$\nabla \cdot \mathbf{V} = 0, \quad (2.4)$$

with the dimensionless frequency $\Omega = \omega a^2/\nu$ serving also as the appropriate Reynolds number.

At very high frequencies viscous effects scale out of (2.3), leaving Euler’s equations of motion

$$\partial \mathbf{V}/\partial t + \mathbf{V} \cdot \nabla \mathbf{V} = -\nabla P. \quad (2.5)$$

As will be justified through proper accounting for the Stokes layers (§3.6), the problem can then be treated from the perspective of potential flow theory. For the boundary conditions we then have

$$\mathbf{n} \cdot \mathbf{V}(\mathbf{r}, t) = \begin{cases} (\mathbf{n} \cdot \mathbf{b}) \eta \cos t & \text{on } \mathcal{S}_1(t) \\ (\mathbf{n} \cdot \mathbf{b}) \eta \cos(t + \varphi) & \text{on } \mathcal{S}_2(t), \end{cases}$$

$$\mathcal{S}_\alpha(t) = \{\mathbf{r} : \|\mathbf{r} - (-1)^\alpha h\mathbf{e}_z - q_\alpha(t)\mathbf{b}\| = 1\}. \quad (2.6)$$

For calculating particle dynamics in potential flow it is advantageous to resort to the well-known, equivalent Lagrangian formulation, which encapsulates the effects of fluid degrees of freedom in variable virtual ‘masses’ so that only ‘generalized’ particle coordinates need be considered. Although a standard derivation – expressing the total kinetic energy of the fluid as a quadratic form in the generalized particle velocities – readily yields expressions for the various virtual mass components, it is much more difficult to demonstrate that Lagrange’s generalized forces obtained therefrom actually correspond to the pressure forces calculable (at least in principle) from the hydrodynamic equations. Theoretical arguments available in the literature typically regard the problem as one of *eliminating* fluid degrees of freedom from an overall variational formulation involving both fluid and particle coordinates; cf. Lamb (1932), Birkhoff (1950). A conceptually simpler derivation can be based upon Euler’s equations, and this development, given below, has close connections with the boundary-layer derivation presented in §3.6.

2.1. From Euler’s equations to Lagrangian mechanics

The irrotational flow field can be written as the gradient of a harmonic potential,

$$\mathbf{V}(\mathbf{r}, t) = -\nabla \phi, \quad (2.7)$$

where ϕ is uniquely determined by the instantaneous positions and velocities of all (spherical) particles. Thus, on the surface of each sphere we have the boundary

† Since we are concerned only with incompressible flows, all velocity fields will subsequently be understood to be solenoidal without explicit mention of the divergence-free condition (2.4).

condition†

$$n_j \partial \phi / \partial r_j = -n_j \dot{X}_j^\beta \quad \text{on } \mathcal{S}^\beta = \{ \mathbf{r} : \| \mathbf{r} - \mathbf{X}^\beta(t) \| = R^\beta \}.$$

Once the velocity potential has been obtained at any instant, Euler’s equation (2.5) gives for the pressure field, within an arbitrary additive constant,

$$P = \partial \phi / \partial t - V^2 / 2. \tag{2.8}$$

Owing to linearity of Laplace’s equation, one can factor out the dependence of ϕ on the individual velocities as follows (Lamb 1932, Chap. VI):

$$\phi = \dot{X}_i^\alpha(t) \Phi_i^\alpha(\mathbf{r}_j, X_k^\beta), \tag{2.9}$$

where the individual potentials Φ_i^α are given by the boundary value problems

$$\nabla^2 \Phi_i^\alpha = 0 \quad \text{in } \mathcal{V}(t), \tag{2.10}$$

$$n_j \frac{\partial \Phi_i^\alpha}{\partial r_j} = -n_i \delta^{\alpha\beta} \quad \text{on } \mathcal{S}^\beta, \tag{2.11}$$

$$\Phi_i^\alpha \rightarrow \text{constant, say } 0, \quad \text{as } r \rightarrow \infty. \tag{2.12}$$

The generalized virtual masses are defined as the coefficients in the quadratic form expressing total fluid kinetic energy in terms of the individual velocities \dot{X}_i^α :

$$2T = \int_{\mathcal{V}} \| \nabla \phi \|^2 d^3 \mathbf{r} = \int_{\mathcal{V}} \frac{\partial}{\partial r_k} \left(\phi \frac{\partial \phi}{\partial r_k} \right) d^3 \mathbf{r}. \tag{2.13}$$

Utilizing the divergence theorem (with \mathcal{S} denoting the collection of all sphere surfaces and \mathbf{n} the normal vector directed into the fluid), the linear decomposition (2.9), and the boundary condition (2.11) we obtain

$$\begin{aligned} 2T &= - \int_{\mathcal{S}} (\dot{X}_i^\alpha \Phi_i^\alpha) \left(\dot{X}_j^\gamma \frac{\partial \Phi_j^\gamma}{\partial r_k} \right) n_k d^2 \mathbf{r} \\ &= \dot{X}_i^\alpha \dot{X}_j^\gamma \left[\int_{\mathcal{S}} \Phi_i^\alpha \left(-n_k \frac{\partial \Phi_j^\gamma}{\partial r_k} \right) d^2 \mathbf{r} \right] \\ &= \dot{X}_i^\alpha \dot{X}_j^\gamma \left[\int_{\mathcal{S}^\beta} \Phi_i^\alpha (n_j \delta^{\beta\gamma}) d^2 \mathbf{r} \right] \\ &= \dot{X}_i^\alpha \dot{X}_j^\beta \left[\int_{\mathcal{S}^\beta} \Phi_i^\alpha n_j d^2 \mathbf{r} \right]. \end{aligned}$$

Thus, one obtains the desired quadratic form for the kinetic energy and the associated formulas for the configuration-dependent virtual masses $\mathcal{M}_{ij}^{\alpha\beta}$:

$$2T = \dot{X}_i^\alpha \dot{X}_j^\beta \mathcal{M}_{ij}^{\alpha\beta}, \quad \mathcal{M}_{ij}^{\alpha\beta} = \int_{\mathcal{S}^\beta} \Phi_i^\alpha n_j d^2 \mathbf{r}. \tag{2.14}$$

Standard arguments based upon Green’s theorem demonstrate that the virtual mass tensor is symmetric (Lamb 1932, Art. 136), i.e.

$$\mathcal{M}_{ij}^{\alpha\beta} = \mathcal{M}_{ji}^{\beta\alpha} \quad \text{for } i, j = 1, 2, 3. \tag{2.15}$$

By the usual interpretation, expression (2.14) suggests that one should regard the

† Here we use Latin affices to distinguish Cartesian components, while individual particles are indexed with Greek letters. Repeated indices denote summation, but only when they are both subscripts or both superscripts.

positions X_i^α as generalized coordinates in a Lagrangian formulation, which now involves only particle degrees of freedom. According to Lagrange's equations the generalized (external) forces acting on each degree of freedom take the form

$$F_k^\gamma = \frac{d}{dt} \left(\frac{\partial T}{\partial \dot{X}_k^\gamma} \right) - \frac{\partial T}{\partial X_k^\gamma}. \tag{2.16}$$

But it is not obvious *a priori* that the F_k^γ possess the same physical significance as the corresponding hydrodynamic pressure forces

$$\int_{\mathcal{G}^\gamma} P n_k d^2r, \tag{2.17}$$

an assertion for which available proofs rely upon either (i) a Hamiltonian formulation applied to fluid and particle degrees of freedom together (Lamb 1932, Arts. 135–136; Birkhoff 1950, Chap. V, §15) or (ii) arguments involving virtual motions of the fluid and the associated virtual power (Milne-Thomson 1968). The derivation below proceeds by calculating the generalized forces in Lagrange's equations (2.16) directly from the hydrodynamic equations of potential flow (2.7), (2.8), (2.17).†

It follows from (2.14) that

$$\begin{aligned} 2 \frac{\partial T}{\partial X_k^\gamma} &= \dot{X}_i^\alpha \dot{X}_j^\beta \left[\int_{\mathcal{G}^\beta} \frac{\partial \Phi_i^\alpha}{\partial X_k^\gamma} n_j d^2r + \delta^{\beta\gamma} \int_{\mathcal{G}^\gamma} \frac{\partial \Phi_i^\alpha}{\partial r_k} n_j d^2r \right] \\ &= \dot{X}_i^\alpha \dot{X}_j^\beta \int_{\mathcal{G}^\beta} \frac{\partial \Phi_i^\alpha}{\partial X_k^\gamma} n_j d^2r - \dot{X}_j^\gamma \int_{\mathcal{G}^\gamma} V_k n_j d^2r, \end{aligned} \tag{2.18}$$

where summation over γ has been suppressed in the second integral. From (2.13) we also know that

$$\frac{\partial T}{\partial X_k^\gamma} = -\frac{1}{2} \int_{\mathcal{G}^\gamma} V^2 n_k d^2r + \int_{\mathcal{V}} \frac{\partial}{\partial X_k^\gamma} \left(\frac{1}{2} V^2 \right) d^3r.$$

Noting the identity

$$-\frac{\partial}{\partial r_j} \left(V_j \frac{\partial \phi}{\partial X_k^\gamma} \right) = -V_j \frac{\partial}{\partial X_k^\gamma} \left(\frac{\partial \phi}{\partial r_j} \right) = V_j \frac{\partial V_j}{\partial X_k^\gamma} = \frac{\partial}{\partial X_k^\gamma} \left(\frac{1}{2} V^2 \right)$$

the volume integral can be rewritten using the divergence theorem and subsequently incorporating the boundary condition (2.11):

$$\begin{aligned} \int_{\mathcal{V}} \frac{\partial}{\partial X_k^\gamma} \left(\frac{1}{2} V^2 \right) d^3r &= \int_{\mathcal{G}} n_j V_j \frac{\partial \phi}{\partial X_k^\gamma} d^2r \\ &= \dot{X}_j^\beta \int_{\mathcal{G}^\beta} n_j \frac{\partial}{\partial X_k^\gamma} (\dot{X}_i^\alpha \Phi_i^\alpha) d^2r \\ &= \dot{X}_i^\alpha \dot{X}_j^\beta \int_{\mathcal{G}^\beta} \frac{\partial \Phi_i^\alpha}{\partial X_k^\gamma} n_j d^2r. \end{aligned}$$

Thus results another expression for the X_k^γ derivative of the kinetic energy:

$$\frac{\partial T}{\partial X_k^\gamma} = - \int_{\mathcal{G}^\gamma} \frac{1}{2} V^2 n_k d^2r + \dot{X}_i^\alpha \dot{X}_j^\beta \int_{\mathcal{G}^\beta} \frac{\partial \Phi_i^\alpha}{\partial X_k^\gamma} n_j d^2r. \tag{2.19}$$

† *Footnote added in proof.* For the simpler case of an isolated body, a direct hydrodynamic derivation of Kirchhoff's equations (to which Lagrange's equations reduce in the absence of configurational dependence of the virtual masses) was given by H. Lamb (*Q. J. Pure Appl. Maths*, vol xix, 1883, pp. 66–70). This involved angular forms, which do not arise for the spherical bodies considered here.

Subtracting (2.19) from (2.18) one obtains for the velocity contribution to the pressure integral about sphere γ :

$$\int_{\mathcal{S}^\gamma} \left(-\frac{1}{2}V^2\right) n_k d^2\mathbf{r} = -\frac{\partial T}{\partial X_k^\gamma} - \dot{X}_j^\gamma \int_{\mathcal{S}^\gamma} V_k n_j d^2\mathbf{r} \quad (2.20)$$

For the time derivative term we first note that

$$\frac{\partial \phi}{\partial t} = \frac{\partial}{\partial t} (\dot{X}_i^\alpha \Phi_i^\alpha) = \ddot{X}_i^\alpha \Phi_i^\alpha + \dot{X}_i^\alpha \dot{X}_j^\beta \frac{\partial \Phi_i^\alpha}{\partial X_j^\beta}.$$

Integrating around \mathcal{S}^γ , and adding and subtracting the expression

$$\delta^{\beta\gamma} \dot{X}_i^\alpha \dot{X}_j^\beta \int_{\mathcal{S}^\beta} \frac{\partial \Phi_i^\alpha}{\partial r_j} n_k d^2\mathbf{r} = -\dot{X}_j^\gamma \int_{\mathcal{S}^\gamma} V_j n_k d^2\mathbf{r}$$

on the left-hand side, gives

$$\begin{aligned} \int_{\mathcal{S}^\gamma} \frac{\partial \phi}{\partial t} n_k d^2\mathbf{r} &= \ddot{X}_i^\alpha \left[\int_{\mathcal{S}^\gamma} \Phi_i^\alpha n_k d^2\mathbf{r} \right] \\ &\quad + \dot{X}_i^\alpha \dot{X}_j^\beta \left[\int_{\mathcal{S}^\gamma} \frac{\partial \Phi_i^\alpha}{\partial X_j^\beta} n_k d^2\mathbf{r} + \delta^{\beta\gamma} \int_{\mathcal{S}^\beta} \frac{\partial \Phi_i^\alpha}{\partial r_j} n_k d^2\mathbf{r} \right] \\ &\quad + \dot{X}_j^\gamma \int_{\mathcal{S}^\gamma} V_j n_k d^2\mathbf{r} \\ &= \ddot{X}_i^\alpha \mathcal{M}_{ik}^{\alpha\gamma} + \dot{X}_i^\alpha \dot{X}_j^\beta \frac{\partial \mathcal{M}_{ik}^{\alpha\gamma}}{\partial X_j^\beta} + \dot{X}_j^\gamma \int_{\mathcal{S}^\gamma} V_j n_k d^2\mathbf{r}. \end{aligned}$$

Noting that

$$\frac{d}{dt} \left(\frac{\partial T}{\partial \dot{X}_k^\gamma} \right) = \frac{d}{dt} (\dot{X}_i^\alpha \mathcal{M}_{ik}^{\alpha\gamma}) = \ddot{X}_i^\alpha \mathcal{M}_{ik}^{\alpha\gamma} + \dot{X}_i^\alpha \dot{X}_j^\beta \frac{\partial \mathcal{M}_{ik}^{\alpha\gamma}}{\partial X_j^\beta}$$

the above equation reduces to the simpler form

$$\int_{\mathcal{S}^\gamma} \frac{\partial \phi}{\partial t} n_k d^2\mathbf{r} = \frac{d}{dt} \left(\frac{\partial T}{\partial \dot{X}_k^\gamma} \right) + \dot{X}_j^\gamma \int_{\mathcal{S}^\gamma} V_j n_k d^2\mathbf{r}. \quad (2.21)$$

Combining (2.20) with (2.21), we find

$$\int_{\mathcal{S}^\gamma} P n_k d^2\mathbf{r} = \frac{d}{dt} \left(\frac{\partial T}{\partial \dot{X}_k^\gamma} \right) - \frac{\partial T}{\partial X_k^\gamma} + \dot{X}_j^\gamma \int_{\mathcal{S}^\gamma} (V_j n_k - V_k n_j) d^2\mathbf{r}. \quad (2.22)$$

The apparent discrepancy detracting from an otherwise correct Lagrangian force equation can be shown to vanish by the following argument.

Consider any (closed) curve \mathcal{C} formed by the intersection of \mathcal{S}^γ with a plane $x_3 = \text{constant}$. If $d\mathbf{l} = (dx_1, dx_2, 0)$ is the local line element at some point on \mathcal{C} , then $(n_1, n_2, 0)d\mathbf{l} = (-dx_2, dx_1, 0)$. Taking \mathcal{A} to be a surface which spans \mathcal{C} while lying

entirely within the fluid, it then follows that

$$\begin{aligned} \int_{\mathcal{C}} (V_1 n_2 - V_2 n_1) dl &= \int_{\mathcal{C}} [V_1 dx_1 - V_2 (-dx_2)] \\ &= \int_{\mathcal{C}} \mathbf{V} \cdot d\mathbf{l} = \int_{\mathcal{A}} (\nabla \times \mathbf{V}) \cdot \mathbf{n} d^2\mathbf{r}, \end{aligned}$$

which must vanish for potential flow. Therefore

$$\int_{\mathcal{S}^\gamma} (V_1 n_2 - V_2 n_1) d^2\mathbf{r} = 0,$$

and the same is true of any permutation of the indices, so that the discrepancy term in (2.22) vanishes (Lamb 1883). Thus we have

$$F_k^\gamma \stackrel{\text{def}}{=} \int_{\mathcal{S}^\gamma} P n_k d^2\mathbf{r} = \frac{d}{dt} \left(\frac{\partial T}{\partial \dot{X}_k^\gamma} \right) - \frac{\partial T}{\partial X_k^\gamma}, \quad (2.23)$$

where F_k^γ is the external force exerted on \mathcal{S}^γ , and thereby the force exerted by \mathcal{S}^γ on the surrounding fluid. Subsequent computations of the mean drift force will involve the configuration gradient of the kinetic energy $\partial T / \partial X_k^\gamma$ and its relation to hydrodynamic quantities appearing in (2.20).

2.2. Linear oscillations in potential flow: integral formulas

The purpose of this subsection is to express the mean drift force for linear oscillations in potential flow in terms of surface integrals over the two spheres. This will establish the connection between potential flow and the subsequent general perturbative formulation for arbitrary frequencies (§3). Actual calculations will be carried out in §2.3 using Lagrange’s equations.

The sphere–sphere interaction force is given, at each instant, by

$$\begin{aligned} \Delta F &= - \int_{\mathcal{S}_1(t)} P n_3 d^2\mathbf{r} + \int_{\mathcal{S}_2(t)} P n_3 d^2\mathbf{r} \\ &= - \frac{d}{dt} \left(\frac{\partial T}{\partial \dot{z}_1} \right) + \frac{\partial T}{\partial z_1} + \frac{d}{dt} \left(\frac{\partial T}{\partial \dot{z}_2} \right) - \frac{\partial T}{\partial z_2}, \end{aligned} \quad (2.24)$$

$\Delta F > 0$ for attraction. Owing to time periodicity, the time-derivative terms vanish upon taking the temporal average over one period, so that one obtains for the mean interaction force

$$\langle \Delta F \rangle = \left\langle \frac{\partial T}{\partial z_1} \right\rangle - \left\langle \frac{\partial T}{\partial z_2} \right\rangle. \quad (2.25)$$

From (2.20) it then follows that

$$\begin{aligned} \langle \Delta F \rangle &= \left\langle \int_{\mathcal{S}_1} \left[\frac{1}{2} V^2 n_3 - \eta \cos t V_3 (\mathbf{n} \cdot \mathbf{b}) \right] d^2\mathbf{r} \right\rangle \\ &\quad - \left\langle \int_{\mathcal{S}_2} \left[\frac{1}{2} V^2 n_3 - \eta \cos(t + \varphi) V_3 (\mathbf{n} \cdot \mathbf{b}) \right] d^2\mathbf{r} \right\rangle. \end{aligned} \quad (2.26)$$

Relying on the decomposition (2.9) we now write the velocity field \mathbf{V} as the sum of two contributions,

$$\mathbf{V}(\mathbf{r}, t) = \eta \cos t \mathbf{V}^{[1]}(\mathbf{r}; t) + \eta \cos(t + \varphi) \mathbf{V}^{[2]}(\mathbf{r}; t), \quad (2.27)$$

where

$$\mathbf{n} \cdot \mathbf{V}^{[\alpha]} = \delta_{\alpha\beta} \mathbf{n} \cdot \mathbf{b} \text{ on } \mathcal{S}_\beta \quad (\alpha, \beta = 1, 2). \tag{2.28}$$

Here, the dependence of $\mathbf{V}^{[1]}$ and $\mathbf{V}^{[2]}$ on t is only parametric, tied to the domain of definition $\mathcal{V}(t)$. Equation (2.26) becomes

$$\begin{aligned} \langle \Delta F \rangle &= \eta^2 \left\langle \int_{\mathcal{S}_1} \left\{ \frac{1}{2} [\cos^2 t \|\mathbf{V}^{[1]}\|^2 + 2 \cos t \cos(t + \varphi) \mathbf{V}^{[1]} \cdot \mathbf{V}^{[2]} \right. \right. \\ &\quad \left. \left. + \cos^2(t + \varphi) \|\mathbf{V}^{[2]}\|^2 \right] n_3 - [\cos^2 t V_3^{[1]} + \cos t \cos(t + \varphi) V_3^{[2]}] (\mathbf{n} \cdot \mathbf{b}) \right\} d^2 \mathbf{r} \right\rangle \\ &- \eta^2 \left\langle \int_{\mathcal{S}_2} \left\{ \frac{1}{2} [\cos^2 t \|\mathbf{V}^{[1]}\|^2 + 2 \cos t \cos(t + \varphi) \mathbf{V}^{[1]} \cdot \mathbf{V}^{[2]} \right. \right. \\ &\quad \left. \left. + \cos^2 t \|\mathbf{V}^{[2]}\|^2 \right] n_3 - [\cos t \cos(t + \varphi) V_3^{[1]} + \cos^2(t + \varphi) V_3^{[2]}] (\mathbf{n} \cdot \mathbf{b}) \right\} d^2 \mathbf{r} \right\rangle. \end{aligned} \tag{2.29}$$

In the linear oscillation regime one neglects the motion of the surfaces of integration, regarding \mathcal{S}_1 and \mathcal{S}_2 as fixed. To this approximation the fields $\mathbf{V}^{[1]}$ and $\mathbf{V}^{[2]}$ are then independent of the parameter t , so that the time averages affect only the cosine terms. Noting that

$$\langle \cos^2 t \rangle = \frac{1}{2}, \quad \langle \cos t \cos(t + \varphi) \rangle = \frac{1}{2} \cos \varphi,$$

we define the coefficients,

$$\left. \begin{aligned} \hat{B}_1 &= \frac{1}{2} \int_{\mathcal{S}_1^{(0)}} \left\{ \frac{1}{2} [\|\mathbf{V}^{[1]}\|^2 + \|\mathbf{V}^{[2]}\|^2] n_3 - V_3^{[1]} (\mathbf{n} \cdot \mathbf{b}) \right\} d^2 \mathbf{r} \\ &\quad - \frac{1}{2} \int_{\mathcal{S}_2^{(0)}} \left\{ \frac{1}{2} [\|\mathbf{V}^{[1]}\|^2 + \|\mathbf{V}^{[2]}\|^2] n_3 - V_3^{[2]} (\mathbf{n} \cdot \mathbf{b}) \right\} d^2 \mathbf{r}, \\ \hat{B}_2 &= \frac{1}{2} \int_{\mathcal{S}_1^{(0)}} \left\{ \mathbf{V}^{[1]} \cdot \mathbf{V}^{[2]} n_3 - V_3^{[2]} (\mathbf{n} \cdot \mathbf{b}) \right\} d^2 \mathbf{r} \\ &\quad - \frac{1}{2} \int_{\mathcal{S}_2^{(0)}} \left\{ \mathbf{V}^{[1]} \cdot \mathbf{V}^{[2]} n_3 - V_3^{[1]} (\mathbf{n} \cdot \mathbf{b}) \right\} d^2 \mathbf{r}, \end{aligned} \right\} \tag{2.30}$$

which depend only upon the distance between the spheres (e.g. as given by the gap spacing, $L = 2h - 2$).

Then the mean interaction force can be expressed simply as

$$\langle \Delta F \rangle_{\text{linear}} = \eta^2 \left[\hat{B}_1 + \hat{B}_2 \cos \varphi \right], \tag{2.31}$$

based upon the characteristic inertial pressure scale $\rho a^2 \omega^2$. Starting with §3 we will non-dimensionalize with respect to the viscous pressure scale $\mu \ell \omega / a$. Thus, we must multiply the above result by Ω / η to put it on the latter basis. For comparison with future results we thus have

$$\langle \Delta F \rangle_{\text{linear}} = \Omega \eta \langle \Delta F \rangle_*, \quad \langle \Delta F \rangle_*(L, \varphi) = \hat{B}_1(L) + \hat{B}_2(L) \cos \varphi. \tag{2.32}$$

To avoid confusion with the subsequent pseudo-Brinkman velocity field $\mathbf{v}(\mathbf{r})$, we will henceforth denote potential velocity fields by \mathbf{w} instead of \mathbf{V} . Thereby, with reference to the boundary conditions (2.28) we have

$$\mathbf{V}^{[1]} \rightarrow \mathbf{w}^{[1]}, \quad \mathbf{V}^{[2]} \rightarrow \mathbf{w}^{[2]}. \tag{2.33}$$

The potential velocity field

$$\mathbf{w}(\mathbf{r}) \stackrel{\text{def}}{=} \mathbf{w}^{[1]}(\mathbf{r}) + \cos \varphi \mathbf{w}^{[2]}(\mathbf{r}) \tag{2.34}$$

satisfies the boundary conditions

$$\mathbf{n} \cdot \mathbf{w} = \mathbf{n} \cdot \mathbf{b} \text{ on } \mathcal{S}_1^{(0)}, \quad \mathbf{n} \cdot \mathbf{w} = \cos \varphi \mathbf{n} \cdot \mathbf{b} \text{ on } \mathcal{S}_2^{(0)}. \tag{2.35}$$

2.3. Linear oscillations via Lagrange’s equations

For problems of potential flow that involve two spheres or one sphere near an infinite plane wall, Lamb (1932, Arts. 137, 138) presents the Lagrangian formulation, and applies it to the leading-order interaction at large separations. As details are provided by Lamb, we present only a very brief summary, which applies for any direction of oscillation \mathbf{b} relative to the line of centres.

Noting that the virtual mass coefficients depend only on the separation $L = z_2 - z_1 - 2$, the total kinetic energy of the the fluid is

$$T = \eta^2 \left[\frac{1}{2} \mathcal{M}_a(L) \dot{q}_1^2 + \mathcal{M}_b(L) \dot{q}_1 \dot{q}_2 + \frac{1}{2} \mathcal{M}_a(L) \dot{q}_2^2 \right],$$

where for spheres of equal size we can write

$$\mathcal{M}_a \stackrel{\text{def}}{=} \mathcal{M}^{11} = \mathcal{M}^{22}, \quad \mathcal{M}_b \stackrel{\text{def}}{=} \mathcal{M}^{12} = \mathcal{M}^{21}. \tag{2.36}$$

Taking the derivatives with respect to z_1 and z_2 and subtracting according to (2.25) gives for the mean interaction force (positive for attraction),

$$\langle \Delta F \rangle = -\eta^2 \left\langle \frac{d\mathcal{M}_a}{dL} [\dot{q}_1^2 + \dot{q}_2^2] \right\rangle - 2\eta^2 \left\langle \frac{d\mathcal{M}_b}{dL} \dot{q}_1 \dot{q}_2 \right\rangle. \tag{2.37}$$

If the amplitudes of vibration are small then any accompanying temporal variations in the argument L can be neglected at leading order, leaving

$$\langle \Delta F \rangle = -\eta^2 \frac{d\mathcal{M}_a}{dL} \langle \cos^2 t + \cos^2(t + \varphi) \rangle - 2\eta^2 \frac{d\mathcal{M}_b}{dL} \langle \cos t \cos(t + \varphi) \rangle.$$

Therefore,

$$\langle \Delta F \rangle = -\eta^2 \left[\frac{d\mathcal{M}_a}{dL} + \frac{d\mathcal{M}_b}{dL} \cos \varphi \right], \tag{2.38}$$

which applies equally to axial and transverse oscillations.

There is no coupling between motions in the x -, y - and z -directions, owing to the specific azimuthal harmonics involved in each case, viz.

$$\mathcal{M}_{ij}^{\alpha\beta} = 0 \quad \text{for } i \neq j. \tag{2.39}$$

This fact, together with (2.15), means that the set of virtual mass coefficients (2.14) can be reduced to four independent quantities,

$$\left. \begin{aligned} \mathcal{M}_a^\parallel &\leftarrow \mathcal{M}_{33}^{11} = \mathcal{M}_{33}^{22}, \\ \mathcal{M}_b^\parallel &\leftarrow \mathcal{M}_{33}^{12} = \mathcal{M}_{33}^{21}, \\ \mathcal{M}_a^\perp &\leftarrow \mathcal{M}_{11}^{11} = \mathcal{M}_{11}^{22} = \mathcal{M}_{22}^{11} = \mathcal{M}_{22}^{22}, \\ \mathcal{M}_b^\perp &\leftarrow \mathcal{M}_{11}^{12} = \mathcal{M}_{11}^{21} = \mathcal{M}_{22}^{12} = \mathcal{M}_{22}^{21}. \end{aligned} \right\} \tag{2.40}$$

The coefficients in (2.32) are therefore given by

$$\left. \begin{aligned} \hat{B}_1^\parallel &= -d\mathcal{M}_a^\parallel/dL, & \hat{B}_2^\parallel &= -d\mathcal{M}_b^\parallel/dL, \\ \hat{B}_1^\perp &= -d\mathcal{M}_a^\perp/dL, & \hat{B}_2^\perp &= -d\mathcal{M}_b^\perp/dL. \end{aligned} \right\} \tag{2.41}$$

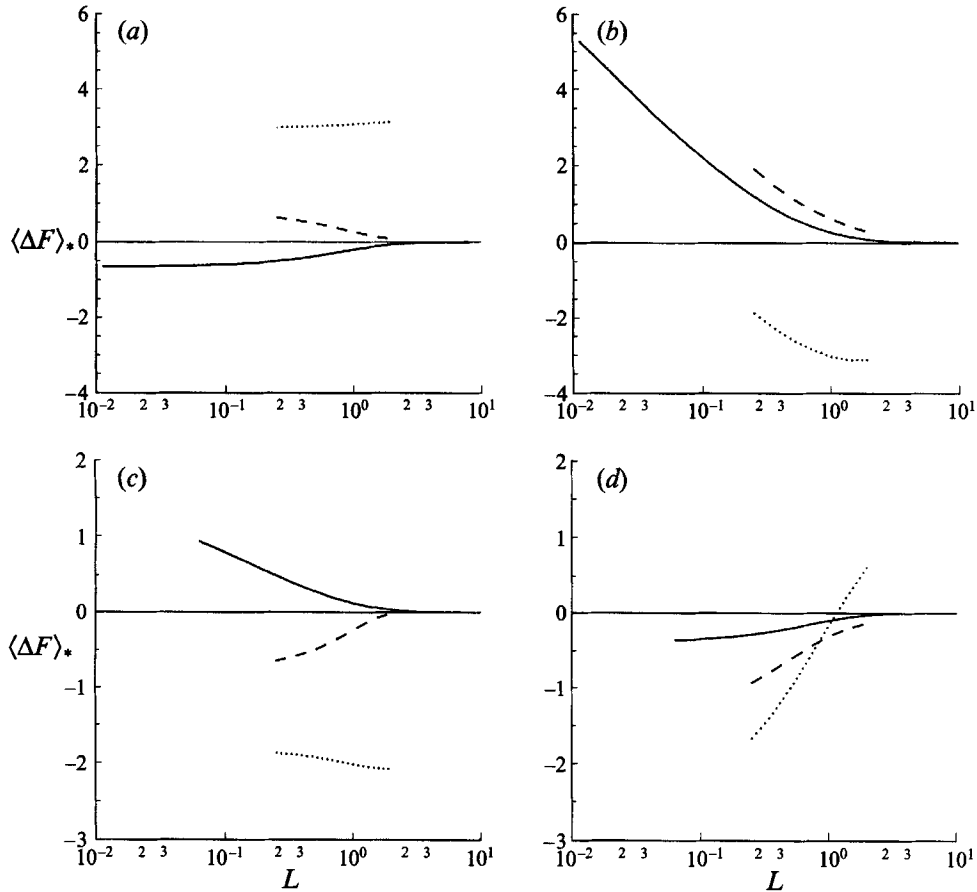


FIGURE 1. Linear oscillations in potential flow *vs.* viscous flow. The reduced mean interaction force $\langle \Delta F \rangle_*$ (positive for attraction) between two vibrating spheres is plotted as a function of separation L for in-phase ($\varphi = 0$) and opposite-phase ($\varphi = \pi$) oscillations, both parallel and perpendicular to the line of centres. Solid curves represent the limit of potential flow, whereas the cases $\Omega = 1/16$ and $\Omega = 4$ are distinguished using dotted *vs.* dashed curves, respectively. (a) Axial oscillations with $\varphi = 0$. (b) Axial oscillations with $\varphi = \pi$. (c) Transverse oscillations with $\varphi = 0$. (d) Transverse oscillations with $\varphi = \pi$.

For two spheres moving along their line of centres, the method of images (Lamb 1932, Art. 98) can readily be carried to high order by computer to evaluate the functions $\mathcal{M}_a^{\parallel}(L)$ and $\mathcal{M}_b^{\parallel}(L)$ with arbitrary accuracy. Details of this calculation appear in Appendix A. To compute the variable masses $\mathcal{M}_a^{\perp}(L)$ and $\mathcal{M}_b^{\perp}(L)$ we apply a numerical surface integration of (2.14) to the potentials Φ_1^{α} ($\alpha = 1, 2$), which are calculated numerically with a least-squares boundary singularity method as described in §4.6. In either case, numerical differentiation (by central differences) with respect to L then yields the mean force coefficients according to (2.41). These are tabulated as functions of separation L in table 1, along with the virtual masses.

Figure 1 shows how the reduced mean interaction forces $\langle \Delta F \rangle_*^{\parallel}(L, \varphi)$ and $\langle \Delta F \rangle_*^{\perp}(L, \varphi)$, cf. (2.32), vary with L for in-phase ($\varphi = 0$) and opposite-phase ($\varphi = \pi$) vibrations of the two spheres. Relative motion *along* the axis leads to higher velocity – therefore, lower pressure – in the gap, and hence to net attraction between the spheres; net

repulsion accompanies the centre-of-mass mode (Lamb 1932, Art. 138). The opposite behaviour is observed for motion *perpendicular* to the axis. For both axial and transverse oscillations, the attractive and repulsive forces become asymptotically the same, decaying like L^{-3} , as $L \rightarrow \infty$ (Lamb 1932, Arts. 98, 99, 137, 138). For comparison (to be discussed in §5), the graphs also show some corresponding results pertaining to the case of viscous oscillatory flow. Only at high frequencies ($\Omega \gtrsim 100$) does the viscous interaction force come quantitatively close to the asymptotic limit from potential flow; this will be seen in figure 3, below.

3. Nonlinear drift forces at arbitrary frequencies

Below we begin with the full nonlinear Navier–Stokes equations describing the flow field surrounding two oscillating spheres of equal radius. Once again, the general derivation applies for any direction of oscillation \mathbf{b} . The mathematical problem is then simplified by expressing the inertial nonlinearities arising at the moving boundaries and within the volume of the fluid as small perturbations of the time-dependent Stokes equations. Computation of the resulting nonlinear force is facilitated by application of a reciprocal theorem. In the limit of infinite frequency, the general formula reduces to the result from Lagrange’s equations in potential flow.

3.1. Model formulation for two vibrating spheres

We refer again to oscillations of the two spheres according to (2.1) and (2.2). In dealing with viscous flow it is advantageous to non-dimensionalize velocity with respect to $\ell\omega$ rather than $a\omega$, utilizing the corresponding characteristic viscous pressure scale $\mu(\ell\omega)/a$ (Landau & Lifshitz 1959, §24). Then the Navier–Stokes equations appear in the following dimensionless form, posed on the time-varying fluid domain $\mathcal{V}(t)$:

$$\Omega \frac{\partial \mathbf{V}}{\partial t} + \Omega \eta \mathbf{V} \cdot \nabla \mathbf{V} = -\nabla P + \nabla^2 \mathbf{V}, \tag{3.1}$$

with the boundary conditions

$$\mathbf{V}(\mathbf{r}, t) = \mathbf{b} \dot{q}_\alpha(t) \text{ on } \mathcal{S}_\alpha(t) = \{\mathbf{r} : \|\mathbf{r} - (-1)^\alpha \mathbf{h}e_z - \eta \mathbf{q}_\alpha(t)\mathbf{b}\| = 1\}. \tag{3.2}$$

Nonlinear effects, which are due to (i) inertia within the bulk fluid and (ii) motion of the boundaries on which the no-slip conditions are imposed, are thus seen to appear as corrections at $O(\eta)$. The relevant Reynolds number is now

$$Re = \frac{(\ell\omega)a}{\nu} = \frac{\omega a^2}{\nu} \frac{\ell}{a} = \Omega \eta. \tag{3.3}$$

At high frequencies we need $\eta \ll \Omega^{-1}$ in order to be able to linearize about negligible inertia in the fluid ($Re \ll 1$). This condition is satisfied in the case of Brownian motion, as will be verified in §6.4.

3.2. Perturbation about small inertia and amplitude

To linearize the equations we introduce a perturbation expansion in powers of η , defined on the *undeformed* fluid domain $\mathcal{V}^{(0)}$:

$$\mathbf{V}(\mathbf{r}, t) = \mathbf{V}^{(0)}(\mathbf{r}, t) + \eta \mathbf{V}^{(1)}(\mathbf{r}, t) + O(\eta^2). \tag{3.4}$$

Substituting this expansion into (3.1), and transferring the boundary conditions (3.2) to the *fixed* surfaces $\mathcal{S}_\alpha^{(0)}$, we obtain

$$-\Omega \frac{\partial \mathbf{V}^{(0)}}{\partial t} - \nabla P^{(0)} + \nabla^2 \mathbf{V}^{(0)} = \mathbf{0}, \quad (3.5)$$

$$\mathbf{V}^{(0)}(\mathbf{r}, t) = \mathbf{b} \dot{q}_\alpha(t) \quad \text{on} \quad \mathcal{S}_\alpha^{(0)}, \quad (3.6)$$

$$-\Omega \frac{\partial \mathbf{V}^{(1)}}{\partial t} - \nabla P^{(1)} + \nabla^2 \mathbf{V}^{(1)} = \Omega \mathbf{V}^{(0)} \cdot \nabla \mathbf{V}^{(0)}, \quad (3.7)$$

$$\mathbf{V}^{(1)}(\mathbf{r}, t) = -q_\alpha(t) \mathbf{b} \cdot \nabla \mathbf{V}^{(0)}(\mathbf{r}, t) \quad \text{on} \quad \mathcal{S}_\alpha^{(0)}. \quad (3.8)$$

3.3. Mean nonlinear force of interaction

We shall briefly skip ahead in more detail to the first-order problem to determine what is needed from the zeroth-order solution. In order to obtain the leading-order mean drift force it is sufficient to solve for time-averaged quantities. Applying the time average to (3.7) and (3.8) gives the following Stokes flow problem, wherein the zeroth-order inertial term appears as a prescribed volumetric force:†

$$-\nabla \langle P^{(1)} \rangle + \nabla^2 \langle \mathbf{V}^{(1)} \rangle = \Omega \langle \mathbf{V}^{(0)} \cdot \nabla \mathbf{V}^{(0)} \rangle, \quad \mathbf{r} \in \mathcal{V}^{(0)}, \quad (3.9)$$

$$\langle \mathbf{V}^{(1)} \rangle = -\langle q_\alpha(t) \mathbf{b} \cdot \nabla \mathbf{V}^{(0)}(\mathbf{r}, t) \rangle \quad \text{on} \quad \mathcal{S}_\alpha^{(0)}. \quad (3.10)$$

To make use of the reciprocal theorem, let $\mathbf{u}'(\mathbf{r})$ and $\mathbf{T}'(\mathbf{r}) = -Ip' + [\nabla \mathbf{u}' + (\nabla \mathbf{u}')^\dagger]$ represent the velocity and stress fields resulting from the 'test' Stokes flow problem

$$-\nabla p' + \nabla^2 \mathbf{u}' = 0, \quad \mathbf{r} \in \mathcal{V}^{(0)}, \quad (3.11)$$

$$\mathbf{u}' = \mathbf{e}_z \quad \text{on} \quad \mathcal{S}_1^{(0)}, \quad \mathbf{u}' = -\mathbf{e}_z \quad \text{on} \quad \mathcal{S}_2^{(0)}. \quad (3.12)$$

By substituting (3.9) – (3.12) into the reciprocal theorem,

$$\begin{aligned} \int_{\mathcal{S}_1^{(0)}} \mathbf{u}' \cdot \mathbf{T} \cdot \mathbf{n} d^2 \mathbf{r} + \int_{\mathcal{S}_2^{(0)}} \mathbf{u}' \cdot \mathbf{T} \cdot \mathbf{n} d^2 \mathbf{r} &= \int_{\mathcal{S}_1^{(0)}} \mathbf{u} \cdot \mathbf{T}' \cdot \mathbf{n} d^2 \mathbf{r} \\ &+ \int_{\mathcal{S}_2^{(0)}} \mathbf{u} \cdot \mathbf{T}' \cdot \mathbf{n} d^2 \mathbf{r} - \int_{\mathcal{V}^{(0)}} \mathbf{u}' \cdot (\nabla \cdot \mathbf{T}) d^3 \mathbf{r} + \int_{\mathcal{V}^{(0)}} \mathbf{u} \cdot (\nabla \cdot \mathbf{T}') d^3 \mathbf{r}, \end{aligned} \quad (3.13)$$

one then obtains for the mean interaction force $\langle \Delta F \rangle = \langle F_1 - F_2 \rangle$ (positive for net attraction)

$$\begin{aligned} \langle \Delta F \rangle &= -\eta \left[\int_{\mathcal{S}_1^{(0)}} \langle q_1 \mathbf{b} \cdot \nabla \mathbf{V}^{(0)} \rangle \cdot \mathbf{T}' \cdot \mathbf{n} d^2 \mathbf{r} \right. \\ &\left. + \int_{\mathcal{S}_2^{(0)}} \langle q_2 \mathbf{b} \cdot \nabla \mathbf{V}^{(0)} \rangle \cdot \mathbf{T}' \cdot \mathbf{n} d^2 \mathbf{r} \right] - \Omega \eta \left[\int_{\mathcal{V}^{(0)}} \mathbf{u}' \cdot \langle \mathbf{V}^{(0)} \cdot \nabla \mathbf{V}^{(0)} \rangle d^3 \mathbf{r} \right]. \end{aligned} \quad (3.14)$$

By this formula, the effect of fluid inertia appears to be decomposed into finite-amplitude and volumetric contributions, to be described below by separate coefficients. However, it should be borne in mind that the formal distinction is only tied to the Eulerian form of the hydrodynamic equations, and would not arise in the equivalent Lagrangian formulation: for, the latter contains motion of the boundaries within the mapping of material points.

† That inertia of the fluid is negligible – even at high frequencies – in the time-average, first-order problem follows from smallness of the effective Reynolds number for steady streaming, $Re^* = \Omega \eta^2 = \eta Re$ (Batchelor 1967, §5.13; Tabakova & Zapryanov 1982 *a, b*); cf. (3.3).

By using the divergence theorem the inertia volume integral can be rewritten in either of the following two equivalent forms:

$$\begin{aligned}
 & - \int_{\mathcal{V}^{(0)}} \mathbf{u}' \cdot \langle \mathbf{V}^{(0)} \cdot \nabla \mathbf{V}^{(0)} \rangle d^3\mathbf{r} \\
 & = \Omega\eta \int_{\mathcal{V}^{(0)}} \mathbf{u}' \cdot \langle \mathbf{V}^{(0)} \times (\nabla \times \mathbf{V}^{(0)}) \rangle d^3\mathbf{r}
 \end{aligned} \tag{3.15}$$

$$= \Omega\eta \int_{\mathcal{V}^{(0)}} \nabla \mathbf{u}' : \langle \mathbf{V}^{(0)} \mathbf{V}^{(0)} \rangle d^3\mathbf{r}, \tag{3.16}$$

where $\nabla \mathbf{u}'$ can be replaced by the symmetric rate-of-strain tensor

$$\mathbf{D}' = \frac{1}{2} [\nabla \mathbf{u}' + (\nabla \mathbf{u}')^\dagger].$$

At high frequencies the first alternative representation (3.15) consolidates the volumetric contribution of inertia within the Stokes layers surrounding the particles. The latter volume integral (3.16) involves only $\mathbf{V}^{(0)}$, not its derivatives, so that the contribution from the Stokes layers decays asymptotically like their thickness ($\Omega^{\frac{1}{2}}$) as $\Omega \rightarrow \infty$. In effect, the high-frequency behaviour is banished to the far field: inserting the irrotational outer solution into (3.16) should reproduce the results from potential flow. This will be verified below in §3.5.

3.4. The drift force coefficients

In order to solve the zeroth-order problem (§3.2) it is convenient to write the solution in complex form, ultimately taking real parts at the end to form the time-average quantities entering the drift force expression (3.14), (3.16). We shall also decouple the disturbances due to the individual particle motions. For this purpose we define

$$Q_1(t) = i^{-1} e^{it} \quad \text{and} \quad Q_2(t) = i^{-1} e^{i(t+\phi)}, \tag{3.17}$$

so that

$$q_\alpha = \text{Re}[Q_\alpha] \quad (\alpha = 1, 2). \tag{3.18}$$

Furthermore, we introduce the two complex velocity fields $\mathbf{v}^{[1]}(\mathbf{r})$ and $\mathbf{v}^{[2]}(\mathbf{r})$, each of which satisfies the Brinkman-like equation

$$-i\Omega \mathbf{v} - \nabla p + \nabla^2 \mathbf{v} = \mathbf{0}, \tag{3.19}$$

but with different boundary conditions:

$$\mathbf{v}^{[\alpha]} = \delta^{\alpha\beta} \mathbf{b} \quad \text{on} \quad \mathcal{S}_\beta^{(0)} \quad (\alpha, \beta = 1, 2). \tag{3.20}$$

Then

$$\mathbf{V}^{(0)}(\mathbf{r}, t) = \text{Re}[\dot{Q}_1(t)\mathbf{v}^{[1]}(\mathbf{r}) + \dot{Q}_2(t)\mathbf{v}^{[2]}(\mathbf{r})]. \tag{3.21}$$

The mean drift force of interaction between the two spheres is then obtained by substituting (3.18) and (3.21) into (3.14), (3.16). To simplify the expressions, we note that

$$\left. \begin{aligned}
 \langle Q_{1R} \dot{Q}_{1R} \rangle &= \langle Q_{2R} \dot{Q}_{2R} \rangle = \langle Q_{1I} \dot{Q}_{1I} \rangle = \langle Q_{2I} \dot{Q}_{2I} \rangle = 0, \\
 \langle Q_{1R} \dot{Q}_{1I} \rangle &= \langle Q_{2R} \dot{Q}_{2I} \rangle = -\langle Q_{1I} \dot{Q}_{1R} \rangle = -\langle Q_{2I} \dot{Q}_{2R} \rangle = \frac{1}{2}, \\
 \langle Q_{2R} \dot{Q}_{1R} \rangle &= \langle Q_{2I} \dot{Q}_{1I} \rangle = -\langle Q_{1R} \dot{Q}_{2R} \rangle = -\langle Q_{1I} \dot{Q}_{2I} \rangle = \frac{1}{2} \sin \varphi, \\
 \langle Q_{1R} \dot{Q}_{2I} \rangle &= \langle Q_{2R} \dot{Q}_{1I} \rangle = -\langle Q_{1I} \dot{Q}_{2R} \rangle = -\langle Q_{2I} \dot{Q}_{1R} \rangle = \frac{1}{2} \cos \varphi.
 \end{aligned} \right\} \tag{3.22}$$

with analogous equations for $\langle \dot{Q}_{1R} \dot{Q}_{1R} \rangle$, etc. Furthermore, whether the spheres oscillate

parallel or perpendicular to the line of centres, the integrand in (3.16) has mirror symmetry about the plane $z = 0$. This follows from fore-aft symmetry of the axisymmetric Stokes test problem (3.11), (3.12), whereby

$$D'_{zz}(-z, \rho) = D'_{zz}(z, \rho), \quad D'_{\rho\rho}(-z, \rho) = D'_{\rho\rho}(z, \rho),$$

$$D'_{z\rho}(-z, \rho) = -D'_{z\rho}(z, \rho), \quad D'_{\phi\phi}(-z, \rho) = D'_{\phi\phi}(z, \rho),$$

together with (3.49), (3.50) and (3.52) appearing in §3.9 below.

Thus, the mean interaction force $\langle \Delta F \rangle$ – for oscillation either parallel or perpendicular to the line of centres – can be written in the concise general form

$$\langle \Delta F \rangle = \Omega \eta \langle \Delta F \rangle. = \Omega \eta [\mathcal{C}_1(\Omega; L) + \mathcal{C}_2(\Omega; L) \cos \varphi], \tag{3.23}$$

with the (real) coefficients C_i decomposed into the finite-amplitude and volumetric contributions, viz.

$$C_i = A_i + B_i, \tag{3.24}$$

$$\left. \begin{aligned} A_1 &= \frac{1}{\Omega} \int_{\mathcal{S}_2^{(0)}} (\mathbf{b} \cdot \nabla \mathbf{v}_I^{[2]}) \cdot \mathbf{T}' \cdot \mathbf{n} \, d^2 \mathbf{r} = \frac{1}{\Omega} \int_{\mathcal{S}_1^{(0)}} (\mathbf{b} \cdot \nabla \mathbf{v}_I^{[1]}) \cdot \mathbf{T}' \cdot \mathbf{n} \, d^2 \mathbf{r}, \\ A_2 &= \frac{1}{\Omega} \int_{\mathcal{S}_2^{(0)}} (\mathbf{b} \cdot \nabla \mathbf{v}_I^{[1]}) \cdot \mathbf{T}' \cdot \mathbf{n} \, d^2 \mathbf{r} = \frac{1}{\Omega} \int_{\mathcal{S}_1^{(0)}} (\mathbf{b} \cdot \nabla \mathbf{v}_I^{[2]}) \cdot \mathbf{T}' \cdot \mathbf{n} \, d^2 \mathbf{r}, \\ B_1 &= \int_{\hat{\mathcal{V}}^{(0)}} \mathbf{D}' : (\mathbf{v}_R^{[1]} \mathbf{v}_R^{[1]} + \mathbf{v}_R^{[2]} \mathbf{v}_R^{[2]} + \mathbf{v}_I^{[1]} \mathbf{v}_I^{[1]} + \mathbf{v}_I^{[2]} \mathbf{v}_I^{[2]}) \, d^3 \mathbf{r}, \\ B_2 &= 2 \int_{\hat{\mathcal{V}}^{(0)}} \mathbf{D}' : (\mathbf{v}_R^{[1]} \mathbf{v}_R^{[2]} + \mathbf{v}_I^{[1]} \mathbf{v}_I^{[2]}) \, d^3 \mathbf{r}. \end{aligned} \right\} \tag{3.25}$$

Here $\hat{\mathcal{V}}^{(0)}$ denotes the semi-infinite fluid domain on one side, either right or left, of the plane $z = 0$.

3.5. The limit of potential flow

We are now in a position to establish the connection between the inertial drift force at high frequency and linear oscillations in potential flow (§2.2). As observed for (3.16), the formulas (3.25) giving B_1 and B_2 relegate the *effect* of vorticity to the far field, even though vorticity is actually generated at the boundaries. Thus, we can take the limit

$$\mathbf{v}_R^{[\alpha]} \rightarrow \mathbf{w}^{[\alpha]}, \quad \mathbf{v}_I^{[\alpha]} \rightarrow \mathbf{0} \quad \text{as} \quad \Omega \rightarrow \infty$$

throughout the whole fluid – in particular, right up to the sphere surfaces, without considering Stokes layers. In this limit the equation for B_2 becomes

$$\begin{aligned} B_2 &= 2 \int_{\hat{\mathcal{V}}^{(0)}} \mathbf{D}' : \mathbf{w}^{[1]} \mathbf{w}^{[2]} \, d^3 \mathbf{r} \\ &= \int_{\mathcal{V}^{(0)}} \mathbf{D}' : \mathbf{w}^{[1]} \mathbf{w}^{[2]} \, d^3 \mathbf{r} \\ &= \frac{1}{2} \int_{\mathcal{V}^{(0)}} \nabla \mathbf{u}' : (\mathbf{w}^{[1]} \mathbf{w}^{[2]} + \mathbf{w}^{[2]} \mathbf{w}^{[1]}) \, d^3 \mathbf{r}. \end{aligned} \tag{3.26}$$

To reduce this expression we first note that, owing to the irrotational nature of $\mathbf{w}^{[1]}$ and $\mathbf{w}^{[2]}$,

$$\mathbf{u}' \cdot [\mathbf{w}^{[1]} \cdot \nabla \mathbf{w}^{[2]} + \mathbf{w}^{[2]} \cdot \nabla \mathbf{w}^{[1]}] = \nabla \cdot [\mathbf{u}' (\mathbf{w}^{[1]} \cdot \mathbf{w}^{[2]})].$$

Combining this with the general identity

$$\mathbf{u}' \cdot [\mathbf{w}^{[1]} \cdot \nabla \mathbf{w}^{[2]} + \mathbf{w}^{[2]} \cdot \nabla \mathbf{w}^{[1]}] = \nabla \cdot [\mathbf{w}^{[1]}(\mathbf{w}^{[2]} \cdot \mathbf{u}') + \mathbf{w}^{[2]}(\mathbf{w}^{[1]} \cdot \mathbf{u}')] - \nabla \mathbf{u}' : (\mathbf{w}^{[1]} \mathbf{w}^{[2]} + \mathbf{w}^{[2]} \mathbf{w}^{[1]})$$

there follows

$$\begin{aligned} \nabla \mathbf{u}' : (\mathbf{w}^{[1]} \mathbf{w}^{[2]} + \mathbf{w}^{[2]} \mathbf{w}^{[1]}) &= \nabla \cdot [\mathbf{w}^{[1]}(\mathbf{w}^{[2]} \cdot \mathbf{u}') + \mathbf{w}^{[2]}(\mathbf{w}^{[1]} \cdot \mathbf{u}')] - \nabla \cdot [\mathbf{u}'(\mathbf{w}^{[1]} \cdot \mathbf{w}^{[2]})]. \end{aligned} \tag{3.27}$$

Now we can apply the divergence theorem to the volume integral (3.26), to obtain

$$\begin{aligned} B_2 &= -\frac{1}{2} \int_{\mathcal{V}_1^{(0)}} \{(\mathbf{n} \cdot \mathbf{w}^{[1]})(\mathbf{u}' \cdot \mathbf{w}^{[2]}) + (\mathbf{n} \cdot \mathbf{w}^{[2]})(\mathbf{u}' \cdot \mathbf{w}^{[1]})\} d^2\mathbf{r} \\ &\quad + \frac{1}{2} \int_{\mathcal{V}_1^{(0)}} (\mathbf{n} \cdot \mathbf{u}') (\mathbf{w}^{[1]} \cdot \mathbf{w}^{[2]}) d^2\mathbf{r} \\ &\quad - \frac{1}{2} \int_{\mathcal{V}_2^{(0)}} \{(\mathbf{n} \cdot \mathbf{w}^{[1]})(\mathbf{u}' \cdot \mathbf{w}^{[2]}) + (\mathbf{n} \cdot \mathbf{w}^{[2]})(\mathbf{u}' \cdot \mathbf{w}^{[1]})\} d^2\mathbf{r} \\ &\quad + \frac{1}{2} \int_{\mathcal{V}_2^{(0)}} (\mathbf{n} \cdot \mathbf{u}') (\mathbf{w}^{[1]} \cdot \mathbf{w}^{[2]}) d^2\mathbf{r}. \end{aligned}$$

Substitution of the boundary conditions (2.28) and (3.12) then gives

$$B_2 = \frac{1}{2} \int_{\mathcal{V}_1^{(0)}} [\mathbf{w}^{[1]} \cdot \mathbf{w}^{[2]} n_3 - w_3^{[2]}(\mathbf{n} \cdot \mathbf{b})] d^2\mathbf{r} - \frac{1}{2} \int_{\mathcal{V}_2^{(0)}} [\mathbf{w}^{[1]} \cdot \mathbf{w}^{[2]} n_3 - w_3^{[1]}(\mathbf{n} \cdot \mathbf{b})] d^2\mathbf{r}. \tag{3.28}$$

Comparing with (2.30) we see that $B_2 \rightarrow \hat{B}_2$ as $\Omega \rightarrow \infty$. In a similar fashion one can show that $B_1 \rightarrow \hat{B}_1$ as well, thereby establishing that the general perturbative formulation is consistent with potential flow in the high-frequency limit.

Owing to the $\Omega^{-\frac{1}{2}}$ scaling of the boundary-layer thickness (§3.7), the finite-amplitude coefficients A_1 and A_2 decay like $\Omega^{-\frac{1}{2}}$ as $\Omega \rightarrow \infty$. This is consistent with the fact that the mean interaction force in potential flow is, at leading order, unaffected by the motion of the boundaries.†

3.6. High frequencies and thin Stokes layers

The integral formula (3.16) enabled us to pass from viscous flow at high frequencies to potential flow without having to deal with vorticity boundary layers. Nevertheless, it is worthwhile to re-examine the high-frequency limit from the boundary-layer perspective. Returning to the volume integral in (3.14), we divide the domain $\mathcal{V}^{(0)}$ into a subset \mathcal{V}^{BL} , composed of thin boundary layers at the sphere surfaces, and the remaining volume \mathcal{V}^∞ , throughout which the velocity field $\mathbf{v}(\mathbf{r}) = \mathbf{v}^{[1]}(\mathbf{r}) + e^{i\varphi} \mathbf{v}^{[2]}(\mathbf{r})$ is effectively irrotational. To leading order the outer field is exactly in phase with the

† For potential flow there is also a finite-amplitude effect, but it is of an entirely different nature, being a second-order correction – at overall order $O(\eta^4)$ – to the leading-order drift force, which is proportional to η^2 ; cf. (2.31). This is readily verified in the formulation using Lagrange’s equations (§2.3) by Taylor expanding the effective mass terms in (2.37) about the mean separation L to take into account the $O(\eta)$ sinusoidal variations in position. The $O(\eta^3)$ terms vanish upon taking the time average, leaving the correction to fourth order.

motion of the boundaries (cf. §3.7). Thereby,

$$\mathbf{v}_R(\mathbf{r}) = \mathbf{w}(\mathbf{r}), \quad \mathbf{v}_I(\mathbf{r}) = \sin \varphi \mathbf{w}^{[2]}(\mathbf{r}), \quad \mathbf{r} \in \mathcal{V}^\infty,$$

with \mathbf{w} given by (2.34).

Noting that $\mathbf{u}' \cdot (\mathbf{w} \cdot \nabla \mathbf{w}) = \frac{1}{2} \nabla \cdot (\mathbf{u}' w^2)$ and using the divergence theorem together with the boundary conditions (3.12), the outer volume integral in (3.14) becomes

$$\begin{aligned} & -\frac{1}{2} \int_{\mathcal{V}^\infty} \mathbf{u}' \cdot [\mathbf{v}_R \cdot \nabla \mathbf{v}_R + \mathbf{v}_I \cdot \nabla \mathbf{v}_I] d^3 \mathbf{r} \\ &= \frac{1}{4} \int_{\mathcal{S}_1^{\text{BL}}} [|\mathbf{w}|^2 + \sin^2 \varphi |\mathbf{w}^{[2]}|^2] n_3 d^2 \mathbf{r} \\ & - \frac{1}{4} \int_{\mathcal{S}_2^{\text{BL}}} [|\mathbf{w}|^2 + \sin^2 \varphi |\mathbf{w}^{[2]}|^2] n_3 d^2 \mathbf{r} \end{aligned} \tag{3.29}$$

Here, $\mathcal{S}_1^{\text{BL}}$ and $\mathcal{S}_2^{\text{BL}}$ are the ‘edges’ of the boundary layers, i.e. the surfaces separating \mathcal{V}^{BL} from \mathcal{V}^∞ . To the present order of approximation, one may take the surface integrals over $\mathcal{S}_1^{(0)}$ and $\mathcal{S}_2^{(0)}$ instead.

To evaluate the boundary-layer contribution to (3.14), one observes that the velocity relative to each sphere is effectively tangential throughout \mathcal{V}^{BL} . Defining the constants U' and V such that $\mathbf{u}' = U' \mathbf{e}_z$ and $\mathbf{v} = V \mathbf{b}$ over the particular sphere in question, one can write

$$\mathbf{v} = V \mathbf{b} + v_\theta^* \mathbf{e}_\theta \quad \text{within } \mathcal{V}_\alpha^{\text{BL}}.$$

To leading order the velocity gradient is then

$$\nabla \mathbf{v} = \frac{\partial v_\theta^*}{\partial r} \hat{\mathbf{r}} \mathbf{e}_\theta,$$

and throughout the boundary layer the integrand can be approximated as follows:

$$\mathbf{u}' \cdot [\mathbf{v}_R \cdot \nabla \mathbf{v}_R + \mathbf{v}_I \cdot \nabla \mathbf{v}_I] = U' \left[V_R \frac{\partial v_{\theta R}^*}{\partial r} + V_I \frac{\partial v_{\theta I}^*}{\partial r} \right] (\mathbf{b} \cdot \hat{\mathbf{r}}) (\mathbf{e}_z \cdot \mathbf{e}_\theta).$$

Integrating this quantity across the boundary layer we obtain at each position θ

$$-U' \{ V_R [(v_{\theta R}^*)^\infty - (v_{\theta R}^*)^0] + V_I [(v_{\theta I}^*)^\infty - (v_{\theta I}^*)^0] \} (\mathbf{b} \cdot \hat{\mathbf{r}}) \sin \theta,$$

where 0 refers to the sphere surface, and ∞ denotes the outer limit of the inner solution. Now, v_θ^0 vanishes owing to the stick boundary conditions, while matching to the inner limit of the outer solution means that

$$-(v_{\theta R}^*)^\infty \sin \theta = w_3 - V_R b_3, \quad -(v_{\theta I}^*)^\infty \sin \theta = \sin \varphi w_3^{[2]} - V_I b_3.$$

Thus, the volume integral over \mathcal{V}^{BL} becomes

$$\begin{aligned} & -\frac{1}{2} \int_{\mathcal{V}^{\text{BL}}} \mathbf{u}' \cdot [\mathbf{v}_R \cdot \nabla \mathbf{v}_R + \mathbf{v}_I \cdot \nabla \mathbf{v}_I] d^3 \mathbf{r} \\ &= -\frac{1}{2} \int_{\mathcal{S}_1^{(0)}} w_3 (\mathbf{n} \cdot \mathbf{b}) d^2 \mathbf{r} + \frac{1}{2} \int_{\mathcal{S}_2^{(0)}} [\cos \varphi w_3 + \sin^2 \varphi w_3^{[2]}] (\mathbf{n} \cdot \mathbf{b}) d^2 \mathbf{r}, \end{aligned} \tag{3.30}$$

with $\mathcal{S}_1^{\text{BL}}$ and $\mathcal{S}_2^{\text{BL}}$ indistinguishable from $\mathcal{S}_1^{(0)}$ and $\mathcal{S}_2^{(0)}$.

Combining the inner and outer contributions to the volume integral in (3.14), there

follows to leading order for high frequencies

$$\begin{aligned} \langle \Delta F \rangle \cdot &= \frac{1}{2} \int_{\mathcal{G}_1^{(0)}} \left\{ \frac{1}{2} [|\mathbf{w}|^2 + \sin^2 \varphi |\mathbf{w}^{[2]}|^2] n_3 - w_3 (\mathbf{n} \cdot \mathbf{b}) \right\} d^2 \mathbf{r} \\ &\quad - \frac{1}{2} \int_{\mathcal{G}_2^{(0)}} \left\{ \frac{1}{2} [|\mathbf{w}|^2 + \sin^2 \varphi |\mathbf{w}^{[2]}|^2] n_3 \right. \\ &\quad \left. - [\cos \varphi w_3 + \sin^2 \varphi w_3^{[2]}] (\mathbf{n} \cdot \mathbf{b}) \right\} d^2 \mathbf{r}. \end{aligned} \tag{3.31}$$

Exploiting the decomposition (2.34), this result can be shown to be equivalent to the representation (2.30), (2.32) derived previously for potential flow. Moreover, via (2.20) and (2.25) one sees a direct connection between the preceding considerations of vanishingly thin Stokes layers and Lagrange's equations.

3.7. Remarks on the $O(\Omega^{-\frac{1}{2}})$ correction; the first reflection

We turn our attention now from potential flow (the limit of infinite frequency) to high-frequency asymptotics for the unsteady Stokes velocity field $\mathbf{v}^{[1]}(\mathbf{r})$. With reference to the friction coefficients $\zeta_{\alpha\beta}^{\parallel}$ and $\zeta_{\alpha\beta}^{\perp}$ that are defined below in §4.5, we note that at leading order the asymptotic behaviour as $\Omega \rightarrow \infty$ is given by the corresponding virtual masses; the first correction appears at order $\Omega^{-\frac{1}{2}}$, viz.

$$\zeta_{\alpha\beta}^{\parallel} / \Omega \sim i \mathcal{M}_{\alpha\beta}^{\parallel} + O(\Omega^{-\frac{1}{2}}), \quad \zeta_{\alpha\beta}^{\perp} / \Omega \sim i \mathcal{M}_{\alpha\beta}^{\perp} + O(\Omega^{-\frac{1}{2}}). \tag{3.32}$$

The nonlinear drift force $\langle \Delta F \rangle$, also becomes linear in $\Omega^{-\frac{1}{2}}$ as $\Omega \rightarrow \infty$ at fixed separation L .

The $O(\Omega^{-\frac{1}{2}})$ corrections stem from two effects: (i) finite thickness of the Stokes layers; and (ii) rearrangement of the outer irrotational solution relative to the motion of the boundaries. This can readily be seen from the simpler problem of an isolated vibrating sphere, for which the solution can be written in the form

$$\mathbf{v}_i(\mathbf{r}) = b_j P_{ij}(\mathbf{r}), \tag{3.33}$$

with

$$P_{ij}(\mathbf{r}) = \frac{G(\gamma)}{2r^3} [3\hat{r}_i \hat{r}_j - \delta_{ij}] - \frac{3}{2r} e^{\gamma-r} [G(\gamma r) \hat{r}_i \hat{r}_j - H(\gamma r) \delta_{ij}]. \tag{3.34}$$

Here

$$\gamma = (1 + i)(\Omega/2)^{\frac{1}{2}}, \quad \hat{\mathbf{r}} = r^{-1} \mathbf{r}, \tag{3.35}$$

and

$$\left. \begin{aligned} G(x) &= 1 + 3x^{-1} + 3x^{-2}, \\ H(x) &= 1 + x^{-1} + x^{-2}. \end{aligned} \right\} \tag{3.36}$$

The first term appears like the dipole solution in potential flow – except for the factor $G(\gamma)$ which mixes real and imaginary parts (in-phase and out-of-phase components), and therefore appears like a shift in phase relative to the motion of the sphere. The second term represents the Stokes layer, whose contribution to the velocity field decays exponentially with distance from the surface.

A more precise interpretation of the first term is as follows: owing to mass conservation, the oscillatory boundary layer drives a flux *normal* to the surface given by the surface divergence of the tangential flux, integrated across the boundary layer. Explicitly,

$$\text{Efflux} = -\gamma^{-1} \nabla_s \cdot \left[U_{\tan}^{\text{solid}} - U_{\tan}^{\circ} \right]$$

at leading order, where the superscript \circ denotes the zeroth-order irrotational velocity field evaluated at the surface (Batchelor 1967, §5.13). The solution for an isolated sphere in potential flow, a source dipole, is such that the boundary-layer efflux has the form

$$\text{Efflux} = 3\gamma^{-1}(\mathbf{b} \cdot \mathbf{n}),$$

which happens to coincide with the normal velocity component at the surface due to motion of the sphere as a whole (with velocity $3\gamma^{-1}\mathbf{b}$). Thus, the boundary-layer efflux can be *interpreted* as a phase shift of the outer irrotational field at order γ^{-1} . In the presence of hydrodynamic interactions between the spheres, the symmetry necessary for this simple interpretation does not generally exist† – hence the need for some kind of matching procedure to determine the boundary conditions for the outer irrotational field. (See Sangani, Zhang & Prosperetti 1991, for many-particle problems associated with the acoustic behaviour of bubbly liquids.)

Because our problem involves only two spheres, we can proceed more simply by the method of reflections. This is developed by Kim & Russel (1985) for calculating drag coefficients in the analogous case of Brinkman flow – with arbitrary screening length. As will be discussed below, their general procedure must be modified in order to obtain an explicit, uniformly valid expression for the velocity field.

As long as the Stokes layers are well separated ($\Omega \gg L^{-2}$), each particle experiences only the disturbance due to the outer irrotational field of the other (cf. Sangani 1991). Therefore, the hydrodynamic interaction is as weak as that characteristic of potential flow, even if the Stokes layers are not thin compared with the radius of the spheres. The first reflected field, originating from sphere 2 to cancel out the disturbance felt at its surface due to the incident field $\mathbf{b} \cdot \mathbf{P}(\mathbf{r} + h\mathbf{e}_z)$ centred about sphere 1, gives the velocity field uniformly within an error of $O(\epsilon^6)$, where $\epsilon = (L + 2)^{-1}$. To this order of approximation, it is sufficient to cancel only the constant, linear and quadratic components of the incident field. Any higher corrections in the Taylor series would be mixed with the second reflection from sphere 1, and are neglected here. (This simple approximation will be seen to give very accurate results in §§5 and 6, below.) Explicitly, one can write

$$\begin{aligned} v_i^{[1]}(\mathbf{r}) = & b_j P_{ij}(\mathbf{r} + h\mathbf{e}_z) - (\epsilon^3/2)G(\gamma)X_j P_{ij}(\mathbf{r} - h\mathbf{e}_z) \\ & + (\epsilon^4/2)G(\gamma)(1 + \gamma^{-1})^{-1}Y_{jk}Q_{ijk}(\mathbf{r} - h\mathbf{e}_z) \\ & + (3\epsilon^5/16)Z_{jkl}R_{ijkl}(\mathbf{r} - h\mathbf{e}_z) + O(\epsilon^6), \end{aligned} \quad (3.37)$$

with

$$\left. \begin{aligned} Q_{ijk}(\mathbf{r}) = & I(\gamma)r^{-4}[\delta_{ij}\hat{r}_k + \delta_{ik}\hat{r}_j - 5\hat{r}_i\hat{r}_j\hat{r}_k] \\ & - 5r^{-1}e^{\gamma-r} [J(\gamma r)\delta_{ij}\hat{r}_k + (\gamma r)^{-1}G(\gamma r)\delta_{ik}\hat{r}_j - I(\gamma r)\hat{r}_i\hat{r}_j\hat{r}_k], \\ R_{ijkl}(\mathbf{r}) = & L(\gamma)r^{-5}[(\delta_{ij}\hat{r}_k\hat{r}_l + \delta_{ik}\hat{r}_j\hat{r}_l + \delta_{il}\hat{r}_j\hat{r}_k) - 7\hat{r}_i\hat{r}_j\hat{r}_k\hat{r}_l] \\ & - 7r^{-1}e^{\gamma-r} [(\gamma r)^{-1}I(\gamma r)(\delta_{ik}\hat{r}_j\hat{r}_l + \delta_{il}\hat{r}_j\hat{r}_k) + K(\gamma r)\delta_{ij}\hat{r}_k\hat{r}_l \\ & - L(\gamma r)\hat{r}_i\hat{r}_j\hat{r}_k\hat{r}_l] \end{aligned} \right\} \quad (3.38)$$

† See also Lawrence & Weinbaum (1988) in connection with the unsteady drag on a spheroid.

and

$$\left. \begin{aligned} X_j &= 3b_3\delta_{3j} - b_j, \\ Y_{jk} &= (b_j\delta_{3k} + b_k\delta_{3j}) + b_3(\delta_{jk} - 5\delta_{3j}\delta_{3k}), \\ Z_{jkl} &= b_j(\delta_{kl} - 5\delta_{3k}\delta_{3l}) + b_k(\delta_{jl} - 5\delta_{3j}\delta_{3l}) + b_l(\delta_{jk} - 5\delta_{3j}\delta_{3k}) \\ &\quad - 5b_3(\delta_{jk}\delta_{3l} + \delta_{jl}\delta_{3k} + \delta_{kl}\delta_{3j} - 7\delta_{3j}\delta_{3k}\delta_{3l}). \end{aligned} \right\} \quad (3.39)$$

Here we have defined the following functions:

$$\left. \begin{aligned} I(x) &= 1 + 6x^{-1} + 15x^{-2} + 15x^{-3}, \\ J(x) &= 1 + 2x^{-1} + 3x^{-2} + 3x^{-3}, \\ K(x) &= 1 + 4x^{-1} + 9x^{-2} + 15x^{-3} + 15x^{-4}, \\ L(x) &= 1 + 10x^{-1} + 45x^{-2} + 105x^{-3} + 105x^{-4}. \end{aligned} \right\} \quad (3.40)$$

The expressions for Q_{ijk} and R_{ijkl} have been simplified by using the facts that

$$Y_{kk} = 0 \quad \text{and} \quad Z_{jkk} = Z_{kjk} = Z_{kkj} = 0_j.$$

The first reflected field appears only at $O(\epsilon^6)$ in the vicinity of the moving sphere. To the degree of approximation represented by (3.37), the sphere–sphere interaction is therefore not felt inside its Stokes layer. Furthermore, within an error of $O(\epsilon^4)$ both Stokes layers induce only a phase shift between the outer field and their respective spheres. Starting with the $O(\epsilon^4)$ correction, the simple phase-shift interpretation ceases to apply. We note that, as long as Ω and ϵ are chosen such that the Stokes layers do not overlap, we have the following asymptotic behaviour of the finite-amplitude drift-force coefficients of (3.25):

$$A_1 = O(1), \quad A_2 = O(\epsilon^3). \quad (3.41)$$

It is worthwhile to compare (3.37) with the multipole expansion given by Kim & Russel (1985) for the first reflection. With the aim of calculating drag coefficients, they proceed by systematically cancelling the *moments* of the disturbance *stress field* felt at the surface of sphere 2 (monopole, dipole, quadrupole, etc.), rather than by cancelling the successive *gradients* of the incident velocity field. For our case of well-separated Stokes layers, (3.37) is, of course, equivalent to their formulation; but it involves a reordering of the terms. For example, because the force dipole does not completely cancel the linear part of the incident field, our $O(\epsilon^4)$ term contains the contribution of a higher multipole.

3.8. Asymptotic behaviour at low frequencies

Based upon the asymptotic form of the pseudo-Brinkman velocity fields $v^{[i]}(\mathbf{r})$ at low frequency, one can deduce the scaling of the coefficients A_i, B_i of (3.25). Although general results are available in terms of inner and outer expansions (see e.g. Kanwal 1964), our present aim does not require such detailed arguments. First of all, if we denote by $\mathbf{u}^{[1]}(\mathbf{r})$ and $\mathbf{u}^{[2]}(\mathbf{r})$ the Stokes velocity fields that satisfy the same boundary conditions (3.20) as the Brinkman velocity fields $\mathbf{v}^{[1]}(\mathbf{r})$ and $\mathbf{v}^{[2]}(\mathbf{r})$, then

$$\mathbf{v}_R^{[\alpha]}(\mathbf{r}) \rightarrow \mathbf{u}^{[\alpha]}(\mathbf{r}), \quad \mathbf{v}_I^{[\alpha]}(\mathbf{r}) \rightarrow \mathbf{0} \quad \text{as } \Omega \rightarrow 0,$$

uniformly in position \mathbf{r} within any bounded region of space.

Exact expressions for the singular solutions will be given in §4; but for now it is sufficient to note the following expansion of the pseudo-Brinkman point force singularity $\mathbf{S}(\mathbf{r})$ in powers of $\Omega^{\frac{1}{2}}$ (Howells 1974; Pozrikidis 1989b):

$$\mathbf{S}(\mathbf{r}) = \mathbf{S}^{(0)} - \frac{4}{3}\gamma\mathbf{l} + \frac{1}{4}\gamma^2r(3\mathbf{l} - \hat{\mathbf{r}}\hat{\mathbf{r}}) + \dots, \quad (3.42)$$

with $\mathbf{S}^{(0)}(\mathbf{r})$ the Stokeslet. This expansion converges at any fixed position \mathbf{r} , but not, of course, uniformly in \mathbf{r} – precisely due to the far-field singular behaviour.

If one considers the solutions $\mathbf{v}^{[\alpha]}(\mathbf{r})$ as being generated by areal distributions of the force singularity over the two sphere surfaces (Howells 1974), then it is clear that the near-field correction at $O(\gamma)$ is a uniform flow, which has no effect on $\nabla\mathbf{v}^{[\alpha]}(\mathbf{r})$. The frequency dependence of the *gradient* is therefore felt first at $O(\gamma^2) = O(\Omega)$. Therefore, from (3.25) it follows that

$$A_i(\Omega; L) \sim \Psi_i^{(0)}(L) + \Psi_i^{(1)}(L)\Omega \quad \text{as } \Omega \rightarrow 0. \quad (3.43)$$

Proceeding to the inertia drift force, we observe that the volume integrals (3.25) giving the coefficients B_i do converge if we insert $\{\mathbf{u}^{[\alpha]}, \mathbf{0}\}$ in place of $\{\mathbf{v}_R^{[\alpha]}, \mathbf{v}_I^{[\alpha]}\}$, i.e.

$$B_i(\Omega; L) \sim \Upsilon_i^{(0)}(L) + \Upsilon_i^{(1)}(L)\Omega^{\frac{1}{2}} \quad \text{as } \Omega \rightarrow 0. \quad (3.44)$$

Thus, the *dimensional* drift force $\langle \Delta F \rangle$ scales asymptotically like $\Omega\eta\langle \Delta F \rangle_*(0; L)$ at low frequencies; cf. (3.23).

It is also true that $B_1^{\parallel}(0; L) = B_2^{\parallel}(0; L)$. To show this, observe that $\mathbf{u}^{[1]} - \mathbf{u}^{[2]}$ is precisely the Stokes test velocity field \mathbf{u}' from (3.11), (3.12). At $\Omega = 0$ the alternative volume integrals in (3.14) and (3.16) are then seen to be equivalent, whereby

$$B_1^{\parallel}(0; L) - B_2^{\parallel}(0; L) = - \int_{\mathcal{V}^{(0)}} \nabla\mathbf{u}' : \mathbf{u}'\mathbf{u}' d^3\mathbf{r} = \int_{\mathcal{V}^{(0)}} \nabla\mathbf{u}' : \mathbf{u}'\mathbf{u}' d^3\mathbf{r} = 0. \quad (3.45)$$

Although there appears to be no simple relation between $A_1(0; L)$ and $A_2(0; L)$, the above result *does* have a counterpart involving the finite-amplitude coefficients – (6.21) below, which arises in the stochastic considerations of Brownian motion (§6.3).

Finally, in connection with §4.5 below it is useful to consider the expansion (3.42) with reference to the frequency-dependent friction coefficients, for motions both parallel and perpendicular to the line of centres. The contribution from the uniform field gives rise to an $O(\Omega^{\frac{1}{2}})$ correction to the *individual* friction coefficient of each sphere with the other held stationary, i.e.

$$\zeta_{\alpha\beta} = \zeta_{\alpha\beta}^{(0)} + O(\Omega^{\frac{1}{2}}) \quad (\alpha = 1, 2) \quad (3.46)$$

But these two corrections exactly cancel out in the sphere–sphere interaction when the spheres move in opposite directions. Consequently, the friction coefficient describing *relative* motion has the following asymptotic behaviour at low frequencies:

$$\zeta_{11} - \zeta_{12} = \zeta_{\text{relative}} = \zeta_{\text{relative}}^{(0)} + O(\Omega). \quad (3.47)$$

3.9. Axial and transverse modes

At this point we introduce different notation for oscillations parallel and perpendicular to the line of centres. Axial modes ($\mathbf{b}^{\parallel} = \mathbf{e}_z$) are described by the axisymmetric velocity fields $\mathbf{v}^{[\alpha],\parallel}(z, \rho)$, for which the no-slip boundary conditions (3.20) need only be imposed along the generating arcs of the spheres, $\mathcal{L}_{\alpha}^{(0)}$. Explicitly,

$$v_z^{[\alpha],\parallel} = \delta^{\alpha\beta}, \quad v_{\rho}^{[\alpha],\parallel} = 0 \quad \text{on } \mathcal{L}_{\beta}^{(0)} \quad (\alpha, \beta = 1, 2). \quad (3.48)$$

Note the following relations in circular cylindrical coordinates (z, ρ) :

$$v_z^{[2],\parallel}(z, \rho) = v_z^{[1],\parallel}(-z, \rho), \quad v_{\rho}^{[2],\parallel}(z, \rho) = -v_{\rho}^{[1],\parallel}(-z, \rho); \quad (3.49)$$

there are, of course, no azimuthal components.

For transverse oscillations ($\mathbf{b}^{\perp} = \mathbf{e}_x$), we exploit the fact that the azimuthal dependence of the flow is contained entirely within the first harmonic in ϕ , whereby each

velocity field $\mathbf{v}^{[\alpha],\perp}(\mathbf{r})$ can be expressed in terms of a corresponding set of *axisymmetric* functions, denoted by \perp^* , viz.

$$\left. \begin{aligned} v_z^{[\alpha],\perp}(z, \rho, \phi) &= v_z^{[\alpha],\perp^*}(z, \rho) \cos \phi, \\ v_\rho^{[\alpha],\perp}(z, \rho, \phi) &= v_\rho^{[\alpha],\perp^*}(z, \rho) \cos \phi, \\ v_\phi^{[\alpha],\perp}(z, \rho, \phi) &= v_\phi^{[\alpha],\perp^*}(z, \rho) \sin \phi. \end{aligned} \right\} \quad (3.50)$$

With the ϕ dependence factored out in this way, the boundary conditions (3.20) again reduce to conditions imposed on the generating arcs $\mathcal{L}_\alpha^{(0)}$; cf. Kim & Russel (1985), Karrila & Kim (1989) :

$$v_z^{[\alpha],\perp^*} = 0, \quad v_\rho^{[\alpha],\perp^*} = \delta^{\alpha\beta}, \quad v_\phi^{[\alpha],\perp^*} = -\delta^{\alpha\beta} \quad \text{on } \mathcal{L}_\alpha^{(0)} \quad (\alpha, \beta = 1, 2). \quad (3.51)$$

We then observe the relations

$$\left. \begin{aligned} v_z^{[2],\perp^*}(z, \rho) &= -v_z^{[1],\perp^*}(-z, \rho), \\ v_\rho^{[2],\perp^*}(z, \rho) &= v_\rho^{[1],\perp^*}(-z, \rho), \\ v_\phi^{[2],\perp^*}(z, \rho) &= v_\phi^{[1],\perp^*}(-z, \rho). \end{aligned} \right\} \quad (3.52)$$

Given axisymmetry of $\mathbf{v}^{[\alpha],\parallel}$ and (3.50), one can immediately carry out the azimuthal part of each surface or volume integral appearing in the coefficient formulas (3.25). It follows that there are no coupling translational modes in the x -, y - and z -directions; the drift-force contributions from these perpendicular modes simply add to each other. The surface integrals reduce to line integrals over the arcs $\mathcal{L}_\alpha^{(0)}$, while the volume integrals become areal integrals over the z, ρ projection $\hat{\mathcal{A}}^{(0)}$ of $\hat{\mathcal{V}}^{(0)}$. With these simplifications the coefficient formulas (3.25) for both axial and transverse oscillations can ultimately be written in the general form

$$A_i^\square = \frac{1}{\Omega} \int_{\mathcal{L}_2^{(0)}} A_i^\square(z, \rho) 2\pi\rho dl, \quad B_i^\square = \int_{\hat{\mathcal{A}}^{(0)}} \Gamma_i^\square(z, \rho) 2\pi\rho dzd\rho. \quad (3.53)$$

Explicit expressions for the functions $A_i^\parallel, A_i^\perp, \Gamma_i^\parallel, \Gamma_i^\perp$ are given in Appendix B.

4. Numerical solutions via a boundary singularity method

In order to evaluate (numerically) the coefficient integrals (3.53) one requires accurate solutions of the Stokes flow problem (3.11), (3.12) and of the imaginary-permeability version of the Brinkman equation (3.19), (3.20) for both axial and transverse motion of the spheres. Moreover, for calculating the virtual masses and checking overall consistency of the computational scheme, it is also useful to carry out the corresponding calculations for potential flow.

Although separation of variables in bipolar coordinates yields an exact series solution of the axisymmetric Stokes problem (Stimson & Jeffrey 1926; Brenner 1961), the Brinkman equation is not similarly separable (Kim & Russel 1985). For both Stokes and Brinkman flow, numerical techniques based upon singular solutions prove to be efficient for calculating hydrodynamic coefficients for two spheres at fairly small separations; e.g. the multipole-collocation technique (Gluckman *et al.* 1971; Kim & Mifflin 1985; Kim & Russel 1985).

We utilized a least-squares boundary singularity method (Mathon & Johnston 1977; Bogomolny 1985; Dąbrosz 1985; Nitsche & Brenner 1990), 'LSBSM', to calculate the flow fields and hydrodynamic coefficients for all cases except the *axisymmetric* potential problem, which was tractable more efficiently by the method of images

(Lamb 1932, Art. 98); cf. Appendix A. Based upon this numerical scheme, the calculations in this paper could readily be extended to treat nonlinear drift phenomena in pores (§7.3); cf. Nitsche & Brenner 1990).

The LSBSM algorithms for potential, Stokes and Brinkman flow are all analogous, differing mainly in the respective sets of singular basis functions, and in the details of the boundary conditions for inviscid versus viscous flow. Two separate FORTRAN codes were developed to treat the respective cases of axial and transverse oscillations. In combining the LSBSM subroutines for quasi-static and transient Stokes flow (and, in the latter case, also potential flow) into each program, the implementation was streamlined by pooling certain elements of the calculations, as will be discussed below in §4.9.

4.1. General description of the method

Numerical methods based upon hydrodynamic singularities have been reviewed very recently and comprehensively in the works of Weinbaum, Ganatos & Yan (1990), Kim & Karrila (1991), and Pozrikidis (1992). The description that follows is therefore kept short.

In the traditional boundary integral method, the flow fields are given by a continuous distribution of singular solutions over the solid surfaces, of which the unknown density is the solution of an integral equation that results from imposing the no-slip boundary conditions (Youngren & Acrivos 1975; Karrila & Kim 1989; Pozrikidis 1989*a*). Because the generating singularities lie precisely on the surface(s) at which the fluid velocity is to be prescribed, one must evaluate singular integrals.

The boundary singularity method avoids singular integrals by representing the solution as a superposition of singular solutions whose poles lie on an auxiliary-boundary which is displaced a certain distance *behind* the physical boundary, i.e. inside the solid phase (Weinbaum *et al.* 1990). The strengths of the singularities are optimized in a least-squares sense with respect to no-slip residuals calculated at discrete points on the sphere surfaces. Overdetermining the system with an excess of boundary criteria is intended to make the method more robust with respect to the choice of boundary points than collocation; cf. Gluckman *et al.* (1971), Kim & Russel (1985), Nitsche & Brenner (1990).

Reasonably accurate results have been obtained in Stokes flow with star-shaped clusters of a few (e.g. 7 or 13) poles positioned around the centres of the particles (Dąbrosz 1985), a scheme which could be regarded as a pseudo-multipole technique in which difference quotients approximate higher-order singularities. Nevertheless, systematic mesh refinement seems to favour the auxiliary-boundary approach. As with boundary elements the dimension of the singularity mesh is then one lower than that of the fluid domain, while displacement of the generating boundary offers advantages for evaluating derivatives at the solid surfaces (Han & Olson 1987). This feature is desirable in view of the formulas (3.25) for the finite-amplitude coefficients A_i .

Excursion into the particle interiors necessitates the introduction of the point-source solution in addition to the force singularity (Dąbrosz 1985). In contrast, boundary elements via single-layer potentials require only the latter solution. This can be rationalized intuitively by observing that the exact solution for Stokes or Brinkman flow past a sphere is just an appropriate superposition (3.34) of the point force and the source doublet, both placed at the sphere centre.

In a manner significantly different from our least-squares, pseudo-boundary-element approach, Pozrikidis (1989*b*) has employed Brinkman-type singularities to obtain an

approximate solution of the time-dependent Stokes equations for the problem of a prolate spheroid vibrating along its axis symmetry (this in addition to some exact solutions for solid particles and droplets). His numerical procedure utilized continuous lineal distributions of point forces and dipoles along the focal length, the densities being given by truncated expansions in Chebyshev polynomials. The corresponding coefficients were determined by imposing the no-slip boundary conditions at an equal number of positions on the surface (collocation).

Because the LSBSM algorithms for quasi-static and unsteady Stokes flow are exactly analogous, our description is restricted to the unsteady case. First we present the method for the axisymmetric problem of axial oscillations (§§4.2, 4.3), and subsequently we describe how the scheme must be generalized to deal with the non-axisymmetric flow generated by transverse oscillation (§4.4). Section 4.5 develops formulas to express the hydrodynamic forces acting on each sphere in terms of the singularity strengths. The LSBSM procedure is simpler when applied to potential flow; this implementation is sketched very briefly in §4.6 for transverse modes. (Axial modes in potential flow were treated by the method of images.) Section 4.7 gives formulas for the velocity fields and friction coefficients corresponding to the leading-order reflection scheme (§3.7) that is utilized at very high frequencies. Calculation of the drift-force coefficients via numerical integration of (3.53) is discussed in §4.8. Finally, in §4.9 we describe checks on the accuracy and overall consistency of our numerical approach. Note that explicit expressions for the singular basis functions appear in Appendices C and D.

4.2. Axisymmetric singular basis functions

For the time-dependent Stokes equations in the frequency domain – equivalently, the Brinkman equation with imaginary-permeability – the point force singularity of (vector) strength \mathbf{f} is as follows (Howells 1974; Pozrikidis 1989a):

$$\left. \begin{aligned} \mathbf{S}(\mathbf{r}) \cdot \mathbf{f} &= \frac{1}{\gamma^2} \frac{1}{4\pi r^3} [3A(\gamma r)\hat{\mathbf{r}}\hat{\mathbf{r}} - B(\gamma r)\mathbf{I}] \cdot \mathbf{f}, \\ A(x) &= 1 - (1 + x + x^2/3)e^{-x}, \\ B(x) &= 1 - (1 + x + x^2)e^{-x}, \end{aligned} \right\} \tag{4.1}$$

with γ defined in (3.35). At a given value of r this singularity appears like the dipole solution in potential flow at high frequencies such that $\Omega^{\frac{1}{2}} \gg r^{-1}$. In the low-frequency limit ($\Omega^{\frac{1}{2}} \ll r^{-1}$) the singularity approaches

$$\frac{1}{8\pi} \frac{1}{r} (\hat{\mathbf{r}}\hat{\mathbf{r}} + \mathbf{I}),$$

which is just the Stokeslet. The point-source solution of (scalar) strength Q is simply

$$\mathbf{q}(\mathbf{r}) = \frac{Q}{4\pi} \frac{\hat{\mathbf{r}}}{r^2}, \tag{4.2}$$

and applies also to Stokes flow and potential flow.

Axisymmetric singular basis functions are generated by integrating the force and source singularities, with uniform lineal density, around circular rings centred on the z -axis (Pozrikidis 1989a). The flow fields $\{v_z^{[a],\parallel}(z, \rho), v_\rho^{[a],\parallel}(z, \rho)\}$ are resolvable in terms of three kinds of basis functions, respectively associated with (i) radial forces, (ii)

Parameter set, 'PS'	1	2
Intervals for azimuthal integration	12	24
Singularity points (N)	18	34
Boundary points	78	150
Matrix: axial modes, viscous flow	156 × 50	300 × 98
transverse modes, viscous flow	234 × 60	450 × 124
transverse modes, potential flow	79 × 14	151 × 30

TABLE 2. Computational parameters for the LSBSM numerics

axial forces, and (iii) sources at each position ϕ' around the ring:

$$\left. \begin{aligned} U^{(1),\parallel}(z, \rho, \phi; z_*, \rho_*) &= U^{(\rho),\parallel} = \frac{1}{2\pi} \int_0^{2\pi} \mathbf{S}[\mathbf{r}(z, \rho, \phi; z_*, \rho_*, \phi')] \cdot \mathbf{e}'_\rho(\phi') \, d\phi', \\ U^{(2),\parallel}(z, \rho, \phi; z_*, \rho_*) &= U^{(z),\parallel} = \frac{1}{2\pi} \int_0^{2\pi} \mathbf{S}[\mathbf{r}(z, \rho, \phi; z_*, \rho_*, \phi')] \cdot \mathbf{e}_z \, d\phi', \\ U^{(3),\parallel}(z, \rho, \phi; z_*, \rho_*) &= U^{(q),\parallel} = \frac{1}{2\pi} \int_0^{2\pi} \mathbf{q}[\mathbf{r}(z, \rho, \phi; z_*, \rho_*, \phi')] \, d\phi', \end{aligned} \right\} \quad (4.3)$$

with

$$\left. \begin{aligned} \mathbf{r}(z, \rho, \phi; z_*, \rho_*, \phi') &= [z - z_*] \mathbf{e}_z + [\rho - \rho_* \cos(\phi - \phi')] \mathbf{e}_\rho + [\rho_* \sin(\phi - \phi')] \mathbf{e}_\phi, \\ r(z, \rho, \phi; z_*, \rho_*, \phi') &= [\rho^2 + \rho_*^2 - 2\rho\rho_* \cos(\phi - \phi') + (z - z_*)^2]^{\frac{1}{2}}. \end{aligned} \right\} \quad (4.4)$$

Symmetry reduces the azimuthal integrations from the interval $0 < \phi' < 2\pi$ to $0 < \phi' < \pi$, and ensures that the azimuthal component must vanish identically. By the above prescription one then obtains the following equations for the axial and radial components of $U^{(i)}$:

$$\left. \begin{aligned} U_z^{(i),\parallel}(z, \rho; z_*, \rho_*) &= \frac{1}{4\pi^2} \int_0^\pi f_z^{(i),\parallel}(\phi'; z, \rho, z_*, \rho_*) \, d\phi', \\ U_\rho^{(i),\parallel}(z, \rho; z_*, \rho_*) &= \frac{1}{4\pi^2} \int_0^\pi f_\rho^{(i),\parallel}(\phi'; z, \rho, z_*, \rho_*) \, d\phi' \end{aligned} \right\} \quad (4.5)$$

($i = 1, 2, 3$). Expressions for the corresponding integrands $f_z^{(i),\parallel}(\phi'; z, \rho, z_*, \rho_*)$, $f_\rho^{(i),\parallel}(\phi'; z, \rho, z_*, \rho_*)$ appear in Appendix C. Analogous formulas define the basis functions needed to evaluate $\mathbf{b}^\parallel \cdot \nabla \mathbf{v}^{[z],\parallel} = \partial \mathbf{v}^{[z],\parallel} / \partial z$, which are required to compute the drift-force coefficients A_i^\parallel via (3.25).

The integrands in (4.3) are periodic, analytic functions of ϕ' , being integrated precisely over one period. When applied to evaluate the right-hand sides in (4.5), the trapezoid integration rule therefore converges faster than any power of the step size (Dahlquist & Björck 1974, p. 300). Very accurate results were obtained with relatively few azimuthal subdivisions; see table 2 and figure 2.

In the limit as the singularity ring shrinks to a point on the axis of symmetry, the axial-force and source solutions simply approach the corresponding point singularities, whereas the radial-force solution collapses to zero. For those singularity points lying on the z -axis the corresponding degenerate coefficients are eliminated from the boundary optimization.

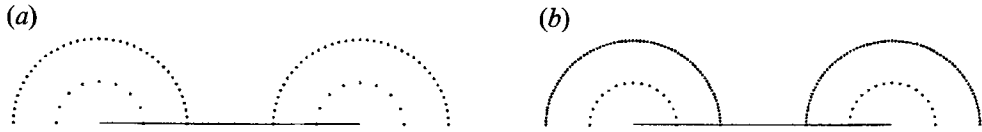


FIGURE 2. Coarse and fine meshes of singularities and boundary points for $L = 1, R = 0.5$; see table 2. (a) Parameter set 1. (b) Parameter set 2

4.3. The numerical algorithm for axisymmetric flow

Because details of the LSBSM technique (as applied to the analogous case of axisymmetric Stokes flow) appear in Nitsche & Brenner (1990), we restrict our discussion to a brief summary. The velocity field $\{v_z^{[1],\parallel}(z, \rho), v_\rho^{[1],\parallel}(z, \rho)\}$ is approximated by a linear combination of singular basis functions centred at $(z_n, \rho_n), n = 1, \dots, N$,

$$\left. \begin{aligned} v_z^{[1],\parallel}(z, \rho) &= \sum_{i=1}^3 \sum_{n=1}^N G_n^{(i),\parallel} U_z^{(i)}(z, \rho; z_n, \rho_n), \\ v_\rho^{[1],\parallel}(z, \rho) &= \sum_{i=1}^3 \sum_{n=1}^N G_n^{(i),\parallel} U_\rho^{(i)}(z, \rho; z_n, \rho_n), \end{aligned} \right\} \quad (4.6)$$

where the unknown coefficients $G_n^{(i),\parallel}$ are chosen so as to minimize, in a least-squares sense, residuals evaluated at discrete points along the solid boundaries. The boundary points on each sphere were taken to lie at equal angular intervals, and the individual residuals were weighted so that the coefficient optimization was equivalent to minimizing the Simpson’s rule approximation \mathcal{E}^\parallel of the following error criterion:

$$\begin{aligned} \mathcal{E}^\parallel &\stackrel{\text{def}}{=} \sum_{\alpha=1}^2 \int_{\mathcal{S}_\alpha^{(0)}} \left\| \mathbf{v}^{[1],\parallel} - \delta_{1\alpha} \mathbf{b}^\parallel \right\|^2 d^2\mathbf{r} \\ &= \sum_{\alpha=1}^2 \int_{\mathcal{S}_\alpha^{(0)}} \{ |v_z^{[1],\parallel} - \delta_{1\alpha}|^2 + |v_\rho^{[1],\parallel}|^2 \} 2\pi\rho dl. \end{aligned} \quad (4.7)$$

Solution of the linear least-squares problem was carried out using a LINPACK QR algorithm (Dongarra *et al.* 1979, Chap. 9). Although there cannot, of course, be a net source of fluid within either sphere, we did not explicitly incorporate the condition

$$\sum_n G_n^{(q),\parallel} = 0 \quad \text{inside } \mathcal{S}_\alpha^{(0)} \quad (\alpha = 1, 2) \quad (4.8)$$

into the optimization. Instead, we monitored the left-hand side as an overall check on consistency of the numerical results.

If $H_n^{(i),\parallel}$ are the coefficients for the velocity field $\mathbf{v}^{[2],\parallel}$, then the relation (3.49) means that

$$H_n^{(\rho),\parallel} = -G_{N+1-n}^{(\rho),\parallel}, \quad H_n^{(z),\parallel} = G_{N+1-n}^{(z),\parallel}, \quad H_n^{(q),\parallel} = -G_{N+1-n}^{(q),\parallel}, \quad (4.9)$$

with the singular points placed at mirror-image positions inside the two spheres and numbered in order of increasing (or decreasing) values of z_n , whereby $(z_{N+1-n}, \rho_{N+1-n}) = (-z_n, \rho_n)$.

The final computation parameters are summarized in table 2.

With a fixed number ($N/2 = 9$ or 17) of singularities evenly spaced in arclength along the concentric auxiliary boundary of radius R inside each sphere, trials were

carried out at each frequency Ω in order to optimize the choice of $R_*(\Omega)$, at least approximately, with respect to the boundary residual criterion (4.7). The total source strength, (4.8), and maximum residual were also factored into the considerations. Thus we arrived at the values of R_* listed in tables 3 and 4. At high frequencies the fundamental solutions were many decay lengths distant from the boundaries. This is not surprising if one considers, for example, that the exact solution (3.34) for a single vibrating sphere consists of the force singularity (4.1) together with a source doublet, both placed at the sphere centre: at high frequencies the point force is many decay lengths distant from the surface. In all cases, the number of conditions exceeded the number of unknowns by at least a factor of 3 in the linear least-squares optimization.

4.4. *Extension to transverse oscillation: non-axisymmetric flow*

Although transverse motion of the sphere(s) ($\mathbf{b}^\perp = \mathbf{e}_x$) induces a non-axisymmetric velocity field, the azimuthal dependence can readily be factored out of the solution via (3.50), so that the stick boundary conditions need only be explicitly imposed on the generating arcs $\mathcal{L}_\alpha^{(0)}$ of the spheres; cf. (3.51). Thus, the LSBSM scheme, while somewhat more complicated in detail, is entirely analogous to that for axisymmetric flow. This simplifying feature has counterparts in both the multipole-collocation technique (Kim & Russel 1985) and the boundary element method (Karrila & Kim 1989).

To resolve the flow fields $\mathbf{v}^{[\alpha],\perp}(\mathbf{r})$ we now need to enlarge the set of basis functions (4.3) to include ring singularities composed of point forces in the *azimuthal* direction. Moreover, the lineal weighting of point forces and point sources around the rings must now be non-uniform, reflecting the desired azimuthal dependence of each velocity component, (3.50). With these considerations, the respective basis functions (depending on $z, \rho, \phi; z_*, \rho_*$) are specified as follows:

$$\left. \begin{aligned} U^{(1),\perp} = U^{(\rho),\perp} &= \frac{1}{2\pi} \int_0^{2\pi} \mathbf{S}[\mathbf{r}(z, \rho, \phi; z_*, \rho_*, \phi')] \cdot \mathbf{e}'_\rho(\phi') \cos \phi' \, d\phi', \\ U^{(2),\perp} = U^{(z),\perp} &= \frac{1}{2\pi} \int_0^{2\pi} \mathbf{S}[\mathbf{r}(z, \rho, \phi; z_*, \rho_*, \phi')] \cdot \mathbf{e}_z \cos \phi' \, d\phi', \\ U^{(3),\perp} = U^{(\phi),\perp} &= \frac{1}{2\pi} \int_0^{2\pi} \mathbf{S}[\mathbf{r}(z, \rho, \phi; z_*, \rho_*, \phi')] \cdot \mathbf{e}'_\phi(\phi') \sin \phi' \, d\phi', \\ U^{(4),\perp} = U^{(q),\perp} &= \frac{1}{2\pi} \int_0^{2\pi} \mathbf{q}[\mathbf{r}(z, \rho, \phi; z_*, \rho_*, \phi')] \cos \phi' \, d\phi'. \end{aligned} \right\} \quad (4.10)$$

Thus we obtain formulas analogous to (4.5) for the basis functions $U_z^{(i),\perp*}$, $U_\rho^{(i),\perp*}$ and $U_\phi^{(i),\perp*}$ (depending on $(z, \rho; z_*, \rho_*)$), which refer to the azimuthal decomposition (3.50). The corresponding integrands $f_z^{(i),\perp*}$, $f_\rho^{(i),\perp*}$ and $f_\phi^{(i),\perp*}$ (depending on $(\phi'; z, \rho, z_*, \rho_*)$) are given in Appendix C. (Analogous formulas for *quasi-static* Stokes flow appear in Appendix D.)

In the limit as $\rho_* \rightarrow 0$ we have

$$U^{(z),\perp} \rightarrow 0, \quad U^{(\phi),\perp} \rightarrow -U^{(\rho),\perp}, \quad U^{(q),\perp} \rightarrow 0 \quad \text{as } \rho_* \rightarrow 0.$$

Thus, for singularity points lying on the z -axis we remove the corresponding degenerate coefficients $G_n^{(z),\perp}$, $G_n^{(\phi),\perp}$ and $G_n^{(q),\perp}$ from the boundary optimization.

The unknown coefficients $G_n^{(i),\perp}$ are then optimized with respect to the error criterion

$$\begin{aligned} \mathcal{E}^\perp &\stackrel{\text{def}}{=} 2 \sum_{\alpha=1}^2 \int_{\mathcal{L}_\alpha^{(0)}} \left\| \mathbf{v}^{[1],\perp} - \delta_{1\alpha} \mathbf{b}^\perp \right\|^2 d^2\mathbf{r} \\ &= \sum_{\alpha=1}^2 \int_{\mathcal{L}_\alpha^{(0)}} \left\{ |v_z^{[1],\perp*}|^2 + |v_\rho^{[1],\perp*} - \delta_{1\alpha}|^2 + |v_\phi^{[1],\perp*} + \delta_{1\alpha}|^2 \right\} 2\pi\rho d\ell, \end{aligned} \quad (4.11)$$

as approximated with Simpson’s rule. The counterpart of (4.9) in the case of transverse motion is

$$H_n^{(\rho),\perp} = G_{N+1-n}^{(\rho),\perp}, \quad H_n^{(z),\perp} = -G_{N+1-n}^{(z),\perp}, \quad H_n^{(\phi),\perp} = G_{N+1-n}^{(\phi),\perp}, \quad H_n^{(q),\perp} = G_{N+1-n}^{(q),\perp}. \quad (4.12)$$

4.5. Frequency-dependent friction coefficient

In order to integrate over the spectrum of frequencies in §6.4, we will require the frequency-dependent friction coefficient for each sphere in the linearized problem (3.19), (3.20). This is formally defined by integrating the normal stress over the surface, but can also be written quite simply in terms of the singularity strengths. Pozrikidis (1989*b*) derives such an expression, for the case of one particle oscillating in an infinite fluid, by taking the stress surface integral to infinity and utilizing the fact that the far-field behaviour is dominated by the point-force solutions. This device loses its utility if there are two or more particles present and one wants to find the force on each particle. Thus, we choose to move the surface integrals *inside* the spheres, i.e. around the poles. Furthermore, in addition to the point forces, the point sources also contribute to the net force. This issue did not arise for Pozrikidis, who constructed his solutions using source doublets (dipoles) – among other singularities – but not point sources.

Using fluid incompressibility (2.4) the velocity field \mathbf{v} can be rewritten in the form $\mathbf{v} = \nabla \cdot (\mathbf{v}\mathbf{r})$. Together with (3.19) this means that

$$\nabla \cdot \mathbf{T} = i\Omega \nabla \cdot (\mathbf{v}\mathbf{r}).$$

Application of the divergence theorem then yields for the force exerted by the fluid on any particle,

$$\mathbf{F}(\epsilon) = \int_{\mathcal{S}} \mathbf{n} \cdot \mathbf{T} d^2\mathbf{r} = \sum_{k=1}^K \int_{\mathcal{S}'_k(\epsilon)} [\mathbf{n} \cdot \mathbf{T} - i\Omega \mathbf{n} \cdot \mathbf{v}\mathbf{r}] d^2\mathbf{r} + i\Omega \int_{\mathcal{S}} \mathbf{n} \cdot \mathbf{v}\mathbf{r} d^2\mathbf{r},$$

with $\mathcal{S}'_k(\epsilon)$ a spherical surface of radius ϵ centred at the k th singularity inside the particle, and \mathbf{n} the outward-pointing normal on all surfaces. If the particle, of volume V_φ , moves (without rotation) at velocity \mathbf{U} , then the surface integral over \mathcal{S} gives $V_\varphi \mathbf{U}$. As $\epsilon \rightarrow 0$, only the point force (strength \mathbf{f}_k) contributes to the stress integral over $\mathcal{S}'_k(\epsilon)$, giving $-\mathbf{f}_k$; there is no contribution from the point source. Conversely, the velocity integral over $\mathcal{S}'_k(\epsilon)$ picks out only a term proportional to the source strength Q_k . Thus, we find

$$\lim_{\epsilon \rightarrow 0} \mathbf{F}(\epsilon) = -\sum_{k=1}^K \mathbf{f}_k - i\Omega \sum_{k=1}^K c_k Q_k + i\Omega V_\varphi \mathbf{U}, \quad (4.13)$$

with c_k the locations of the poles. This is Pozrikidis’s formula (1989*b*, equation 39) except for the additional source terms. Despite a superficial appearance to the contrary, the source contribution must be independent of the choice of origin from

which the positions c_k are measured. This invariance follows from the fact that $\sum_{k=1}^K Q_k = 0$ inside any particle.

In terms of the present numerical formulation, (4.13) reduces to

$$\left. \begin{aligned} F_z^\parallel &= i\Omega \frac{4\pi}{3} U_z - \sum_n [i\Omega z_n G_n^{(q),\parallel} + G_n^{(z),\parallel}], \\ F_x^\perp &= i\Omega \frac{4\pi}{3} U_x - \frac{1}{2} \sum_n [i\Omega \rho_n G_n^{(q),\perp} + G_n^{(\rho),\perp} - G_n^{(\phi),\perp}], \end{aligned} \right\} \quad (4.14)$$

where \sum_n denotes the sum over those ring singularities that lie inside the particle in question. Axisymmetry precludes coupling between axial motions ($\mathbf{b}^\parallel = \mathbf{e}_z$) and transverse motions ($\mathbf{b}^\perp = \mathbf{e}_x$), whereby these two cases can be treated separately. In either case, the friction coefficient $\zeta_{\alpha\beta} = \zeta_{\alpha\beta}(L)$ is defined as the constant of proportionality between the external force exerted upon sphere α and the velocity of sphere β , with the other sphere held stationary, viz.†

$$(F_z^\parallel)_\alpha = \zeta_{\alpha\beta}^\parallel (U_z)_\beta, \quad (F_x^\perp)_\alpha = \zeta_{\alpha\beta}^\perp (U_x)_\beta \quad (\alpha, \beta = 1, 2). \quad (4.15)$$

Because the two spheres are of equal size, there are only four independent friction coefficients:

$$\left. \begin{aligned} \zeta_a^\parallel &\stackrel{\text{def}}{=} \zeta_{11}^\parallel = \zeta_{22}^\parallel, & \zeta_b^\parallel &\stackrel{\text{def}}{=} \zeta_{12}^\parallel = \zeta_{21}^\parallel, \\ \zeta_a^\perp &\stackrel{\text{def}}{=} \zeta_{11}^\perp = \zeta_{22}^\perp, & \zeta_b^\perp &\stackrel{\text{def}}{=} \zeta_{12}^\perp = \zeta_{21}^\perp. \end{aligned} \right\} \quad (4.16)$$

4.6. Calculations for transverse motion in potential flow

The numerical scheme for potential flow carries over from viscous flow (§4.4) – with three minor changes.

(i) The solution involves only the source basis functions, whereby we have

$$w_z^{[1],\perp}(z, \rho) = \sum_{n=1}^N G_n U_z^{(q),\perp}(z, \rho, z_n, \rho_n), \quad (4.17)$$

with analogous equations for the ρ and ϕ components of \mathbf{w} .

(ii) The boundary conditions require only a vanishing *normal* component of velocity relative to the surfaces; no restriction is placed on the tangential component. Thus, the boundary criterion becomes

$$\begin{aligned} \mathcal{E}^\perp &\stackrel{\text{def}}{=} 2 \sum_{\alpha=1}^2 \int_{\mathcal{S}_\alpha^{(0)}} [\mathbf{n} \cdot \mathbf{w}^{[1]} - \delta_{1\alpha} \mathbf{n} \cdot \mathbf{e}_x]^2 d^2\mathbf{r} \\ &= \sum_{\alpha=1}^2 \int_{\mathcal{S}_\alpha^{(0)}} [w_z^{[1],\perp} n_z + w_\rho^{[1],\perp} n_\rho - \delta_{1\alpha} n_\rho]^2 2\pi\rho dl. \end{aligned} \quad (4.18)$$

(iii) In addition to the velocity field \mathbf{w} we require the potentials $\Phi^{[\alpha],\perp}$ themselves‡ ($\mathbf{w} = -\nabla\Phi^{[\alpha],\perp}$) in order to calculate the added masses via (2.14). Factoring out the azimuthal dependence as before,

$$\Phi^{[\alpha],\perp}(z, \rho, \phi) = \Phi^{[\alpha],\perp*}(z, \rho) \cos \phi,$$

† Summation over β is suppressed.

‡ These correspond to Φ_i^α in the notation of §2.1.

the basis functions for $\Phi^{[x],\perp*}(z, \rho)$ are as follows:

$$\Psi^{\perp*}(z, \rho, z_*, \rho_*) = \frac{1}{4\pi} \int_0^\pi \frac{\cos \phi' d\phi'}{[\rho^2 + \rho_*^2 - 2\rho\rho_* + (z - z_*)^2]^{\frac{1}{2}}}. \tag{4.19}$$

We note the symmetry relation

$$H_n = G_{N+1-n}, \tag{4.20}$$

which is the counterpart of (4.12) above.

Finally, the surface integrals giving the virtual masses (2.14) and (2.40) reduce to line integrals over the generating arcs of the spheres:

$$\mathcal{M}_a^\perp = \int_{\mathcal{L}_1^{(0)}} \pi\rho (\Phi^{[1],\perp*} n_\rho) dl, \quad \mathcal{M}_b^\perp = \int_{\mathcal{L}_2^{(0)}} \pi\rho (\Phi^{[1],\perp*} n_\rho) dl. \tag{4.21}$$

4.7. Formulas pertaining to the reflection solution

Here we rewrite the reflection solution (3.37), (3.38), (3.39) in the form of §3.9 for both axial and transverse modes, whereby the azimuthal dependence is explicitly factored out as in (3.50) in the latter case. From the definitions $b_i^\parallel = \delta_{3i}$ and $b_i^\perp = \delta_{li}$ one ultimately obtains the following expressions, which apply when the Stokes layers are well separated:

$$\left. \begin{aligned} \mathbf{v}^{[1],\parallel}(z, \rho) &= V^{(0),\parallel}(z+h, \rho) - \epsilon^3 G(\gamma) V^{(0),\parallel}(z-h, \rho) \\ &\quad + (\epsilon^4/2)G(\gamma)(1+\gamma^{-1})^{-1} V^{(1),\parallel}(z-h, \rho) \\ &\quad + (15\epsilon^5/4)V^{(2),\parallel}(z-h, \rho) + O(\epsilon^6), \\ \mathbf{v}^{[2],\parallel}(z, \rho) &= V^{(0),\parallel}(z-h, \rho) - \epsilon^3 G(\gamma) V^{(0),\parallel}(z+h, \rho) \\ &\quad - (\epsilon^4/2)G(\gamma)(1+\gamma^{-1})^{-1} V^{(1),\parallel}(z+h, \rho) \\ &\quad + (15\epsilon^5/4)V^{(2),\parallel}(z+h, \rho) + O(\epsilon^6), \end{aligned} \right\} \tag{4.22}$$

$$\left. \begin{aligned} \mathbf{v}^{[1],\perp*}(z, \rho) &= V^{(0),\perp*}(z+h, \rho) + (\epsilon^3/2)G(\gamma) V^{(0),\perp*}(z-h, \rho) \\ &\quad + (\epsilon^4/2)G(\gamma)(1+\gamma^{-1})^{-1} V^{(1),\perp*}(z-h, \rho) \\ &\quad + (3\epsilon^5/16)V^{(2),\perp*}(z-h, \rho) + O(\epsilon^6), \\ \mathbf{v}^{[2],\perp*}(z, \rho) &= V^{(0),\perp*}(z-h, \rho) + (\epsilon^3/2)G(\gamma) V^{(0),\perp*}(z+h, \rho) \\ &\quad - (\epsilon^4/2)G(\gamma)(1+\gamma^{-1})^{-1} V^{(1),\perp*}(z+h, \rho) \\ &\quad + (3\epsilon^5/16)V^{(2),\perp*}(z+h, \rho) + O(\epsilon^6). \end{aligned} \right\} \tag{4.23}$$

The individual components $V_z^{(i),\parallel}(z, \rho)$, $V_\rho^{(i),\parallel}(z, \rho)$, $V_z^{(i),\perp*}(z, \rho)$, $V_\rho^{(i),\perp*}(z, \rho)$, $V_\phi^{(i),\perp*}(z, \rho)$ are given in Appendix E. Using the Faxén law for the unsteady Stokes equations, the frequency-dependent friction coefficients $\tilde{\zeta}_a^\parallel$, $\tilde{\zeta}_b^\parallel$, $\tilde{\zeta}_a^\perp$, $\tilde{\zeta}_b^\perp$ can be extracted through terms of $O(\epsilon^{10})$ using only the multipoles appearing above (Kim & Russel 1985).

$$\left. \begin{aligned} \tilde{\zeta}_a^\parallel/(6\pi) &= \left(1 + \gamma + \frac{\gamma^2}{9} \right) \\ &\quad + \left\{ \epsilon^6 [G(\gamma)]^2 + 3\epsilon^8 \frac{G(\gamma)I(\gamma)}{1+\gamma^{-1}} + 6\epsilon^{10}L(\gamma) \right\} \left(1 + \gamma + \frac{\gamma^2}{3} \right) + O(\epsilon^{11}), \\ \tilde{\zeta}_b^\parallel/(6\pi) &= -\epsilon^3 G(\gamma) \{ 1 + \epsilon^6 [G(\gamma)]^2 \} \left(1 + \gamma + \frac{\gamma^2}{3} \right) + O(\epsilon^{11}), \end{aligned} \right\} \tag{4.24}$$

$$\left. \begin{aligned} \zeta_a^\perp / (6\pi) &= \left(1 + \gamma + \frac{\gamma^2}{9} \right) \\ &+ \left\{ \frac{\epsilon^6}{4} [G(\gamma)]^2 + \epsilon^8 \frac{G(\gamma)I(\gamma)}{1 + \gamma^{-1}} + \frac{9}{4} \epsilon^{10} L(\gamma) \right\} \left(1 + \gamma + \frac{\gamma^2}{3} \right) + O(\epsilon^{11}), \\ \zeta_b^\perp / (6\pi) &= \frac{\epsilon^3}{2} G(\gamma) \left\{ 1 + \frac{\epsilon^6}{4} [G(\gamma)]^2 \right\} \left(1 + \gamma + \frac{\gamma^2}{3} \right) + O(\epsilon^{11}). \end{aligned} \right\} \quad (4.25)$$

4.8. Numerical integration for the mean force coefficients

Once numerical solutions have been obtained for both the quasi-static (3.11), (3.12) and unsteady (3.19), (3.20) Stokes problems, the areal integrals (3.53) for coefficients B_i are transformed to bipolar coordinates, and subsequently approximated with Simpson’s rule. The transformation from bipolar coordinates (ξ, η) to Cartesian coordinates (z, ρ) in the meridian plane is as follows (Happel & Brenner 1983):

$$\rho = \frac{c \sin \xi}{\cosh \eta - \cos \xi}, \quad z = \frac{c \sinh \eta}{\cosh \eta - \cos \xi} \quad (4.26)$$

$(0 \leq \xi \leq \pi, 0 \leq \eta \leq \eta_0)$, with

$$c = (h^2 - 1)^{\frac{1}{2}}, \quad \eta_0 = \ln \left(h + (h^2 - 1)^{\frac{1}{2}} \right). \quad (4.27)$$

The metric becomes

$$\rho \, dz \, d\rho = \frac{c^3 \sin \xi}{(\cosh \eta - \cos \xi)^3} \, d\xi \, d\eta.$$

Simpson’s rule, with a 100×100 (ξ, η) mesh, was used to approximate the areal integrals in (3.53).

Two limiting cases warrant further comment. Firstly, if the vorticity decay length is significantly smaller than half of the inter-sphere gap (non-interacting boundary layers), then the boundary-layer region (thickness taken as $\delta = 2(2/\Omega)^{\frac{1}{2}}$) is integrated separately in polar coordinates with a 100×50 (θ, r) mesh, and the bipolar integration is applied outside the enlarged sphere. Note that in this case, (4.27) is replaced by

$$c = (h^2 - (1 + \delta)^2)^{\frac{1}{2}}, \quad \eta_0 = \ln \left[\left(\frac{h}{1 + \delta} \right) + \left(\left(\frac{h}{1 + \delta} \right)^2 - 1 \right)^{\frac{1}{2}} \right]. \quad (4.28)$$

Secondly, in the low-frequency limit (§3.8) one must resolve the far-field region $r \gtrsim \Omega^{-\frac{1}{2}}$, which contributes an $O(\Omega)$ term to the volume integral. Observing that

$$(\rho^2 + z^2)^{\frac{1}{2}} \sim \frac{2c}{(\xi^2 + \eta^2)^{\frac{1}{2}}}$$

at large distances, it is clear that the corresponding (ξ, η) region can become small relative to any fixed (i.e. Ω -independent) integration mesh.† Thus, when the decay length $\delta' = (2/\Omega)^{\frac{1}{2}}$ is significantly greater than the geometric lengthscale $2h + 2$, the original (ξ, η) domain is subdivided into four rectangles by the perpendicular lines $\xi = 4c/\delta'$, $\eta = 4c/\delta'$. In each subregion the integration is carried out with a 100×100 mesh, thereby ensuring that the far-field exponential decay zone is resolved with reasonable accuracy, no matter how small the corresponding area appears in the (ξ, η) -plane.

† It would be wasteful to refine the entire mesh only to have enough integration points in a tiny corner region and in two adjoining thin strips.

The line integrals (3.53), (4.21) giving the coefficients A_i^{\parallel} , A_i^{\perp} and virtual masses \mathcal{M}_a^{\perp} , \mathcal{M}_b^{\perp} are approximated with Simpson's rule using 100 subdivisions around the arcs $\mathcal{L}_\alpha^{(0)}$.

4.9. Computational details; testing of accuracy and overall consistency

The FORTRAN implementation of the above LSBSM algorithms was streamlined by using the same set of boundary points to enforce, via the error criteria (4.7), (4.11) and (4.18), the respective boundary conditions for viscous flow (quasi-static Stokes, transient Stokes) and inviscid flow. In each case we also used the same number of singularity points,† placed at the same polar angles in each sphere; however, the values of R , (radii of the respective auxiliary boundaries) were chosen independently for each hydrodynamic problem.

Given the extensiveness and complexity of the numerical calculations, it was desirable to provide checks on their accuracy and consistency. Fortunately, the friction coefficients could be compared with values and asymptotic expressions available in the literature. By testing the numerical counterparts of certain theoretical relations involving surface or volume integrals of the various flow fields, we were able to (i) establish the accuracy of the numerical integrations and (ii) verify the overall consistency of the numerics. A summary of these considerations is given below.

For the calculations of viscous flow at unit separation between the spheres ($L = 1$), we tested the invariance of the computed friction coefficients with respect to changes in the radius R , of the singularity boundary about its optimized value at each frequency Ω . Based upon these considerations, we utilized the LSBSM scheme up to $\Omega = 256$ for axial modes and up to $\Omega = 128$ for transverse modes. At higher frequencies we switched to the reflection formulas from §4.7. When both approaches applied, the respective results agreed very closely; see tables 11–13 and §5, below.

The residuals of the boundary conditions are listed in tables 3–5 for all of the calculations reported in this paper. With only 18 singularity points and 78 boundary points at $L = 1$, the total error criteria $\bar{\mathcal{E}}^{\parallel}$ and $\bar{\mathcal{E}}^{\perp}$, (4.7) and (4.11), were bounded by 3×10^{-6} , and the maximum deviation of the fluid velocity‡ at any boundary point by 2×10^{-3} . For axial modes, the net source inside each particle (4.8) was also monitored; it did not exceed 7×10^{-8} in any case. Note that the latter check was not available for the transverse modes, because the cosine weighting of point sources around the rings (4.10) resulted in a zero net source for each individual ring.

The Stokes friction coefficients for $L = 0.2, 0.5, 1.0, 2.0$ were checked against the boundary-multipole collocation results of Kim & Mifflin (1985) as summarized in table 6 (6-digit accuracy at $L = 0.2$). By assigning the parameter γ a real value instead of the complex value given by (3.35), we were able to compare our calculated friction coefficients for what was now Brinkman flow with the results obtained by Kim & Russel (1985) using a multipole-collocation scheme and the method of reflections. The axial and transverse drag coefficients X_F and Y_F used by Kim & Russel can be expressed as follows in terms of our notation:

$$X_F = Z^{\parallel}, \quad Y_F = Z^{\perp},$$

† Owing to the specific basis functions and boundary conditions involved, the corresponding numbers of coefficients and constraints were, however, different for viscous *vs.* potential flow.

‡ The residuals listed refer to unit velocity of the moving sphere.

Ω	A_1^{\parallel}	A_2^{\parallel}	B_1^{\parallel}	B_2^{\parallel}
1/2048	0.330	5.742	-1.209	-1.209
1/1024	0.370	5.672	-1.204	-1.204
1/512	0.427	5.574	-1.198	-1.197
1/256	0.506	5.437	-1.190	-1.189
1/128	0.614	5.246	-1.180	-1.177
1/64	0.759	4.984	-1.170	-1.162
1/32	0.946	4.633	-1.160	-1.143
1/16	1.172	4.178	-1.153	-1.117
1/8	1.420	3.614	-1.154	-1.082
1/4	1.651	2.959	-1.165	-1.034
1/2	1.817	2.254	-1.184	-0.968
1	1.871	1.564	-1.201	-0.883
2	1.793	0.957	-1.197	-0.779
4	1.592	0.484	-1.146	-0.658
8	1.312	0.167	-1.032	-0.531
16	1.011	-0.006	-0.863	-0.416
32	0.742	-0.066	-0.676	-0.338
64	0.531	-0.068	-0.505	-0.296
128	0.378	-0.054	-0.364	-0.274
256	0.267	-0.040	-0.254	-0.260
64	0.529	-0.064	-0.502	-0.295
128	0.375	-0.051	-0.362	-0.272
256	0.265	-0.038	-0.253	-0.259
512	0.188	-0.028	-0.171	-0.250
1024	0.133	-0.020	-0.112	-0.245
2048	0.094	-0.014	-0.070	-0.241
4096	0.066	-0.010	-0.040	-0.239
8192	0.047	-0.007	-0.020	-0.237
16384	0.033	-0.005	-0.005	-0.236
32768	0.023	-0.004	0.005	-0.235

TABLE 12. Drift-force coefficients as functions of frequency for axial modes at $L = 1$. The upper results for $\Omega \leq 256$ are from the LSBSM numerical method, while the lower results for $\Omega \geq 64$ are from the reflection solution.

with

$$Z = \frac{(1/6\pi)(\zeta_a + \zeta_b) + \frac{2}{9}\gamma^2}{1 + \gamma + \gamma^2/3}.$$

They presented graphs of X_F and Y_F as functions of the sphere–sphere separation for $\gamma = 1/10, 1, 10$. Table 7 lists corresponding values of the coefficients X_F and Y_F calculated with our LSBSM scheme for $L = 1$. These results agree with those of Kim & Russel, with 7-digit accuracy.

As described in §4.8, the mesh used to evaluate the integral (3.53) is modified, in a frequency-dependent manner, to resolve the far-field or boundary-layer structure of the integrand at low and high frequencies, respectively. In order to test the accuracy of the numerical integration scheme, we used three different meshes for the same integrand – namely, that obtained by inserting the quasi-static Stokes velocity fields into (3.53). Table 8 shows resulting values of $B_i^{\parallel}(0; 1), B_i^{\perp}(0; 1)$. Note that the numerical results are consistent with (3.45).

The drift force coefficients \hat{B}_i^{\parallel} and \hat{B}_i^{\perp} from potential flow can be calculated in two

Ω	A_1^\perp	A_2^\perp	B_1^\perp	B_2^\perp
1/2048	-2.420	-1.208	1.290	0.135
1/1024	-2.414	-1.198	1.287	0.131
1/512	-2.408	-1.186	1.282	0.127
1/256	-2.400	-1.169	1.275	0.121
1/128	-2.390	-1.147	1.266	0.114
1/64	-2.374	-1.117	1.253	0.106
1/32	-2.352	-1.076	1.235	0.100
1/16	-2.315	-1.020	1.211	0.098
1/8	-2.255	-0.947	1.180	0.105
1/4	-2.156	-0.850	1.141	0.126
1/2	-1.998	-0.726	1.093	0.162
1	-1.764	-0.571	1.032	0.206
2	-1.454	-0.391	0.946	0.242
4	-1.104	-0.211	0.824	0.254
8	-0.782	-0.076	0.672	0.240
16	-0.541	-0.008	0.522	0.217
32	-0.377	0.011	0.397	0.193
64	-0.266	0.013	0.297	0.172
128	-0.187	0.010	0.219	0.156
64	-0.266	0.011	0.296	0.172
128	-0.188	0.009	0.217	0.155
256	-0.133	0.007	0.158	0.143
512	-0.094	0.005	0.114	0.135
1024	-0.066	0.004	0.082	0.129
2048	-0.047	0.003	0.059	0.125
4096	-0.033	0.002	0.044	0.123
8192	-0.023	0.001	0.033	0.121
16384	-0.016	0.001	0.025	0.119
32768	-0.012	0.001	0.020	0.118

TABLE 13. Drift-force coefficients as functions of frequency for transverse modes at $L = 1$. The upper results for $\Omega \leq 128$ are from the LSBSM numerical method, while the lower results for $\Omega \geq 64$ are from the reflection solution.

ways: (i) from the virtual masses via (2.41); and (ii) by inserting the potential velocity fields in place of the transient Stokes fields in the areal integrals (3.53), (B1), (B2) that result from the volume integration formulas (3.25). Table 9 compares the values obtained with both methods. Similarly, the numerical surface integrals corresponding to (6.21) below were checked against the Stokes friction coefficients using (6.22), as indicated in table 10. Tables 8–10 establish the accuracy of the numerical integrations, and also confirm the consistency of the overall numerical scheme.

5. Calculated results and discussion for oscillatory motions

For a sphere–sphere gap equal to one radius ($L = 1$), table 11 gives values of the friction coefficients over a wide spectrum of frequencies. At low and intermediate frequencies these were calculated via (4.14)–(4.16) as part of the LSBSM numerical scheme. In the case of well-separated Stokes layers (Ω exceeding 256 and 128, respectively, for axial *vs.* transverse modes), we employed (4.24) and (4.25) from the reflection solution. The corresponding drift-force coefficients appear in tables 12 and 13. At those frequencies where the numerical and asymptotic solutions of the

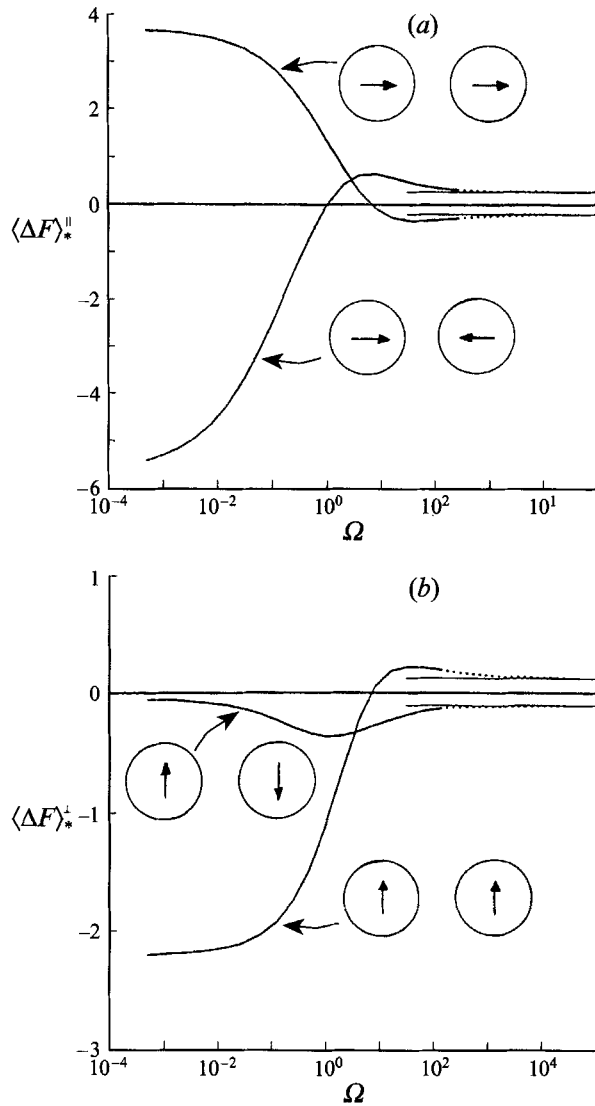


FIGURE 3. Reduced nonlinear drift force $\langle \Delta F \rangle_*$ as a function of frequency for in-phase ($\varphi = 0$) and opposite-phase ($\varphi = \pi$) oscillations at $L = 1$. (a) Axial modes. (b) Transverse modes.

unsteady Stokes equations both apply, very good agreement is observed between the respective results. Even for the friction coefficients $\tilde{\zeta}_b^{\parallel}$ and $\tilde{\zeta}_b^{\perp}$, which are much smaller than $\tilde{\zeta}_a^{\parallel}$ and $\tilde{\zeta}_a^{\perp}$ owing to the weakness of the hydrodynamic interaction in the outer field, the difference amounts to less than 1%. The numerical and asymptotic drift-force coefficients differ by at most 4 in the (rounded) third decimal place.

Figure 3 shows how the reduced mean forces of interaction $\langle \Delta F \rangle_*^{\parallel}$ and $\langle \Delta F \rangle_*^{\perp}$ vary with Ω for oscillations of the spheres (i) with the same phase ($\varphi = 0$), and (ii) with opposite phase ($\varphi = \pi$) at $L = 1$. These quantities are also plotted as functions of L for $\Omega = 1/16, 4$ in figure 1; see tables 14 and 15. The reduced forces must be multiplied

$\Omega = 1/16:$				
L	A_1^{\parallel}	A_2^{\parallel}	B_1^{\parallel}	B_2^{\parallel}
1/4	1.730	3.569	-1.169	-1.142
$\sqrt{2}/4$	1.542	3.770	-1.169	-1.141
1/2	1.385	3.943	-1.168	-1.138
$\sqrt{2}/2$	1.261	4.082	-1.164	-1.131
1	1.172	4.178	-1.153	-1.117
$\sqrt{2}$	1.115	4.213	-1.128	-1.086
2	1.078	4.158	-1.075	-1.026

$\Omega = 4:$				
L	A_1^{\parallel}	A_2^{\parallel}	B_1^{\parallel}	B_2^{\parallel}
1/4	2.646	0.251	-1.372	-0.895
$\sqrt{2}/4$	2.393	0.395	-1.351	-0.868
1/2	2.141	0.490	-1.315	-0.827
$\sqrt{2}/2$	1.880	0.524	-1.254	-0.762
1	1.592	0.484	-1.146	-0.658
$\sqrt{2}$	1.262	0.365	-0.970	-0.501
2	0.904	0.202	-0.731	-0.310

TABLE 14. Drift-force coefficients as functions of separation for axial modes.

by the Reynolds number $Re = \Omega\eta$ in order to obtain the actual (dimensionless) forces $\langle \Delta F \rangle^{\parallel}$ and $\langle \Delta F \rangle^{\perp}$ in (3.23).

For all modes except transverse oscillation with opposite phase, the nonlinear drift force ultimately changes sign in figure 3 as frequency is reduced from the limit of potential flow ($\Omega \rightarrow \infty$). The actual cross-over frequencies for these three modes are similar, and indicate that the qualitative behaviour characteristic of inviscid, irrotational flow persists roughly until the Stokes layers begin to overlap.

It is useful to compare this qualitative behaviour with the results of Tabakova & Zapryanov (1982*a, b*), who develop a singular perturbation scheme for treating steady streaming at high frequencies. Their problem differs from ours in two important respects:

(i) Tabakova & Zapryanov consider an oscillating field at infinity incident upon stationary spheres, whereas our spheres oscillate with arbitrary relative phase in an infinite expanse of quiescent fluid. Thus, the nonlinear effect is different even when $\varphi = 0$ (for which our sphere-sphere gap remains constant).

(ii) Their analysis is restricted to high frequencies $\Omega^{\frac{1}{2}} \gg 1$, but only requires that the Reynolds number for steady streaming ($Re^* = \Omega\eta^2$) be small, i.e. $\eta \ll \Omega^{-\frac{1}{2}}$. In particular, the Reynolds number of the incident flow field ($Re = \Omega\eta$) need not be small, and can even be asymptotically large. They ultimately obtain a singular perturbation expansion (in powers of both $\Omega^{-\frac{1}{2}}$ and η) which, within their prescribed limits, is uniformly valid in both frequency and amplitude. By contrast, we treat the whole spectrum of frequencies, but apply the more severe restriction $\eta \ll \Omega^{-1}$ on the amplitude, so that $Re \ll 1$ even when Ω is large – the case of interest in Brownian motion (§6.4). Ours is a regular perturbation in η at each fixed value of Ω . It should, therefore, be possible to compare the leading-order and $O(\eta)$ terms at any fixed (large) value of Ω . Unfortunately, Tabakova & Zapryanov do not give numerical values for their perturbation coefficients.

$\Omega = 1/16:$				
L	A_1^\perp	A_2^\perp	B_1^\perp	B_2^\perp
1/4	-3.379	0.065	1.596	-0.161
$\sqrt{2}/4$	-3.166	-0.161	1.525	-0.098
1/2	-2.915	-0.425	1.439	-0.031
$\sqrt{2}/2$	-2.628	-0.718	1.335	0.037
1	-2.315	-1.020	1.211	0.098
$\sqrt{2}$	-1.983	-1.298	1.066	0.143
2	-1.649	-1.512	0.902	0.164

$\Omega = 4:$				
L	A_1^\perp	A_2^\perp	B_1^\perp	B_2^\perp
1/4	-2.247	-0.044	1.452	0.192
$\sqrt{2}/4$	-2.042	-0.136	1.352	0.238
1/2	-1.785	-0.210	1.219	0.271
$\sqrt{2}/2$	-1.467	-0.240	1.042	0.280
1	-1.104	-0.211	0.824	0.254
$\sqrt{2}$	-0.754	-0.143	0.595	0.201
2	-0.482	-0.074	0.398	0.135

TABLE 15. Drift-force coefficients as functions of separation for transverse modes.

It is interesting to note the result of Tabakova & Zapryanov that, at $\Omega = 400$ and $\eta = 0.033$ ($Re = 13.2$, $Re^* = 0.44$),[†] the stationary interaction has the *opposite* sign compared with potential flow. At the same frequency – but much smaller amplitude, such that the Reynolds number is small – we recover a mean drift force that is quantitatively *very close* to the limiting value from potential flow. This emphasizes the singular nature of the high-frequency limit; for, the sign of the mean drift interaction depends upon the order of taking the limits $\Omega \rightarrow \infty$ and $\eta \rightarrow 0$.

6. Nonlinear drift in Brownian motion

In previous sections we have derived the time-average nonlinear drift force, (3.23), (3.24) and (3.53), for two spheres oscillating at given (dimensionless) frequency Ω and amplitude η . We now apply these results to the stochastic motion associated with thermal fluctuations in the suspending fluid. First we recall some linear theory of Brownian motion in order to find various (ensemble average) correlations involving the random forcing and thence the positions and velocities of the two particles. We can then integrate numerically over the spectrum of frequencies to obtain the net stochastic drift force. This result is later examined in §7 from the perspective of a general theory of small nonlinearities in the Langevin equation description of Brownian motion, as derived using the appropriate Lagrangian formulation. Finally the implications of mean nonlinear drift are discussed. We show that – with accounting for all fluid degrees of freedom directly excited by the translational motion of the particles – the thermodynamic equilibrium distribution of particles would not be uniform in a dilute colloidal suspension, unless one modified the random forcing of the Langevin equation to include a small cancelling non-zero mean part.

[†] In this case the amplitude is appreciable compared with the thickness of the Stokes layers, and therefore lies outside the range of applicability of our regular perturbation scheme.

For stochastic motions, nonlinear terms represent a ‘mixing’ of different frequencies; for, a product of two functions leads to the convolution of their respective Fourier transforms in the frequency domain. Our spectral integration quantifies how each translational disturbance mode interacts with all others to yield the observable effect, which is a systematic force of interaction between the two particles. This feature has no counterpart in the case of pure oscillatory modes.

6.1. Dimensional formulation using stochastic particle coordinates

To make the transition from pure oscillatory modes to stochastic disturbances, we first convert certain dimensionless quantities appearing in (3.14) and (3.16) to dimensional form, denoted with an underbar:

$$\underline{Q}_\alpha = a\eta Q_\alpha, \quad \underline{t} = \omega^{-1}t, \quad \underline{V} = a\eta\omega V^{(0)}, \quad \underline{F} = \mu a^2\eta\omega F.$$

Equations (3.18) and (3.21) then have the following dimensional counterparts:

$$\left. \begin{aligned} \underline{q}_\alpha(t) &= \text{Re}\{\underline{Q}_\alpha(t)\} = \text{Re}\{(i\omega)^{-1}\dot{\underline{Q}}_\alpha(t)\} \\ \underline{V}(\mathbf{r}, t) &= \text{Re}\{\underline{Q}_1(t)v^{[1]}(\mathbf{r}) + \underline{Q}_2(t)v^{[2]}(\mathbf{r})\}, \end{aligned} \right\} \quad (6.1)$$

and the relevant form of the result (3.14), (3.16) is thus

$$\begin{aligned} \langle \Delta \underline{F} \rangle &= -\mu \left\langle \int_{\mathcal{S}_1^{(0)}} \underline{q}_1(\mathbf{b} \cdot \nabla \underline{V}) \cdot \mathbf{T}' \cdot \mathbf{n} \, d^2\mathbf{r} \right\rangle \\ &\quad - \mu \left\langle \int_{\mathcal{S}_2^{(0)}} \underline{q}_2(\mathbf{b} \cdot \nabla \underline{V}) \cdot \mathbf{T}' \cdot \mathbf{n} \, d^2\mathbf{r} \right\rangle + \rho a^2 \left\langle \int_{\mathcal{V}^{(0)}} \mathbf{D}' : \underline{V} \underline{V} \, d^3\mathbf{r} \right\rangle. \end{aligned} \quad (6.2)$$

Note that, aside from the underlined quantities, the surface and volume integrals have been left in dimensionless form.

In order to deal with Brownian motion, we replace pure oscillatory quantities with stochastic quantities. Thus, in place of (6.1) we now have

$$\left. \begin{aligned} \underline{q}_\alpha(t) &= \frac{1}{(2\pi)^{\frac{1}{2}}} \int_{-\infty}^{\infty} d\omega \tilde{q}_\alpha(\omega) e^{i\omega t} = \frac{1}{(2\pi)^{\frac{1}{2}}} \int_{-\infty}^{\infty} d\omega \frac{1}{i\omega} \tilde{\dot{q}}_\alpha(\omega) e^{i\omega t}, \\ \underline{V}(\mathbf{r}, t) &= \frac{1}{(2\pi)^{\frac{1}{2}}} \int_{-\infty}^{\infty} d\omega \left[\tilde{q}_1(\omega) v^{[1]}(\mathbf{r}; \omega) + \tilde{q}_2(\omega) v^{[2]}(\mathbf{r}; \omega) \right] e^{i\omega t}. \end{aligned} \right\} \quad (6.3)$$

Here a factor of $1/(2\pi)^{\frac{1}{2}}$ has been absorbed into the definition of the Fourier transform, i.e.

$$\tilde{f}(\omega) = \frac{1}{(2\pi)^{\frac{1}{2}}} \int_{-\infty}^{\infty} dt f(t) e^{-i\omega t}.$$

Defining the Fourier transform by integrating against $\exp(-i\omega t)$ is consistent with the formulation given in §3 for pure oscillations (6.1). As will be seen below, the stochastic mean force of interaction is given by (6.2), except with two changes: (i) \underline{q}_α and \underline{V} are now given by (6.3) instead of (6.1); and (ii) the angle brackets denote ensemble-average correlations instead of time averages over one period of the oscillation.

6.2. The Langevin equation with nonlinear drift terms

The linear theory of Brownian motion, including the frequency-dependent friction law, is discussed by a number of authors, including Case (1971), Chow & Hermans (1974), Hinch (1975), and Russel (1981). Here we restrict our discussion to those elements needed to evaluate the nonlinear interaction force between the two spheres.

The positions $q_\alpha(t)$ of the two spheres (of equal mass m) are governed by a stochastic Langevin equation,

$$\left. \begin{aligned} m\ddot{q}_1 + \zeta_{11} * \dot{q}_1 + \zeta_{12} * \dot{q}_2 &= f_1(t) + \mathcal{F}_1(t), \\ m\ddot{q}_2 + \zeta_{21} * \dot{q}_1 + \zeta_{22} * \dot{q}_2 &= f_2(t) + \mathcal{F}_2(t), \end{aligned} \right\} \quad (6.4)$$

with $f_\alpha(t)$ the stochastic force acting on each sphere α in consequence of thermal fluctuations in the surrounding fluid, and \mathcal{F}_α the forces due to nonlinear effects – to be discussed below.

In order to account for Basset history dependence, the friction law for each motion $\alpha\beta$ involves a convolution against the corresponding frequency-dependent friction kernel $\zeta_{\alpha\beta}(t)$,

$$F_\alpha(t) = \zeta_{\alpha\beta} * \dot{q}_\beta = \int_{-\infty}^{\infty} dt' \zeta_{\alpha\beta}(t-t') \dot{q}_\beta(t') = \int_{-\infty}^t dt' \zeta_{\alpha\beta}(t-t') \dot{q}_\beta(t') \quad (6.5)$$

(summation over β implied), where causality requires $\zeta_{\alpha\beta}(t)$ to vanish for $t < 0$ (Case 1971). For particles of density $\rho^{(p)}$ similar to that of the fluid, the transient effect is associated with the timescale on which vorticity diffuses over a distance of order the particle diameter (Hinch 1975). At low frequencies the quasi-static Stokes friction law

$$F_\alpha(t) = \zeta_{\alpha\beta}^{(0)} \dot{q}_\beta(t) \quad (6.6)$$

is a good approximation, while at high frequencies virtual mass is the dominant contribution. The latter is clearly seen from the asymptotic behaviour of the Fourier transform,

$$\tilde{\zeta}_{\alpha\beta}(\omega) \sim i\omega \mathcal{M}_{\alpha\beta} \quad \text{as } \omega \rightarrow \infty, \quad (6.7)$$

with $\mathcal{M}_{\alpha\beta}$ the virtual mass associated with the $\alpha\beta$ motion, which is calculable from potential flow. The factor of $i\omega$ explicitly shows that at high frequency the drag is proportional to the instantaneous acceleration instead of the velocity, leading to a mass ‘renormalization’ (Case 1971).

For the case of an isolated sphere the quasi-static Stokes friction law leads to the following exponential form for the velocity autocorrelation:

$$R(\tau) \stackrel{\text{def}}{=} \langle \dot{q}(t+\tau) \dot{q}(t) \rangle = \frac{kT}{m} e^{-\zeta^{(0)}|\tau|/m}.$$

In contrast, proper accounting for the full spectrum of the friction coefficients leads to

$$\lim_{\tau \rightarrow 0} R(\tau) = \frac{kT}{m + \mathcal{M}} \quad (6.8)$$

with a long-tailed $|\tau|^{-3/2}$ asymptotic decay (Case 1971; Chow & Hermans 1974; Hinch 1975). However, this transient effect does not significantly affect the mean-square displacement, which is dominated by low-frequency contributions. For this reason the quasi-static friction law gives the correct result for the diffusivity; explicitly (cf. Batchelor 1977; Russel 1981),

$$D = \lim_{t \rightarrow \infty} \frac{1}{2} \frac{d}{dt} \langle [q(t)]^2 \rangle = \int_0^\infty R(\tau) d\tau = \frac{1}{2} (2\pi)^{1/2} \tilde{R}(0) = \frac{kT}{\zeta}.$$

In studying dynamic light scattering of dispersions of Brownian macroparticles, Altenberger (1979) considers the effect of fluid inertia, but only in the linearized theory (frequency-dependent friction), and using the point particle approximation.

The nonlinear interaction force $\mathcal{F}_1 - \mathcal{F}_2$ between the two spheres, arising from the two nonlinear terms in (3.7) and (3.8), is given by

$$\begin{aligned} \mathcal{F}_1(t) - \mathcal{F}_2(t) = & -\mu \int_{\mathcal{V}_1^{(0)}} \underline{q}_1(\mathbf{b} \cdot \nabla \underline{V}) \cdot \mathbf{T}'' \cdot \mathbf{n} \, d^2\mathbf{r} \\ & - \mu \int_{\mathcal{V}_2^{(0)}} \underline{q}_2(\mathbf{b} \cdot \nabla \underline{V}) \cdot \mathbf{T}'' \cdot \mathbf{n} \, d^2\mathbf{r} + \rho a^2 \int_{\mathcal{V}^{(0)}} \mathbf{D}'' \cdot \underline{V} \underline{V} \, d^3\mathbf{r}. \end{aligned} \quad (6.9)$$

Here the double primes ($\prime\prime$) denote the flow field which satisfies a test problem analogous to (3.11), (3.12) but for the *transient* Stokes equations; the arguments are otherwise analogous to those which led to (3.14) and (3.16). The asterisk (*) indicates a convolution product in time compounded upon the relevant vector or tensor product.

To linearize the Langevin equation (6.4) we replace $f_x(t)$ by $\epsilon f_x(t)$, subsequently inserting the corresponding regular perturbation expansion for $\underline{q}_\alpha(t)$,

$$\underline{q}_\alpha(t) = \underline{q}_\alpha^{(0)}(t) + \epsilon \underline{q}_\alpha^{(1)}(t) + \epsilon^2 \underline{q}_\alpha^{(2)}(t) + \dots \quad (\alpha = 1, 2). \quad (6.10)$$

The zeroth-order displacements $\underline{q}_\alpha^{(0)}(t)$ are constant in time, leaving the linear Langevin equation at first order:

$$\left. \begin{aligned} m\ddot{\underline{q}}_1^{(1)} + \underline{\zeta}_{11} * \dot{\underline{q}}_1^{(1)} + \underline{\zeta}_{12} * \dot{\underline{q}}_2^{(1)} &= \underline{f}_1(t), \\ m\ddot{\underline{q}}_2^{(1)} + \underline{\zeta}_{21} * \dot{\underline{q}}_1^{(1)} + \underline{\zeta}_{22} * \dot{\underline{q}}_2^{(1)} &= \underline{f}_2(t). \end{aligned} \right\} \quad (6.11)$$

Correlating between different realizations, the sphere–sphere interaction terms are, on ensemble average,

$$\begin{aligned} \langle \Delta \mathcal{F} \rangle = \epsilon^2 \left\{ -\mu \int_{\mathcal{V}_1^{(0)}} \langle \underline{q}_1^{(1)}(\mathbf{b} \cdot \nabla \underline{V}^{(0)}) \cdot \mathbf{T}'' \cdot \mathbf{n} \rangle \, d^2\mathbf{r} \right. \\ \left. - \mu \int_{\mathcal{V}_2^{(0)}} \langle \underline{q}_2^{(1)}(\mathbf{b} \cdot \nabla \underline{V}^{(0)}) \cdot \mathbf{T}'' \cdot \mathbf{n} \rangle \, d^2\mathbf{r} \right. \\ \left. + \rho a^2 \int_{\mathcal{V}^{(0)}} \langle \mathbf{D}'' \cdot \underline{V}^{(0)} \underline{V}^{(0)} \rangle \, d^3\mathbf{r} \right\}, \end{aligned} \quad (6.12)$$

with

$$\underline{V}^{(0)}(\mathbf{r}, t) = \frac{1}{(2\pi)^{\frac{1}{2}}} \int_{-\infty}^{\infty} d\omega \left[\tilde{\underline{q}}_1^{(1)}(\omega) \mathbf{v}^{[1]}(\mathbf{r}; \omega) + \tilde{\underline{q}}_2^{(1)} \mathbf{v}^{[2]}(\mathbf{r}; \omega) \right] e^{i\omega t}. \quad (6.13)$$

Note that the superscript (0) in the symbol $\underline{V}^{(0)}$ refers to the regular perturbation (3.4) and subsequent application of the reciprocal theorem (3.13) to yield (3.14) and (3.16). This is directly equivalent to the linearization (6.10) of stochastic particle coordinates represented by the superscript {1}. Henceforth we shall omit the superscript {1} from all quantities in the above linearized formulation, and drop the ϵ^2 factor in (6.12).

Using the symmetry relations (4.16) one can write the Fourier transform of the Langevin equation (6.11) in the form

$$\left. \begin{aligned} [mi\omega + \tilde{\zeta}_a(\omega)] \tilde{\underline{q}}_1(\omega) + \tilde{\zeta}_b(\omega) \tilde{\underline{q}}_2(\omega) &= \tilde{\underline{f}}_1(\omega), \\ \tilde{\zeta}_b(\omega) \tilde{\underline{q}}_1(\omega) + [mi\omega + \tilde{\zeta}_a(\omega)] \tilde{\underline{q}}_2(\omega) &= \tilde{\underline{f}}_2(\omega). \end{aligned} \right\} \quad (6.14)$$

It follows that

$$\left. \begin{aligned} \tilde{q}_1(\omega) &= \frac{[mi\omega + \tilde{\zeta}_a(\omega)]\tilde{f}_1(\omega) - \tilde{\zeta}_b(\omega)\tilde{f}_2(\omega)}{[mi\omega + \tilde{\zeta}_a(\omega)]^2 - [\tilde{\zeta}_b(\omega)]^2}, \\ \tilde{q}_2(\omega) &= \frac{-\tilde{\zeta}_b(\omega)\tilde{f}_1(\omega) + [mi\omega + \tilde{\zeta}_a(\omega)]\tilde{f}_2(\omega)}{[mi\omega + \tilde{\zeta}_a(\omega)]^2 - [\tilde{\zeta}_b(\omega)]^2}. \end{aligned} \right\} \quad (6.15)$$

In substituting the above expressions into equation (6.12) for the stochastic interaction force, we will require the following results for the correlations of the stochastic forces (cf. Case 1971; Hauge & Martin-Löf 1973; Chow & Hermans 1974):

$$\left. \begin{aligned} \langle \tilde{f}_1(\omega)\tilde{f}_1(\omega') \rangle &= \langle \tilde{f}_2(\omega)\tilde{f}_2(\omega') \rangle = 2kT \delta(\omega + \omega') \operatorname{Re}\{\tilde{\zeta}_a(\omega)\}, \\ \langle \tilde{f}_1(\omega)\tilde{f}_2(\omega') \rangle &= \langle \tilde{f}_2(\omega)\tilde{f}_1(\omega') \rangle = 2kT \delta(\omega + \omega') \operatorname{Re}\{\tilde{\zeta}_b(\omega)\}. \end{aligned} \right\} \quad (6.16)$$

Thus, the frequency dependence of the friction coefficients effectively ‘colours’ the spectrum of random disturbances, which would be white noise in the case of the simple quasi-static friction law. In the absence of a correlation between the components of the stochastic force at different frequencies (6.16) the mean drift interaction between the spheres becomes steady at a value given by (6.12) – but with the tensor fields \mathbf{T}'' and \mathbf{D}'' replaced by the the corresponding fields \mathbf{T}' and \mathbf{D}' from the *quasi-static* Stokes flow problem (3.11), (3.12). With this last input from the linear theory of Brownian motion we can now evaluate the nonlinear interaction force.

6.3. Nonlinear stochastic drift on ensemble average

To find the mean nonlinear drift force in Brownian motion we substitute (6.13), (6.15) and (6.16) into (6.12). For the surface integrals on the right-hand side of (6.12) lengthy manipulations yield

$$\begin{aligned} \langle \Delta \mathcal{F} \rangle_{(\mathcal{A})} &\stackrel{\text{def}}{=} \\ &= -\mu \int_{\mathcal{S}_1^{(0)}} \langle \mathbf{q}_1 \mathbf{b} \cdot \nabla \underline{\mathbf{V}} \rangle \cdot \mathbf{T}' \cdot \mathbf{n} \, d^2r - \mu \int_{\mathcal{S}_2^{(0)}} \langle \mathbf{q}_2 \mathbf{b} \cdot \nabla \underline{\mathbf{V}} \rangle \cdot \mathbf{T}' \cdot \mathbf{n} \, d^2r \\ &= -\frac{\mu kT}{\pi} \int_{-\infty}^{\infty} \frac{d\omega}{i\omega} \left\{ \int_{\mathcal{S}_1^{(0)}} [\underline{\mathcal{W}}_1(\omega) \mathbf{b} \cdot \nabla \overline{\mathbf{v}}^{[1]} + \underline{\mathcal{W}}_2(\omega) \mathbf{b} \cdot \nabla \overline{\mathbf{v}}^{[2]}] \cdot \mathbf{T}' \cdot \mathbf{n} \, d^2r \right. \\ &\quad \left. + \int_{\mathcal{S}_2^{(0)}} [\underline{\mathcal{W}}_1(\omega) \mathbf{b} \cdot \nabla \overline{\mathbf{v}}^{[2]} + \underline{\mathcal{W}}_2(\omega) \mathbf{b} \cdot \nabla \overline{\mathbf{v}}^{[1]}] \cdot \mathbf{T}' \cdot \mathbf{n} \, d^2r \right\} \\ &= -\frac{2\mu kT}{\pi} \int_{-\infty}^{\infty} \frac{d\omega}{i\omega} \int_{\mathcal{S}_2^{(0)}} [\underline{\mathcal{W}}_1(\omega) \mathbf{b} \cdot \nabla \overline{\mathbf{v}}^{[2]} + \underline{\mathcal{W}}_2(\omega) \mathbf{b} \cdot \nabla \overline{\mathbf{v}}^{[1]}] \cdot \mathbf{T}' \cdot \mathbf{n} \, d^2r, \end{aligned} \quad (6.17)$$

where (\mathcal{A}) denotes the contribution from the boundary terms. The weight functions $\underline{\mathcal{W}}_1(\omega)$ and $\underline{\mathcal{W}}_2(\omega)$ are given by

$$\underline{\mathcal{W}}_1(\omega) = \tilde{\zeta}_{aR}(\omega)\underline{\Theta}(\omega) + \tilde{\zeta}_{bR}(\omega)\underline{\Xi}(\omega), \quad \underline{\mathcal{W}}_2(\omega) = \tilde{\zeta}_{bR}(\omega)\underline{\Theta}(\omega) + \tilde{\zeta}_{aR}(\omega)\underline{\Xi}(\omega),$$

with

$$\underline{\Theta}(\omega) = \frac{\tilde{\zeta}_{aR}^2 + (\tilde{\zeta}_{aI} + m\omega)^2 + \tilde{\zeta}_{bR}^2 + \tilde{\zeta}_{bI}^2}{[\tilde{\zeta}_{aR}^2 - (\tilde{\zeta}_{aI} + m\omega)^2 - \tilde{\zeta}_{bR}^2 + \tilde{\zeta}_{bI}^2]^2 + 4[\tilde{\zeta}_{aR}(\tilde{\zeta}_{aI} + m\omega) - \tilde{\zeta}_{bR}\tilde{\zeta}_{bI}]^2},$$

$$\underline{\Xi}(\omega) = \frac{-2 [\underline{\zeta}_{aR} \underline{\zeta}_{bR} + (\underline{\zeta}_{aI} + m\omega) \underline{\zeta}_{bI}]}{[\underline{\zeta}_{aR}^2 - (\underline{\zeta}_{aI} + m\omega)^2 - \underline{\zeta}_{bR}^2 + \underline{\zeta}_{bI}^2]^2 + 4 [\underline{\zeta}_{aR} (\underline{\zeta}_{aI} + m\omega) - \underline{\zeta}_{bR} \underline{\zeta}_{bI}]^2},$$

both even functions of $\omega \in (-\infty, \infty)$. The gap between the spheres is an implicit parameter in these equations. Referring to the pseudo-Brinkman equation (3.19), it is readily verified that

$$\mathbf{v}_R^{[a]}(-\omega) = \mathbf{v}_R^{[a]}(\omega), \quad \mathbf{v}_I^{[a]}(-\omega) = -\mathbf{v}_I^{[a]}(\omega), \tag{6.18}$$

from which arise the complex conjugates in (6.17). The $\mathbf{v}_R^{[a]}$ terms lead to the corresponding part of the integrand in (6.17) being an odd function of ω ; thus, there is no contribution except for a pole at $\omega = 0$. In contrast, the $\mathbf{v}_I^{[a]}$ terms lead to an even function which is regular at $\omega = 0$. Letting the superscript $\{0\}$ indicate the Stokes limit ($\omega \rightarrow 0$) of the friction coefficients, and denoting by $\mathbf{u}^{[a]}$ the Stokes velocity fields that satisfy the boundary conditions (3.20), we ultimately obtain

$$\begin{aligned} \langle \Delta \underline{\mathcal{F}} \rangle_{(\mathcal{S})} &= \frac{-2\mu kT}{[\underline{\zeta}_{a}^{(0)}]^2 - [\underline{\zeta}_{b}^{(0)}]^2} \left\{ \underline{\zeta}_{a}^{(0)} \int_{\mathcal{S}_2^{(0)}} (\mathbf{b} \cdot \nabla \mathbf{u}^{[2]}) \cdot \mathbf{T}' \cdot \mathbf{n} d^2r \right. \\ &\quad \left. - \underline{\zeta}_{b}^{(0)} \int_{\mathcal{S}_2^{(0)}} (\mathbf{b} \cdot \nabla \mathbf{u}^{[1]}) \cdot \mathbf{T}' \cdot \mathbf{n} d^2r \right\} \\ &\quad + \frac{4\mu kT}{\pi} \int_0^\infty d\omega \left\{ \underline{\mathcal{W}}_1(\omega) \frac{1}{\omega} \int_{\mathcal{S}_2^{(0)}} (\mathbf{b} \cdot \nabla \mathbf{v}_I^{[2]}) \cdot \mathbf{T}' \cdot \mathbf{n} d^2r \right. \\ &\quad \left. + \underline{\mathcal{W}}_2(\omega) \frac{1}{\omega} \int_{\mathcal{S}_2^{(0)}} (\mathbf{b} \cdot \nabla \mathbf{v}_I^{[1]}) \cdot \mathbf{T}' \cdot \mathbf{n} d^2r \right\}. \end{aligned} \tag{6.19}$$

This result is now brought back in dimensionless form by writing

$$m\omega = \left(\frac{4\pi}{3} \lambda \Omega \right) \mu a \quad (\lambda = \rho^{(\mathcal{S})} / \rho), \tag{6.20}$$

and noting the relations

$$\begin{aligned} \underline{\zeta} &= \mu a \zeta, \quad \underline{\Theta} = (\mu a)^{-2} \Theta, \quad \underline{\Xi} = (\mu a)^{-2} \Xi, \\ \underline{\mathcal{W}} &= (\mu a)^{-1} \mathcal{W}, \quad \langle \Delta \underline{\mathcal{F}} \rangle_{(\mathcal{S})} = (kT/a) \langle \Delta \mathcal{F} \rangle_{(\mathcal{S})}. \end{aligned}$$

Finally, the pole term is simplified by establishing a connection with two particular quasi-static Stokes flow problems:

(i) *Centre-of-mass motion.* Both spheres move with velocity \mathbf{b} .

(ii) *Relative motion.* Sphere 1 moves with velocity \mathbf{b} while sphere 2 moves with velocity $-\mathbf{b}$.

For both cases we consider a virtual displacement ds of each sphere in the direction of its motion.

The z -component of the interaction force,†

$$\Delta F_z \stackrel{\text{def}}{=} \mathbf{e}_z \cdot (\mathbf{F}_1 - \mathbf{F}_2),$$

is differentiated with respect to s in each case. Using boundary perturbation concepts

† Here, we regard the coordinate system as fixed to the *undisplaced* positions of the spheres. In the case of shearing motion the z -axis coincides with the line of centres *only when* $ds = 0$.

and the reciprocal theorem (3.13) we ultimately obtain

$$\int_{\mathcal{S}_2^{(0)}} (\mathbf{b} \cdot \nabla \mathbf{u}^{[2]}) \cdot \mathbf{T}' \cdot \mathbf{n} \, d^2\mathbf{r} = - \int_{\mathcal{S}_2^{(0)}} (\mathbf{b} \cdot \nabla \mathbf{u}^{[1]}) \cdot \mathbf{T}' \cdot \mathbf{n} \, d^2\mathbf{r} = -\frac{1}{4} \frac{d}{ds} \Delta F_z^{\text{rel}}, \quad (6.21)$$

where the superscript ‘rel’ denotes problem (ii). Expressing ΔF_z^{rel} in terms of the various friction coefficients, one can then write

$$\left. \begin{aligned} \left[\frac{d}{ds} \Delta F_z^{\text{rel}} \right]^{\parallel} &= 4 \frac{d}{dL} \left(\zeta_a^{\{0\},\parallel} - \zeta_b^{\{0\},\parallel} \right), \\ \left[\frac{d}{ds} \Delta F_z^{\text{rel}} \right]^{\perp} &= \frac{4}{L+2} \left[\left(\zeta_a^{\{0\},\parallel} - \zeta_b^{\{0\},\parallel} \right) - \left(\zeta_a^{\{0\},\perp} - \zeta_b^{\{0\},\perp} \right) \right]. \end{aligned} \right\} \quad (6.22)$$

Equations (6.21) and (6.22) can be used to check the accuracy of the numerical surface integrations as well as to establish consistency between different elements of the computational scheme. This was done in §4.9, with reference to (6.28), below.

Substituting (6.21) into the expression (6.19) for the boundary drift force gives

$$\begin{aligned} \langle \Delta \mathcal{F} \rangle_{(\mathcal{S})}(L) &= \frac{1}{2 \left[\zeta_a^{\{0\}}(L) - \zeta_b^{\{0\}}(L) \right]} \frac{d}{ds} \Delta F_z^{\text{rel}}(L) \\ &+ \frac{4}{\pi} \int_0^\infty d\Omega \left[\mathcal{W}_1(\Omega; L) \mathcal{A}_1(\Omega; L) + \mathcal{W}_2(\Omega; L) \mathcal{A}_2(\Omega; L) \right], \end{aligned} \quad (6.23)$$

with

$$\left. \begin{aligned} \mathcal{W}_1(\Omega; L) &= \tilde{\zeta}_{aR}(\Omega; L) \Theta(\Omega; L) + \tilde{\zeta}_{bR}(\Omega; L) \Xi(\Omega; L), \\ \mathcal{W}_2(\Omega; L) &= \tilde{\zeta}_{bR}(\Omega; L) \Theta(\Omega; L) + \tilde{\zeta}_{aR}(\Omega; L) \Xi(\Omega; L), \end{aligned} \right\} \quad (6.24)$$

$$\left. \begin{aligned} \Theta &= \left(\tilde{\zeta}_{aR}^2 + \left(\tilde{\zeta}_{aI} + \frac{4}{3} \pi \lambda \Omega \right)^2 + \tilde{\zeta}_{bR}^2 + \tilde{\zeta}_{bI}^2 \right) / \left[Z_{D1}^2 + 4Z_{D2}^2 \right], \\ \Xi &= \left(-2 \left[\tilde{\zeta}_{aR} \tilde{\zeta}_{bR} + \left(\tilde{\zeta}_{aI} + \frac{4}{3} \pi \lambda \Omega \right) \tilde{\zeta}_{bI} \right] \right) / \left[Z_{D1}^2 + 4Z_{D2}^2 \right], \end{aligned} \right\} \quad (6.25)$$

$$\begin{aligned} Z_{D1} &= \tilde{\zeta}_{aR}^2 - \left(\tilde{\zeta}_{aI} + \frac{4}{3} \pi \lambda \Omega \right)^2 - \tilde{\zeta}_{aR}^2 + \tilde{\zeta}_{bI}^2, \\ Z_{D2} &= \tilde{\zeta}_{aR} \left(\tilde{\zeta}_{aI} + \frac{4}{3} \pi \lambda \Omega \right) - \tilde{\zeta}_{bR} \tilde{\zeta}_{bI}. \end{aligned}$$

Similar computations for the volume integral in (6.12) yield

$$\langle \Delta \mathcal{F} \rangle_{(\mathcal{V})}(L) = \frac{4}{\pi} \int_0^\infty d\Omega \left[\mathcal{W}_1(\Omega; L) B_1(\Omega; L) + \mathcal{W}_2(\Omega; L) B_2(\Omega; L) \right]. \quad (6.26)$$

The drift-force coefficients A_i, B_i are given by (3.25).

By adding the contributions (6.23) and (6.26) one obtains the net nonlinear force of interaction. As noted above in §3.3, the distinction between boundary and volume effects is purely formal. It is physically more meaningful to separate the pole contribution at zero frequency from the spectral integrals. The former drift term is essentially a frictional effect ‘ \mathcal{F} ’, which is well understood (Russel *et al.* 1989, p. 86), whereas the latter represents the action of inertia ‘ \mathcal{I} ’ in the fluid. In §7.2, below, we will interpret both terms in more detail with reference to the dispersion equation. The spectral integrals (6.23) and (6.26) are consolidated using the drift coefficients C_i from (3.24).

With these modifications we can now summarize the result of this section.

The net sphere–sphere interaction force that acts, on ensemble average, owing to

translational Brownian modes in the direction \mathbf{b} is given by

$$\langle \Delta \mathcal{F} \rangle = \frac{kT}{a} \langle \Delta \mathcal{F} \rangle = \frac{kT}{a} [\langle \Delta \mathcal{F} \rangle_{(\mathcal{F})} + \langle \Delta \mathcal{F} \rangle_{(\mathcal{F})}] \quad (6.27)$$

with

$$\left. \begin{aligned} \langle \Delta \mathcal{F} \rangle_{(\mathcal{F})}(L) &= \frac{-2}{\zeta_a^{(0)}(L) - \zeta_b^{(0)}(L)} \int_{\mathcal{S}_2^{(0)}} (\mathbf{b} \cdot \nabla \mathbf{u}^{[2]}) \cdot \mathbf{T}' \cdot \mathbf{n} \, d^2r \\ &= \frac{1/2}{\zeta_a^{(0)}(L) - \zeta_b^{(0)}(L)} \frac{d}{ds} \Delta F_z^{\text{rel}}(L), \\ \langle \Delta \mathcal{F} \rangle_{(\mathcal{F})}(L) &= \frac{4}{\pi} \int_0^\infty d\Omega [\mathcal{W}_1(\Omega; L) C_1(\Omega; L) + \mathcal{W}_2(\Omega; L) C_2(\Omega; L)] \\ &= \frac{4}{\pi} \int_0^\infty d\Omega \mathcal{Z}(\Omega; L). \end{aligned} \right\} \quad (6.28)$$

The crucial observation here – indeed a major result of this paper – is that *the net stochastic drift force* $\langle \Delta \mathcal{F} \rangle_{(\mathcal{F})}$ *is of* $O(1)$ *on the Brownian scale* kT/a , even though nonlinear effects appear only at $O(Re)$ for each frequency in the spectrum of pure-oscillatory modes. This order of magnitude of the drift force can be estimated as the result of pressure forces p acting over an area $O(a^2)$, with pressure fluctuations $O(\rho u^2)$ in which one uses the thermal velocity $u = O(kT/\rho a^3)^{1/2}$. In the next section we evaluate this force at $L = 1$, for both axial ($\mathbf{b}^{\parallel} = \mathbf{e}_z$) and transverse ($\mathbf{b}^{\perp} = \mathbf{e}_x$) modes.

Although *all* fluctuation modes act simultaneously in Brownian motion, nonlinear drift exhibits no coupling between translations in the three mutually perpendicular directions $\mathbf{e}_x, \mathbf{e}_y, \mathbf{e}_z$; this fact follows from the specific azimuthal harmonics involved (3.50). Moreover, the first two are equivalent owing to transverse isotropy. Thus, the total stochastic drift force is given by a simple superposition of the contributions from axial and transverse modes,

$$\langle \Delta \mathcal{F} \rangle^* = 2\langle \Delta \mathcal{F} \rangle^{\perp} + \langle \Delta \mathcal{F} \rangle^{\parallel}. \quad (6.29)$$

6.4. Applicability of the theory to colloidal particles

Before proceeding to evaluate the spectral integral (6.28), we must first justify the physical assumptions whereby our results can be applied to Brownian motion in actual colloidal systems. We have assumed that the classical linear theory of Brownian motion can be applied and that nonlinear effects are small. In particular we have assumed that the Brownian displacements of the particles are small compared with the size of the particles and that the Reynolds number for the fluid motion is small. We have also assumed that the fluid is incompressible. Letting u and τ represent the characteristic velocity and timescale of fluctuations, and denoting by c the velocity of sound in the fluid, we require the following:

- (i) small Reynolds number: $ua/v \ll 1$,
- (ii) small displacements: $u\tau/a \ll 1$,
- (iii) incompressibility: $u/c \ll 1, \quad aL'/(c\tau) \ll 1$,

with $L' = \max\{1, L\}$. Equipartition of energy fixes the characteristic velocity, and for the characteristic relaxation time we take the inertial–viscous relaxation time (Chow & Hermans 1974):

$$u = (kT/m)^{1/2}, \quad \tau = m/(6\pi\mu a).$$

For spheres suspended in water at room temperature, one then finds that

$$\begin{aligned}\frac{ua}{v} &= (1 \times 10^{-2}) \lambda^{-\frac{1}{2}} (a/a_0)^{-\frac{1}{2}}, \\ \frac{u\tau}{a} &= (2 \times 10^{-3}) \lambda^{\frac{1}{2}} (a/a_0)^{-\frac{1}{2}}, \\ \frac{u}{c} &= (7 \times 10^{-4}) \lambda^{-\frac{1}{2}} (a/a_0)^{-\frac{3}{2}}, \\ \frac{aL'}{c\tau} &= (3 \times 10^{-1}) \lambda^{-1} (a/a_0)^{-1} L',\end{aligned}$$

with $a_0 = 0.01\mu\text{m}$ and λ the ratio of particle to fluid density. Thus, when considered in an overall sense, i.e. averaged over the whole spectrum of frequencies, the assumptions underlying our analysis are seen to hold for colloidal particles.

Given that the stochastic drift force $\langle \Delta \mathcal{F} \rangle_{(s)}$ is obtained by integrating over the spectrum of frequencies (6.28) we must also verify the validity of the physical assumptions (i), (ii) and (iii) for pure oscillations at each frequency. These correspond to the respective conditions,

$$\Omega\eta \ll 1, \quad \eta \ll 1, \quad \left(\frac{v}{ac}\right) \Omega\eta \ll 1, \quad \left(\frac{v}{ca}\right) L'\Omega \ll 1. \quad (6.30)$$

The dimensionless factor $v/(ac)$ exceeds unity only when a is on the order of Angstroms: for oscillating colloidal particles, the characteristic velocity will never approach the speed of sound in the liquid (third condition) as long as the Reynolds number is small (first condition). The fourth condition reflects the fact that compressibility becomes important when $\omega \sim \omega^* \stackrel{\text{def}}{=} c/(aL')$. Physically, ω^* represents a period of oscillation of the same order as the time it takes for sound waves to travel across one radius or between the particles, whichever is larger. At unit separation between the spheres, $L = 1$, this corresponds to the following rough upper bound on frequency:

$$\Omega^* \approx 17(a/a_0), \quad a_0 = 0.01\mu\text{m}$$

for water at room temperature.

In order to consider the first two conditions in (6.30) we must determine the stochastic 'amplitude' η corresponding to a given frequency Ω . For this purpose we write the Fourier-space equation of motion that describes the response to an impulse of the appropriate strength at that frequency – as given by the the frequency correlation of the random forces (6.16). In principle, this must be done for each mode of motion of the two spheres: in phase *vs.* out of phase, parallel *vs.* perpendicular to the line of centres. However, one can obtain reasonable estimates more simply by using the frequency-dependent friction law for an isolated sphere (i.e. by neglecting hydrodynamic interactions).

The dimensionless displacement at each frequency is given by

$$\eta(\omega) = a^{-1} |\tilde{q}(\omega)| = \frac{[2kT\tilde{\zeta}_R(\Omega)/(a\mu v)]^{\frac{1}{2}}}{\Omega |\tilde{\zeta}(\Omega) + (4\pi/3)\lambda\Omega i|}.$$

The asymptotic behaviour at low frequencies then yields the following for the requirement of small displacements:

$$\eta(\Omega) \sim \left[\frac{2}{\zeta^{(0)}} \left(\frac{kT}{a\mu v} \right) \right]^{\frac{1}{2}} \frac{1}{\Omega} = (7 \times 10^{-3}) \left(\frac{a}{a_0} \right)^{-\frac{1}{2}} \frac{1}{\Omega} \ll 1.$$

This places a lower bound on the frequency. The Reynolds number $Re(\Omega) = \Omega\eta(\Omega)$ is small throughout the spectrum: $Re(0) = (6\pi)^{-1} \approx 0.053$, and $Re(\Omega)$ decreases monotonically as Ω increases. Hydrodynamic interactions between the spheres do not substantially alter these estimates pertaining to an isolated sphere.

The considerations above lead to the following upper and lower bounds on the dimensionless frequency Ω , between which our theoretical formulation of nonlinear drift can be applied colloidal particles:

$$0.002 \ll \Omega \ll 170 \text{ for } a = 0.1\mu\text{m}, \quad 0.0007 \ll \Omega \ll 1700 \text{ for } a = 1\mu\text{m}. \quad (6.31)$$

The latter, less restrictive range of validity coincides with the portion of the spectrum in which the integrand $\mathcal{Z}(\Omega; 1)$ in (6.28) is appreciable; at higher and lower frequencies $\mathcal{Z}(\Omega; 1)$ is effectively negligible. Thus our formulation of stochastic drift in Brownian motion applies accurately to micron-size and larger colloidal particles. For particles an order of magnitude smaller, some correction to our theory would have to be made at both ends of the spectrum. But the concept of inertial drift would still apply qualitatively.

6.5. Numerical calculation of nonlinear stochastic drift

Figure 4 shows the spectral weight functions $\mathcal{W}_1(\Omega)$ and $\mathcal{W}_2(\Omega)$ for both axial and transverse modes, at various values of the particle/fluid density ratio λ . In the graphs these functions have been modified by a factor of Ω so that one can directly visualize the spectral weighting with Ω plotted on a logarithmic scale. This corresponds to writing the spectral integral (6.28) using $\ln \Omega$ instead of Ω as the variable of integration, viz.

$$\begin{aligned} \langle \Delta \mathcal{F} \rangle_{(s)}(L) &= \frac{4}{\pi} \int_{-\infty}^{\infty} du e^u [\mathcal{W}_1(e^u; L)C_1(e^u; L) + \mathcal{W}_2(e^u; L)C_2(e^u; L)] \\ &= \frac{4}{\pi} \int_0^{\infty} du e^u \mathcal{Z}(e^u; L). \end{aligned} \quad (6.32)$$

The solid portions of the curves, approaching frequencies in the boundary-layer regime, represent the LSBSM numerical solution of the unsteady Stokes equations. The dotted continuations indicate values based upon the reflection solution.

It is difficult to assign a clear physical interpretation to the spectral weights, but several observations are illuminating. In the limit as $L \rightarrow \infty$, $\mathcal{W}_2(\Omega; L)$ is seen to vanish, while $\mathcal{W}_1(\Omega; L)$ simply approaches the spectrum of the velocity correlation function for an isolated sphere. Explicitly, (6.8) can be written in the form

$$\int_0^{\infty} d\Omega \mathcal{W}_1(\Omega; \infty) = \int_{-\infty}^{\infty} du e^u \mathcal{W}_1(e^u; \infty) = \frac{3/4}{1 + 2\lambda}. \quad (6.33)$$

Even given the relatively small sphere–sphere gap $L = 1$, $\mathcal{W}_1^{\parallel}(\Omega; 1)$ and $\mathcal{W}_1^{\perp}(\Omega; 1)$ are both quantitatively very similar to $\mathcal{W}_1(\Omega; \infty)$ (figure 4*a,c*), while $\mathcal{W}_2^{\parallel}(\Omega; 1)$ and $\mathcal{W}_2^{\perp}(\Omega; 1)$ are both smaller by an order of magnitude (figure 4*b,d*). Note that $\mathcal{W}_2(\Omega; L) = O(L^{-3})$ as $L \rightarrow \infty$ at any fixed frequency. Moreover, even in the dual limit $L \rightarrow \infty$, $\Omega \leq L^{-2}$ (i.e. large separations with overlapping Stokes layers) we have $\mathcal{W}_2(\Omega; L) = O(L^{-1})$. Thus, hydrodynamic interactions between the spheres do not strongly influence the spectral weighting of nonlinear stochastic drift: they are manifested primarily by the drift-force coefficients $C_1^{\parallel}(\Omega; L)$, $C_2^{\parallel}(\Omega; L)$, $C_1^{\perp}(\Omega; L)$, $C_2^{\perp}(\Omega; L)$, which are plotted in figure 5.

The functions $\mathcal{Z}^{\parallel}(\Omega; 1)$ and $\mathcal{Z}^{\perp}(\Omega; 1)$ from (6.28) are plotted for various values of

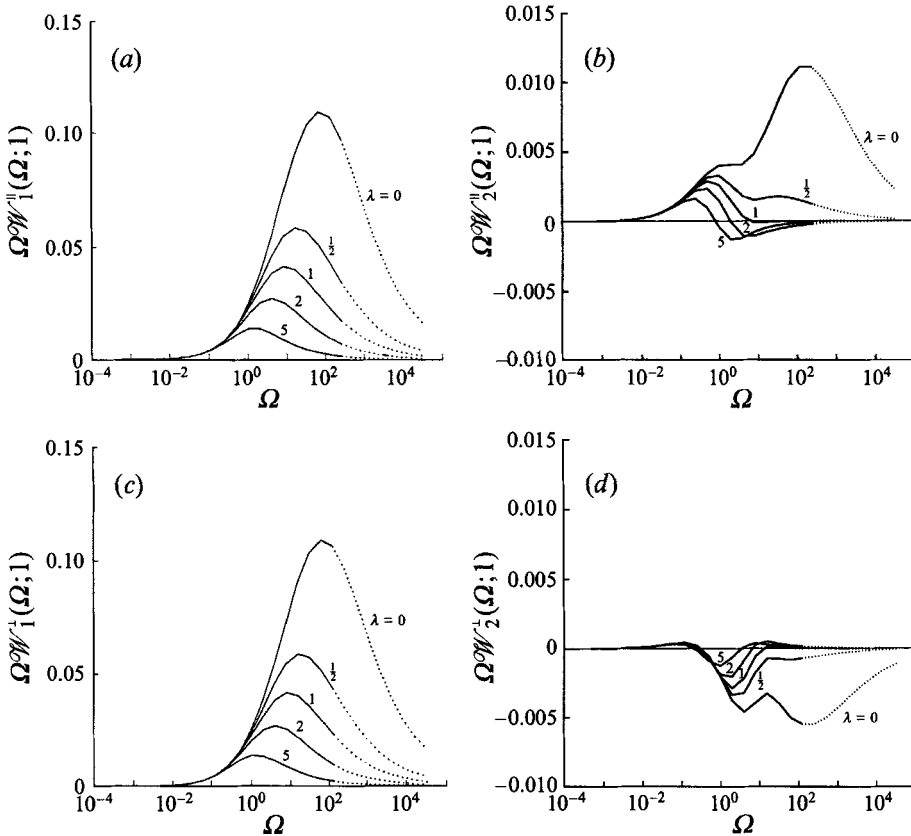


FIGURE 4. Spectral weight functions for several values of the particle/fluid density ratio λ at $L = 1$. Solid curves represent the LSBSM numerics, while dotted curves are based upon the first reflection (§4.7). (a) $\Omega \mathcal{W}_1^{\parallel}(\Omega; 1)$. (b) $\Omega \mathcal{W}_2^{\parallel}(\Omega; 1)$. (c) $\Omega \mathcal{W}_1^{\perp}(\Omega; 1)$. (d) $\Omega \mathcal{W}_2^{\perp}(\Omega; 1)$.

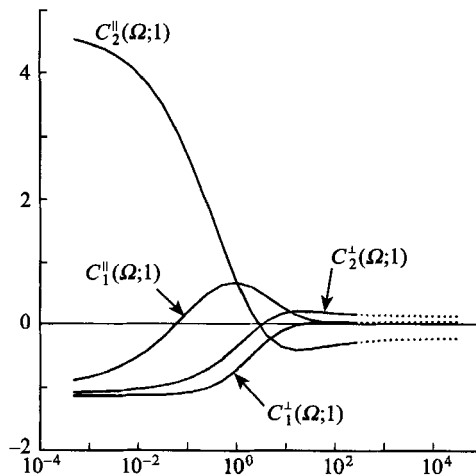


FIGURE 5. Stochastic drift force coefficients $C_1^{\parallel}, C_2^{\parallel}, C_1^{\perp}, C_2^{\perp}$ as functions of frequency at $L = 1$.

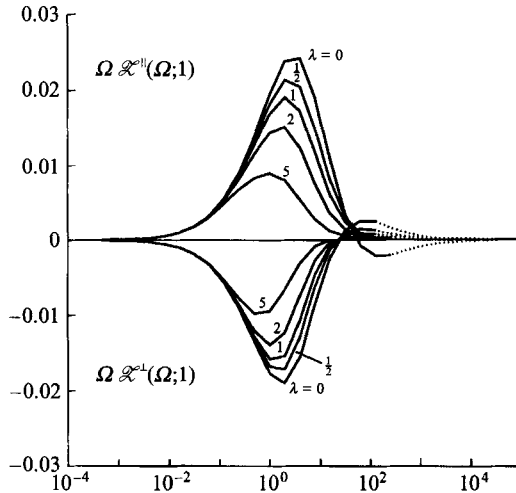


FIGURE 6. Spectrum of nonlinear drift in Brownian motion for several values of the particle/fluid density ratio λ at $L = 1$.

λ	$\langle \Delta \mathcal{F} \rangle_{(\mathcal{F})}^{\parallel}$	$\langle \Delta \mathcal{F} \rangle_{(\mathcal{F})}^{\perp}$	$\langle \Delta \mathcal{F} \rangle_{(\mathcal{F})}^*$	$\langle \Delta \mathcal{F} \rangle_{(\mathcal{A})}^*$
0	0.112	-0.079	-0.047	0.0044
$\frac{1}{2}$	0.108	-0.074	-0.041	0.0115
1	0.096	-0.070	-0.043	0.0097
2	0.077	-0.061	-0.045	0.0068
5	0.047	-0.044	-0.041	0.0035

TABLE 16. Inertial drift forces as functions of particle/fluid density ratio λ at $L = 1$.

λ in figure 6. We note, first of all, that increasing the density of the particles relative to that of the fluid shifts the spectrum of nonlinear drift toward lower frequency. Evidently the most rapid disturbances then have insufficient time to overcome the inertia of the particles. With reference to (6.31) one observes that the integrands have substantially ‘tailed off’ to negligible values outside the range of frequencies indicated for particles 1 μm in radius.

Based upon tables 11, 12 and 13, the functions $\mathcal{Z}^{\parallel}(\Omega;1)$ and $\mathcal{Z}^{\perp}(\Omega;1)$ were computed for $\Omega = 2^{-11}, 2^{-10}, \dots, 2^{14}, 2^{15}$. Simpson’s rule (with the corresponding step size $\Delta u = \Delta \ln \Omega = \ln 2$) was used to evaluate their spectral integrals (6.32) numerically. Table 16 indicates how the inertial drift force $\langle \Delta \mathcal{F} \rangle_{(\mathcal{F})}^* = 2\langle \Delta \mathcal{F} \rangle_{(\mathcal{F})}^{\perp} + \langle \Delta \mathcal{F} \rangle_{(\mathcal{F})}^{\parallel}$ varies with the particle/fluid density ratio λ at the separation $L = 1$. These values are *dimensionless*, referred to the characteristic Brownian force kT/a . The net effect of inertia in the fluid is thus seen to be a repulsion between the diffusing spheres; its magnitude is not negligible compared with that of the well-know *frictional* drift force $\langle \Delta \mathcal{F} \rangle_{(\mathcal{F})}^*(1) = -0.17$ (§7.2). Finally, it is important to point out that both the frictional and inertial drift effects are similar in strength to gravity for particles between 0.1 μm and 1 μm in size.

Inaccuracies introduced by discarding the spectrum outside the interval $2^{-11} \leq \Omega \leq$

2^{15} can be estimated from the asymptotic behaviour,

$$\mathcal{Z}(\Omega; L) \sim O(1) \quad \text{as } \Omega \rightarrow 0, \quad \mathcal{Z}(\Omega; L) \sim O(\Omega^{-\frac{1}{2}}) \quad \text{as } \Omega \rightarrow \infty.$$

The accuracy of the numerical integration itself was checked with reference to the autocorrelation integral (6.33). Compared with these factors, and in view of the accuracy of the spectral weight functions (friction coefficients – tables 6, 7, 11), the predominant numerical uncertainty seems to come from the drift-force coefficients; an approximate bound can be inferred from tables 8, 9, 12, 13. Given (6.33), a reasonable estimate of 0.02 for $(\delta C)_{\max}$ over the whole spectrum leads to the estimate $(\delta \mathcal{Z})_{\max} = 0.02/(1 + 2\lambda)$ for $\langle \Delta \mathcal{Z} \rangle_{(\mathcal{F})}^{\parallel}$ and $\langle \Delta \mathcal{Z} \rangle_{(\mathcal{F})}^{\perp}$. The question of *numerical accuracy* is, of course, distinct from the issue of how accurately the results can be *taken to apply to the physical situation* of particulate diffusion in the colloidal regime – as was discussed in §6.4. The latter is evidently the limiting consideration.

7. Nonlinear drift and the Langevin equation

Stochastic motion of the particles, which is driven by thermal fluctuations within the suspending fluid, involves the whole spectrum of frequencies. Although none of these modes can contribute to any systematic forces or motions in a linearized description, this is no longer true if one accounts for nonlinear hydrodynamic effects. Section 6 represented a synthesis of stochastic theory and frequency-dependent hydrodynamics to yield the net nonlinear effect of fluid disturbance modes that are directly excited by translational motion of the particles. Specifically, the coefficient formulas (3.25) tell us, at each frequency, how to combine the contributions from each region of the fluid. The integration over frequencies embodied in (6.28) quantifies the mutual interactions of all frequencies to yield the net stochastic drift force.

Implicit in the approach of the Langevin equation is the goal of encapsulating the action of thermal fluctuations throughout the fluid in a stochastic equation of motion that involves only particle coordinates. This is possible in the linearized description of Brownian motion. With reference to the hydrodynamic transients responsible for the algebraic – as opposed to exponential – decay of the velocity correlation function, Hinch (1975) has shown that introducing the frequency-dependent friction kernel (6.5) and modified spectrum (6.16) is equivalent to a formal generalization of the Langevin equation that involves fluid degrees of freedom in addition to particle coordinates.† Thus, it is natural to ask whether or not one can incorporate *nonlinear drift forces* into the Langevin equation as well, and thereby avoid having to implement the rather extensive computations presented in the preceding sections.

At high frequencies the effects of fluid inertia can be expressed in terms of virtual mass coefficients. One might therefore suggest splicing the history-dependent friction law (6.5) together with virtual mass coefficients (2.14), (2.16) to yield a nonlinear Langevin equation that accounts for inertia in the fluid – at least at the upper end of the frequency spectrum. The main purpose of §7.1 below is to write such a stochastic equation of motion and compare its prediction of nonlinear drift with the more comprehensive theory developed in §6.

† Evidently, only those fluid modes directly excited by motion of the particles – representing the diffusion of vorticity – are important as far as linear phenomena are concerned.

7.1. The effect of virtual mass

In order to account for the effects of fluid inertia, we modify the traditional linear Langevin equation (Case 1971; Chow & Hermans 1974; Hinch 1975; Russel 1981),†

$$m_{ij}\ddot{\underline{q}}_j + \underline{K}_{ij}\dot{\underline{q}}_j = \underline{f}_i \tag{7.1}$$

by superimposing nonlinear terms that involve the virtual mass associated with each particle degree of freedom, viz.

$$\frac{d}{dt} (\underline{M}_{ij}(\underline{q})\dot{\underline{q}}_j) - \frac{1}{2}\underline{M}_{jki}(\underline{q})\dot{\underline{q}}_j\dot{\underline{q}}_k + \underline{K}_{ij}(\underline{q})\dot{\underline{q}}_j = \underline{f}_i(t). \tag{7.2}$$

We have modified the notation from (6.4) to emphasize that the generalized particle coordinates \underline{q}_i need not coincide with the Cartesian coordinates q_α of individual particles, which we have employed thus far. Indeed, except for explicit results to be derived for the case of two identical spheres, the subsequent formulation is completely general, and applies to arbitrary geometries involving suspended particles as well as confining walls.

The generalized resistance and mass tensors – \underline{K} and \underline{M} , respectively – include all degrees of freedom of the particles; note that \underline{M} embodies the fixed inertia of each mode together with the corresponding virtual inertia of the fluid. The fact that the ‘masses’ now depend upon ‘position’ necessitates using Lagrange’s equations of motion (Goldstein 1951). In order to resolve the long-time mean drift behaviour for this simplified model, it is sufficient to utilize the quasi-static resistance coefficients; hydrodynamic transients could be incorporated in a straightforward fashion. Note that the same was expressly *not true* in §6, where the transient behaviour itself (diffusion of vorticity) was responsible for nonlinear drift.

For weak Brownian forcing (7.2) can be linearized in a manner analogous to that employed in §6.2. We express the position-dependent hydrodynamic coefficients $\underline{K}(\underline{q})$ and $\underline{M}(\underline{q})$ as Taylor expansions about the initial position, viz.

$$\underline{K}_{ij}[\underline{q}(t)] = \underline{K}_{ij}[\underline{q}(0)] + [\underline{q}_k(t) - \underline{q}_k(0)] \underline{K}_{ij,k}[\underline{q}(0)] + \dots, \text{ etc.}$$

Once again the linear Langevin equation (7.1) emerges at first order – the zeroth-order solution being constant in time. If we assume that the stochastic force \underline{f}_i has a mean component $\underline{\mathcal{F}}_i^{(2)}$, at second order we ultimately find the long-time behaviour

$$\begin{aligned} \underline{M}_{ij} \frac{d^2}{dt^2} \langle \underline{q}_j^{(2)} \rangle + \underline{K}_{ij} \frac{d}{dt} \langle \underline{q}_j^{(2)} \rangle &= -\underline{K}_{ij,k} \langle \dot{\underline{q}}_j^{(1)} \underline{q}_k^{(1)} \rangle \\ &+ \frac{1}{2} \underline{M}_{jki} \langle \dot{\underline{q}}_j^{(1)} \dot{\underline{q}}_k^{(1)} \rangle - \underline{M}_{ij,k} \langle \dot{\underline{q}}_j^{(1)} \dot{\underline{q}}_k^{(1)} + \ddot{\underline{q}}_j^{(1)} \underline{q}_k^{(1)} \rangle + \underline{\mathcal{F}}_i^{(2)} \\ &= kT \left[-\underline{K}_{ij,k} (\underline{K}^{-1})_{jk} + \frac{1}{2} \underline{M}_{jki} (\underline{M}^{-1})_{jk} \right] + \underline{\mathcal{F}}_i^{(2)}, \end{aligned} \tag{7.3}$$

where we have used the facts that

$$\begin{aligned} \langle \underline{q}_i^{(1)} \dot{\underline{q}}_j^{(1)} \rangle &= kT (\underline{K}^{-1})_{ij}, \\ \langle \dot{\underline{q}}_i^{(1)} \dot{\underline{q}}_j^{(1)} \rangle &= kT (\underline{M}^{-1})_{ij} \end{aligned}$$

once the initial transients have decayed (Chow & Hermans 1972; Hinch 1975). These represent generalized versions of (6.8), (6.16). In particular, by taking the time

† The fixed inertia tensor m_{ij} is represented by a diagonal matrix.

derivative of the former equation we see that

$$\left\langle \dot{\underline{q}}_j^{(1)} \underline{q}_k^{(1)} + \ddot{\underline{q}}_j^{(1)} \underline{q}_k^{(1)} \right\rangle = 0_{ij}.$$

Further rearrangement then yields

$$\langle \underline{\mathcal{F}}_i \rangle = kT \left[-\underline{K}_{ij,k} (\underline{K}^{-1})_{jk} + \frac{1}{2} \frac{(\det \underline{M})_i}{\det \underline{M}} \right] + \mathcal{F}_i^{(2)},$$

or, in dimensionless form,

$$\langle \underline{\mathcal{F}}_i \rangle = \frac{kT}{a} \left[\langle \mathcal{F}_i \rangle_{(\mathcal{F}')}^* + \langle \mathcal{F}_i \rangle_{(\mathcal{M})}^* + \mathcal{F}_i^{(2)} \right], \tag{7.4}$$

with

$$\langle \mathcal{F}_i \rangle_{(\mathcal{F}')}^* = -K_{ij,k} (K^{-1})_{jk}, \quad \langle \mathcal{F}_i \rangle_{(\mathcal{M})}^* = \left[\ln(\det \underline{M})^{\frac{1}{2}} \right]_i. \tag{7.5}$$

The first term represents a purely frictional drift effect, arising from the \underline{q} -dependence of the quasi-static Stokes friction coefficients. Below we shall establish that this is precisely equivalent to $\langle \Delta \mathcal{F}_i \rangle_{(\mathcal{F}')}^*$, which emerged from a pole at zero frequency in the comprehensive stochastic formulation (§6.3). The second drift force represents the systematic effect of virtual mass; an alternative derivation of this term appears in Rallison (1979). In order to determine how well the simple virtual-mass approximation captures the influence of inertia over the whole spectrum (not just at high frequencies), we shall ultimately compare $\langle \Delta \mathcal{F}_i \rangle_{(\mathcal{M})}^*$ with $\langle \Delta \mathcal{F}_i \rangle_{(\mathcal{F})}^*$ from §6.5.

It is convenient to choose the generalized coordinates \underline{q}_i in such a fashion as to diagonalize the matrix representations of \underline{K} and \underline{M} . To this end we take

$$\left. \begin{aligned} \underline{q}_1 &= x_1 - x_2, & \underline{q}_2 &= y_1 - y_2, \\ \underline{q}_3 &= z_1 - z_2, & \underline{q}_4 &= x_1 + x_2, \\ \underline{q}_5 &= y_1 + y_2, & \underline{q}_6 &= z_1 + z_2, \end{aligned} \right\} \tag{7.6}$$

where we have restricted the considerations to translational degrees of freedom. In evaluating derivatives with respect to the \underline{q}_i we choose to keep the coordinate system *fixed in space*,† considering displacements $d\underline{q}_i$ about $(\underline{q}_1, \underline{q}_2, \underline{q}_3, \underline{q}_4, \underline{q}_5, \underline{q}_6) = (0, 0, -L - 2, 0, 0, 0)$. The diagonal form of \underline{K} in these coordinates is then somewhat deceptive, because it applies only when $\underline{q}_1 = \underline{q}_2 = 0$. Explicitly,

$$\underline{K}(\underline{q}_1, \underline{q}_2, \underline{q}_3) = \begin{bmatrix} \Delta F & 0 \\ 0 & \Sigma F \end{bmatrix}. \tag{7.7}$$

The friction tensor $\underline{K}(0, 0, \underline{q}_3)$ appears as a diagonal matrix because

$$(\Delta F)_{ij}(0, 0, \underline{q}_3) = 0, \quad (\Sigma F)_{ij}(0, 0, \underline{q}_3) = 0 \quad \text{for } i \neq j.$$

The inverse of \underline{K} can therefore be computed simply by inverting the elements on the diagonal:

$$\underline{K}^{-1}(0, 0, \underline{q}_3) = \text{diag} \left(\frac{1}{(\Delta F)_{11}}, \dots, \frac{1}{(\Sigma F)_{11}}, \dots \right). \tag{7.8}$$

But in order to evaluate $K_{ij,k} = \nabla \underline{K}$ we must include the off-diagonal elements, whose

† The alternative would be to tie the z -axis to the line of centres. This would preserve diagonality of the matrix representations, but with the complication of a \underline{q} -dependent coordinate system, which we wish to avoid.

derivatives do *not* vanish when $\mathcal{Q}_1 = \mathcal{Q}_2 = 0$. Straightforward calculations using the relations

$$\left. \begin{aligned} (\Delta F)_{11}(0, 0, \mathcal{Q}_3) &= (\Delta F)_{22}(0, 0, \mathcal{Q}_3) = \frac{1}{2} \left[\zeta_a^{\{0\},\perp}(L) - \zeta_b^{\{0\},\perp}(L) \right], \\ (\Delta F)_{33}(0, 0, \mathcal{Q}_3) &= \frac{1}{2} \left[\zeta_a^{\{0\},\parallel}(L) - \zeta_b^{\{0\},\parallel}(L) \right], \\ (\Sigma F)_{11}(0, 0, \mathcal{Q}_3) &= (\Sigma F)_{22}(0, 0, \mathcal{Q}_3) = \frac{1}{2} \left[\zeta_a^{\{0\},\perp}(L) + \zeta_b^{\{0\},\perp}(L) \right], \\ (\Sigma F)_{33}(0, 0, \mathcal{Q}_3) &= \frac{1}{2} \left[\zeta_a^{\{0\},\parallel}(L) + \zeta_b^{\{0\},\parallel}(L) \right] \end{aligned} \right\} \quad (7.9)$$

(with $L = -\mathcal{Q}_3 - 2$) ultimately show that

$$\begin{aligned} \langle \mathcal{F}_3 \rangle_{(\mathcal{F}')}^* &= -K_{3j,k}(K^{-1})_{jk} = \frac{-2}{(\Delta F)_{11}} \frac{\partial}{\partial \mathcal{Q}_1} (\Delta F)_{31} - \frac{1}{(\Delta F)_{33}} \frac{\partial}{\partial \mathcal{Q}_3} (\Delta F)_{33} \\ &= \frac{1}{2} \left[2 \langle \Delta \mathcal{F} \rangle_{(\mathcal{F})}^\perp + \langle \Delta \mathcal{F} \rangle_{(\mathcal{F})}^\parallel \right] = \frac{1}{2} \langle \Delta \mathcal{F} \rangle_{(\mathcal{F})}^*. \end{aligned} \quad (7.10)$$

All other components ($i = 1, 2, 4, 5, 6$) must vanish. The factor $\frac{1}{2}$ arises in distinguishing between (i) the generalized force acting on the generalized coordinate \mathcal{Q}_3 , and (ii) the difference between the (axial) hydrodynamic forces acting on the two spheres. Thus, this frictional drift force agrees with the corresponding result (6.28) from §6.3.

Only the diagonal form of \mathbf{M} (corresponding to $\mathcal{Q}_1 = \mathcal{Q}_2 = 0$) arises in evaluating the drift force $\langle \mathcal{F}_3 \rangle_{(\mathcal{M})}^*$, whereby $\det \mathbf{M}$ is obtained simply by multiplying the elements on the diagonal:

$$\left. \begin{aligned} \mathbf{M} &= \text{diag} (M_{11}, \dots, M_{66}), \\ M_{11} = M_{22} &= (4\pi\lambda/3 + \mathcal{M}_a^\perp - \mathcal{M}_b^\perp)/2, \\ M_{33} &= (4\pi\lambda/3 + \mathcal{M}_a^\parallel - \mathcal{M}_b^\parallel)/2, \\ M_{44} = M_{55} &= (4\pi\lambda/3 + \mathcal{M}_a^\perp + \mathcal{M}_b^\perp)/2, \\ M_{66} &= (4\pi\lambda/3 + \mathcal{M}_a^\parallel + \mathcal{M}_b^\parallel)/2. \end{aligned} \right\} \quad (7.11)$$

A direct computation yields

$$\begin{aligned} \langle \mathcal{F}_3 \rangle_{(\mathcal{M})}^* &= \frac{1}{2 \det \mathbf{M}} \frac{d(\det \mathbf{M})}{d\mathcal{Q}_3} \\ &= -\frac{1}{2} \left[\frac{2}{M_{11}} \frac{dM_{11}}{dL} + \frac{1}{M_{33}} \frac{dM_{33}}{dL} + \frac{2}{M_{44}} \frac{dM_{44}}{dL} + \frac{1}{M_{66}} \frac{dM_{66}}{dL} \right] \\ &= \frac{1}{2} \left(\frac{1}{M_{44}} + \frac{1}{M_{11}} \right) \hat{B}_1^\perp + \frac{1}{2} \left(\frac{1}{M_{44}} - \frac{1}{M_{11}} \right) \hat{B}_2^\perp \\ &\quad + \frac{1}{4} \left(\frac{1}{M_{66}} + \frac{1}{M_{33}} \right) \hat{B}_1^\parallel + \frac{1}{4} \left(\frac{1}{M_{66}} - \frac{1}{M_{33}} \right) \hat{B}_2^\parallel; \end{aligned} \quad (7.12)$$

cf. (2.41), from which the nonlinear drift force $\langle \mathcal{F}_3 \rangle_{(\mathcal{M})}^*$ due to virtual mass can be obtained using table 1. Table 16 compares $\langle \Delta \mathcal{F} \rangle_{(\mathcal{M})}^* = 2 \langle \mathcal{F}_3 \rangle_{(\mathcal{M})}^*$ with $\langle \Delta \mathcal{F} \rangle_{(\mathcal{F})}^*$ for several values of the particle/fluid density ratio λ . It is seen that considerations of virtual mass do not accurately reflect the action of fluid inertia over the whole spectrum of frequencies: $\langle \Delta \mathcal{F} \rangle_{(\mathcal{M})}^*$ is attractive instead of repulsive, and underestimates the magnitude of $\langle \Delta \mathcal{F} \rangle_{(\mathcal{F})}^*$.

7.2. Nonlinear drift and the dispersion equation

For colloidal particles we can neglect the relaxation time in velocity space. Thereby, the dispersion equation for the probability density P can be constructed in a well-known manner† from considerations of transition probabilities. Under very general assumptions regarding the particle–fluid geometry, one obtains the dimensionless dispersion equation,

$$\left(\frac{\mu^2 a}{kT\rho\lambda}\right) \frac{\partial P}{\partial t} + \left[\left(\frac{d}{dt}\langle\mathcal{Q}_i\rangle\right)P\right]_i = \left[\left(\frac{1}{2}\frac{d}{dt}\langle\mathcal{Q}_i\mathcal{Q}_j\rangle\right)P\right]_{ij}, \tag{7.13}$$

where the appropriate form of the Langevin equation is used to evaluate the long-time mean moments. The latter is proportional to the diffusion dyadic,

$$\frac{1}{2}\frac{d}{dt}\langle\mathcal{Q}_i\mathcal{Q}_j\rangle = (K^{-1})_{ij},$$

and is not affected by nonlinear drift. The new element here is that the drift velocity $d\langle\mathcal{Q}_i\rangle/dt = \langle\dot{\mathcal{Q}}_i\rangle$ includes a term due to inertia in the fluid, in addition to the usual frictional term. Explicitly,

$$\langle\dot{\mathcal{Q}}_i\rangle = (K^{-1})_{im} \left[-K_{mn,j} (K^{-1})_{nj} + \langle\mathcal{F}_m\rangle_{(\mathcal{S})}^* + \mathcal{F}_m^{(2)}\right],$$

with $\langle\mathcal{F}_m\rangle_{(\mathcal{S})}^*$ the inertial drift force computed in §6 (which arises from zero-mean random forcing) and $\mathcal{F}_m^{(2)}$ a possible non-zero mean component of the random force. The inertial part of $\langle\dot{\mathcal{Q}}_i\rangle$ immediately gives rise to the divergence of a flux when it is introduced into the dispersion equation. More work is required, however, in order to bring the frictional part into a similar form. Starting from the identity

$$0_{inl} = (\delta_{in})_l = [(K^{-1})_{im} K_{mn}]_l = (K^{-1})_{im,l} K_{mn} + (K^{-1})_{im} K_{mn,l}$$

it can be shown that

$$-(K^{-1})_{im} [K_{mn,l} (K^{-1})_{nj}] = (K^{-1})_{ij,l}.$$

The mean drift velocity can then be written in the following simpler form:

$$\langle\dot{\mathcal{Q}}_i\rangle = (K^{-1})_{ij,j} + (K^{-1})_{ij} \left(\langle\mathcal{F}_j\rangle_{(\mathcal{S})}^* + \mathcal{F}_j^{(2)}\right).$$

Thus, the frictional drift velocity $(K^{-1})_{ij,j}$ is seen to be precisely that term which must be combined with the right-hand side of (7.13) to yield the divergence of the diffusive flux when diffusivity depends upon (generalized) position, viz.

$$\left(\frac{\mu^2 a}{kT\rho\lambda}\right) \frac{\partial P}{\partial t} + [(K^{-1})_{ij} (\langle\mathcal{F}_j\rangle_{(\mathcal{S})}^* + \mathcal{F}_j^{(2)}) P]_i = [(K^{-1})_{ij} P_j]_i. \tag{7.14}$$

We are now in the position to consider how nonlinear drift could result in equilibrium distributions of probability density that are *non-uniform*. For our problem involving two spheres of equal size, all coordinates except \mathcal{Q}_3 represent unimportant degrees of freedom, whereby the steady-state version of (7.14) yields

$$P_{,3} - (\langle\Delta\mathcal{F}\rangle_{(\mathcal{S})}^* + \mathcal{F}^{(2)}) P = C, \tag{7.15}$$

† See e.g. reprints of the original papers of Uhlenbeck & Ornstein (1930) and Chandrasekhar (1943) in the compilation by Wax (1954).

for some constant C which represents the total flux in the coordinate \mathcal{Q}_3 at equilibrium. The (rigid) spheres cannot penetrate each other when they touch, so that C must be zero. Changing variables from \mathcal{Q}_3 to $L = -\mathcal{Q}_3 - 2$, we find the following equilibrium pair distribution function for a dilute, monodisperse dispersion of colloidal particles:

$$P(L) = P_\infty \exp \left[\int_L^\infty (\langle \Delta \mathcal{F} \rangle_{(\mathcal{F})}^* + \mathcal{F}^{(2)}) (\hat{L}) d\hat{L} \right], \quad (7.16)$$

with P_∞ the bulk number density of particles (the limit of P as $L \rightarrow \infty$). In §6 we carried out the (extensive) calculations required to obtain the inertial drift force at one separation, $L = 1$. By the above prescription, one should find $\langle \Delta \mathcal{F} \rangle_{(\mathcal{F})}^*(L)$ at sufficiently many values of L to enable at least an approximate evaluation of the integral in (7.16).

7.3. Concluding remarks

The fluid forces on Brownian particles fluctuate in time due to the discrete molecular nature of the fluid. In the Langevin description the fluid forces are split into a frictional term on the left-hand side of the momentum equation and a random forcing term placed on the right-hand side. The frictional term is calculated for the particle motion in a smooth continuum fluid. In the linear theory of the random motion of the Brownian particles the random force must have zero mean value to avoid a systematic drift and has the magnitude of its fluctuations set by a fluctuation-dissipation theorem (which can be derived by requiring that the resulting particle motion has a thermal energy $\frac{1}{2}kT$ for each degree of freedom). In the weakly nonlinear theory there are obvious contributions from the nonlinear theory for the continuum fluid. One must also consider the possibility of a non-zero mean component of the random forcing $\mathcal{F}^{(2)}$. We note that in order to maintain the fluctuation-dissipation theorem in the presence of small nonlinear effects the random forcing needs some small corrections, but these occur at the third order and do not include a mean component (cf. El-Kareh & Leal 1993).

If one assumes that there is no mean component of the random forcing, $\mathcal{F}^{(2)} = 0$, then the nonlinear effects from the continuum fluid will make the probability density non-uniform for the relative separation of two equal spheres, (7.16). Now there are good statistical mechanical reasons for expecting that this probability density is uniform. To produce a uniform distribution one must clearly set the mean random force to cancel the mean inertial drift force from the continuum fluid

$$\mathcal{F}^{(2)} = -\langle \Delta \mathcal{F} \rangle_{(\mathcal{F})}^*. \quad (7.17)$$

Note that the mean part of the random force does not cancel all the mean drift force from the continuum fluid: the mean friction drift force $\langle \Delta \mathcal{F} \rangle_{(\mathcal{F})}$ is required to turn the probabilistic dispersion equation (7.13) into a Fickian diffusion process (7.14).

One must therefore decide whether or not the probability density should be uniform. Non-uniform distributions can occur in thermodynamic equilibrium and can be correctly predicted by the nonlinear drift force (7.5). A single Brownian particle moving in a finite container will have a uniform distribution in terms of Cartesian coordinates but an appropriate non-uniform distribution in terms of other generalized coordinates, correctly given as $P \propto [\det \mathbf{M}(\mathcal{Q})]^{1/2}$ by (7.5) in (7.15). Similarly a rigid trumbbell (or trimer) consisting of two particles joined to a third by two freely hinged rigid connectors has a non-uniform distribution of the included angle (Rallison 1979), which can be derived from standard statistical mechanical integration over the momenta of a Maxwellian distribution or from our Langevin equation with $\mathcal{F}^{(2)} = 0$.

In the case of two Brownian spheres in a suspension, we believe that the probability density of their separations should be uniform. The number of configurations of the fluid molecules would seem not to depend on the separation of the Brownian particles since it depends only on the volume available to the fluid so long as the Brownian particles are much larger than the fluid molecules. (We note that a number of standard analyses in statistical mechanics logically cannot address this question after they decouple the 'bath' in a small-mass approximation: the small mass of the individual fluid molecules times their large number displaced by a Brownian particle may not always be negligible.) The many experimental measurements of suspensions have never reported any anomalies which would question the assumed uniformity of the probability distribution in thermodynamic equilibrium, although a complicated compensation must first be made for other known interaction forces. Thus we tentatively conclude that when the Langevin equation is used to describe a suspension of interacting particles, as in computer simulations of non-thermodynamic equilibrium processes like shear flow, the random force has a non-zero mean component given by (7.17). We speculate that the need for this non-zero mean component is related to the constraint that the fluid is attached to the particles, just as the constraint of the rigid connectors of the trumbbell is the source of its non-uniform distribution.

It was pointed out in the introduction that there is no well-established general theory of nonlinear fluctuations to which we can appeal. Were it the case that a single Brownian impact displaced a particle through several diameters or that the thermal motion were at a high Mach number or at a high Reynolds number, then there would be serious difficulties in constructing a suitable theory for such strongly nonlinear fluctuations. On mathematical grounds, van Kampen (1981, p. 244) has argued that in these circumstances squares of delta functions would occur and would be meaningless. And on physical grounds, it is not clear that one would have the right to define a temperature for thermodynamics or that the most probable state would be close to the majority of instantaneous states for statistical mechanics. Fortunately colloidal systems necessarily have only small fluctuations, as estimated in §6.4, with small Brownian displacements compared with the size of the particles and small Reynolds and Mach numbers. For the small fluctuations of the real world, one may expect that a theory of nonlinear fluctuations can be constructed which is but a small and regular perturbation of the classical and successful linear theory, for otherwise the linear theory would be isolated from the real world. In order not to disturb the experimentally tested predictions of the linear Langevin theory, one can only make small changes to the amplitude and frequency spectrum of the random forcing. Such small changes yield small corrections to the successful predictions of the diffusivity and velocity autocorrelation function. Such small changes also yield relatively small changes to the steady drift. The only way to change the steady drift significantly while preserving the diffusivity and the velocity autocorrelation function is to modify the zero-frequency component of the random forcing. In the linear theory one needs zero mean force in order to ensure that the random walk has no mean motion. To preserve the absence of mean motion in the slightly nonlinear theory, it is essential to have a small mean component of the random forcing.

Throughout this paper we have restricted our discussion of stochastic motion to translational modes of the two identical spheres. These two-particle calculations could be generalized in four directions: (i) rotary modes of the spheres, (ii) spheres of different sizes, (iii) non-spherical particles, and (iv) fluid degrees of freedom which do not directly excite particle modes. These aspects are discussed in turn below.

In contrast to translational fluctuations, rotary fluctuations of the spheres would

not lead to displacements of the boundaries. According to the spectral theory of §§ 3 and 6, there would be no boundary drift force (therefore no frictional contribution like $\langle \Delta \mathcal{F} \rangle_{(\mathcal{F})}^*$ from a pole at zero frequency), and the volumetric effect of nonlinearities would be manifested in a manner analogous to (3.25), (6.28). Thus, the rotary drift force would be purely inertial; it would decay to zero with decreasing thickness of the Stokes layers as $\Omega \rightarrow \infty$, because there is no virtual mass associated with the rotation of spheres in potential flow. For the same reason, rotary modes would not appear *at all* in the nonlinear Langevin equation of §7.1. This difference emphasizes the importance of capturing the effects of fluid inertia over the entire spectrum of random motion, not just virtual mass at infinite frequency.

For two spheres of unequal size, nonlinear drift would generally result in a net force on the pair in addition to the relative force of interaction. The analysis of nonlinear drift would, of course, become much more complicated in the case non-spherical particles. Rotary modes would be as important as translational modes at high frequencies, and one would have to consider translational–rotational coupling. Even given *fixed* orientations of the particles, nonlinear drift effects due to translational modes in perpendicular directions would no longer be decoupled, in general.

The issue of fluid degrees of freedom is more subtle, and bears upon the very *approach* of the Langevin equation. Consider an experiment in which an *external device* animates suspended particles in a random fashion. There is no question that this stochastic process would be described by the Langevin equation (6.11), with the spectrum of random forcing *determined by the forcing apparatus*. In particular, only those fluid modes associated with the diffusion of vorticity away from the particles would be excited, and the action of that restricted set of modes is represented entirely by the history-dependent friction kernel (6.5) written in particle coordinates. But in Brownian motion the fluctuating force comes from the suspending fluid itself. Explicit cognizance of this fact is given in the linear Langevin equation via (6.16), whereby the spectrum of forces is modified from white noise using the frequency-dependent friction law. As far as linear phenomena are concerned, the linear friction effectively captures the effects of fluid degrees of freedom.

However, when it comes to *nonlinear drift* it must be recognized that an average force of interaction between particles can be induced by fluid modes which vanish on the solid surfaces (Tabakova & Zapryanov 1982 *a, b*), i.e. modes which are *not excited by motion of the particles*. These disturbances are present owing to thermal fluctuations throughout the fluid. In principle one should consider *all* such modes, calculating the resulting drift-force spectra via (3.25) and (6.28) – there being no finite-amplitude effect of changing geometry in the absence of motion of the boundaries. As a first step, one could treat the problem of a fluctuating point force in an arbitrary location within the fluid, with the particles held fixed. In this connection it is relevant to mention the work of Riley (1987) on acoustic streaming induced at the surface of a stationary cylinder by a parallel acoustic line source.

We would like to acknowledge a fruitful exchange with the referees. Thanks are due to Professor Sangtae Kim for supplying numerical values used in tables 6 and 7. Financial support of L.C.N. in the form of an NSF-NATO Postdoctoral Fellowship during the early stages of this work is gratefully acknowledged.

REFERENCES

- ALTENBERGER, A. R. 1979 The role of inertial effects in macroparticle diffusion. *J. Polymer Sci.: Polymer Phys. Ed.* **17**, 1317–1324.
- BATCHELOR, G. K. 1967 *An Introduction to Fluid Dynamics*. Cambridge University Press.
- BATCHELOR, G. K. 1977 Developments in microhydrodynamics. In *Theoretical and Applied Mechanics* (ed. W. T. Koiter), pp. 33–55. North-Holland.
- BIRKHOFF, G. 1950 *Hydrodynamics. A Study in Logic, Fact, and Similitude*. Princeton University Press.
- BOGOMOLNY, A. 1985 Fundamental solutions method for elliptic boundary value problems. *SIAM J. Numer. Anal.* **22**, 644–669.
- BRENNER, H. 1961 The slow motion of a sphere through a viscous fluid towards a plane surface. *Chem. Engng Sci.* **16**, 242–251.
- CASE, K. M. 1971 Velocity fluctuations of a body in a fluid. *Phys. Fluids* **14**, 2091–2095.
- CHOW, T. S. & HERMANS, J. J. 1974 Limitations of the Langevin equation based on hydrodynamic models. *K. Nederl. Akad. Van Wetenschappen – Amst.* **B 77**, 18–25.
- DĄBROŚ, T. 1985 A singularity method for calculating hydrodynamic forces and particle velocities in low-Reynolds-number flows. *J. Fluid Mech.* **156**, 1–21.
- DAHLQUIST, G. & BJÖRCK, Å. 1974 *Numerical Methods*. (Transl. by N. Anderson) Prentice Hall.
- DONGARRA, J. J., BUNCH, J. R., MOLER, C. B. & STEWART, G. W. 1979 *LINPACK Users' Guide*. Philadelphia: SIAM.
- EL-KAREH, A. W. & LEAL, L. G. 1993 Brownian motion of a slightly deformable drop. II Higher-order fluctuation-dissipation theorems. *J. Statist. Phys.* (submitted).
- GLUCKMAN, M. J., PFEFFER, R. & WEINBAUM, S. 1971 A new technique for treating multiparticle slow viscous flow: axisymmetric flow past spheres and spheroids. *J. Fluid Mech.* **50**, 705–740.
- GOLDSTEIN, H. 1951 *Classical Mechanics*. Addison-Wesley.
- GROTEBERG, J. B. 1984 Volume-cycled oscillatory flow in a tapered channel. *J. Fluid Mech.* **141**, 249–264.
- HALL, P. 1974 Unsteady viscous flow in a pipe of slowly varying cross section. *J. Fluid Mech.* **64**, 209–226.
- HAN, P. S. & OLSON, M. D. 1987 An adaptive boundary element method. *Intl J. Numer. Meth. Engng* **24**, 1187–1202.
- HAPPEL, J. & BRENNER, H. 1983 *Low Reynolds Number Hydrodynamics*. Martinus Nijhoff.
- HAUGE, E. H. & MARTIN-LÖF, A. 1973 Fluctuating hydrodynamics and Brownian motion. *J. Statist. Phys.* **7**, 259–281.
- HINCH, E. J. 1975 Application of the Langevin equation to fluid suspensions. *J. Fluid Mech.* **72**, 499–511.
- HOWELLS, I. D. 1974 Drag due to the motion of a Newtonian fluid through a sparse random array of small fixed rigid objects. *J. Fluid Mech.* **64**, 449–475.
- KAMPEN, N. G. VAN 1981 *Stochastic Processes in Physics and Chemistry*. North-Holland.
- KANWAL, R. P. 1964 Drag on an axially symmetric body vibrating slowly along its axis in a viscous fluid. *J. Fluid Mech.* **19**, 631–636.
- KARRILA, S. J. & KIM, S. 1989 Integral equations of the second kind for Stokes flow: direct solution for physical variables and removal of inherent accuracy limitations. *Chem. Engng Commun.* **82**, 123–161.
- KIM, S. & KARRILA, S. J. 1991 *Microhydrodynamics: Principles and Selected Applications*. Butterworth-Heinemann.
- KIM, S. & MIFFLIN, R. T. 1985 The resistance and mobility functions of two equal spheres in low-Reynolds-number flow. *Phys. Fluids* **28**, 2033–2045.
- KIM, S. & RUSSEL, W. B. 1985 The hydrodynamic interactions between two spheres in a Brinkman medium. *J. Fluid Mech.* **154**, 253–268.
- LAMB, H. 1932 *Hydrodynamics*, 6th edn. Cambridge University Press (Dover edition 1945).
- LANDAU, L. D. & LIFSHITZ, E. M. 1959 *Fluid Mechanics*. (Transl. from the Russian by J. B. Sykes & W. H. Reid; Vol. 6 of *Course of Theoretical Physics*.) Pergamon.
- LAWRENCE, C. J. & WEINBAUM, S. 1988 The unsteady force on a body at low Reynolds number; the axisymmetric motion of a spheroid. *J. Fluid Mech.* **189**, 463–489.
- MATHON, R. & JOHNSTON, R. L. 1977 The approximate solution of elliptic boundary-value problems by fundamental solutions. *SIAM J. Numer. Anal.* **14**, 638–650.

- MILNE-THOMSON, L. M. 1968 *Theoretical Hydrodynamics*, 5th edn. Macmillan.
- NITSCHKE, L. C. & BRENNER, H. 1990 Hydrodynamics of particulate motion in sinusoidal pores via a singularity method. *AIChE J.* **36**, 1403–1419.
- POZRIKIDIS, C. 1989a A study of linearized oscillatory flow past particles by the boundary-integral method. *J. Fluid Mech.* **202**, 17–41.
- POZRIKIDIS, C. 1989b A singularity method for unsteady linearized flow. *Phys. Fluids A* **1**, 1508–1520.
- POZRIKIDIS, C. 1992 *Boundary Integral and Singularity Methods for Linearized Viscous Flow*. Cambridge University Press.
- RALLISON, J. M. 1979 The role of rigidity constraints in the rheology of dilute polymer solutions. *J. Fluid Mech.* **93**, 251–279.
- RILEY, N. 1966 On a sphere oscillating in a viscous fluid. *Q. J. Mech. Appl. Maths* **19**, 461–472.
- RILEY, N. 1987 Streaming from a cylinder due to an acoustic source. *J. Fluid Mech.* **180**, 319–326.
- RUSSEL, W. B. 1981 Brownian motion of small particles suspended in liquids. *Ann. Rev. Fluid Mech.* **13**, 425–455.
- RUSSEL, W. B., SAVILLE, D. A. & SCHOWALTER, W. R. 1989 *Colloidal Dispersions*. Cambridge University Press.
- SANGANI, A. S. 1991 A pairwise interaction theory for determining the linear acoustic properties of dilute bubbly liquids. *J. Fluid Mech.* **232**, 221–284.
- SANGANI, A. S., ZHANG, D. Z. & PROSPERETTI, A. 1991 The added mass, Basset, and viscous drag coefficients in nondilute bubbly liquids undergoing small-amplitude oscillatory motion. *Phys. Fluids A* **3**, 2955–2970.
- SOBEY, I. J. 1980 On flow through furrowed channels. Part 1. Calculated flow patterns. *J. Fluid Mech.* **96**, 1–26.
- STIMSON, M. & JEFFREY, G. B. 1926 The motion of two spheres in a viscous fluid. *Proc. R. Soc. Lond. A* **111**, 110.
- TABAKOVA, S. S. & ZAPRYANOV, Z. D. 1982a On the hydrodynamic interaction of two spheres oscillating in a viscous fluid. I. Axisymmetric case. *Z. Angew. Math. Phys.* **33**, 344–357.
- TABAKOVA, S. S. & ZAPRYANOV, Z. D. 1982b On the hydrodynamic interaction of two spheres oscillating in a viscous fluid. II. Three dimensional case. *Z. Angew. Math. Phys.* **33**, 487–502.
- WAX, N. 1954 *Selected Papers on Noise and Stochastic Processes*. Dover.
- WEINBAUM, S., GANATOS, P. & YAN, Z.-Y. 1990 Numerical multipole and boundary boundary integral equation techniques in Stokes flow. *Ann. Rev. Fluid Mech.* **22**, 275–316.
- YOUNGREN, G. K. & ACRIVOS, A. 1975 Stokes flow past a particle of arbitrary shape: a numerical method of solution. *J. Fluid Mech.* **69**, 377–403.